



DISSERTATION

# Computational Hygro-thermal Analysis of Moisture Problems in Historical Buildings in a Tropical Climate

**ausgeführt zum Zwecke der Erlangung des akademischen Grades  
eines Doktors der technischen Wissenschaften unter der Leitung von**

Univ. Prof. Dipl.-Ing. Dr. techn. Ardeshir Mahdavi  
E 259/3 Abteilung für Bauphysik und Bauökologie  
Institut für Architekturwissenschaften

**eingereicht an der Technischen Universität Wien  
Fakultät für Architektur und Raumplanung**

von

Sarin Pinich M.Arch.  
Matrikelnummer: 1528492  
Clementinengasse 20/7, 1150 Wien

Wien, Dezember 2020

# Zusammenfassung

Wasser in historischem Mauerwerk ist eine der größten Bedrohungen für das architektonische Erbe. Es führt zu Schäden an Fassaden sowie der Struktur von Gebäuden und kann sogar zur Verschlechterung der Luftqualität in Innenräumen führen. Aus dem Grundwasser aufsteigende Feuchtigkeit in Mauerwerk infolge der Kapillarwirkung ist ein weitverbreitetes Phänomen und Grund für das Auftreten von Feuchtigkeit in historischen Gebäuden. Aufgrund der Komplexität der Mechanismen von aufsteigender Feuchtigkeit und der Vielzahl der damit zusammenhängende Faktoren, ist es seit Jahrzehnten eine Herausforderung, passende Lösungen hinsichtlich der Verminderung von aufsteigender Feuchtigkeit zu finden.

Diese Arbeit betrachtet historische Gebäude und deren Komponenten, die im 19. Jahrhundert mit traditionellen Techniken in Thailand errichtet wurden. In diesem südostasiatischen Staat herrscht tropisches Klima und trotz einer Vielzahl von Problemen mit aufsteigender Feuchtigkeit kommen kaum effektive Sanierungsmethoden zum Einsatz. Als Fallbeispiel wird eine historische Kirche mit schweren Feuchtigkeitsschäden betrachtet. Das Auftreten der Feuchtigkeit und die Ursachen für die Feuchtigkeitsschäden wurden in zwei Schritten untersucht – erstens in Form einer Besichtigung des betroffenen Mauerwerks vor Ort und zweitens mit numerischer Simulation des hygrothermischen Verhaltens. Für die hygrothermische Simulation wurden die tatsächlichen Maße der Innenwand und der vier Außenwände, welche in vier verschiedene Himmelsrichtungen zeigen, verwendet. Ferner wurden Methoden zur Sanierung dieser historischen Wände betrachtet und hinsichtlich der Effektivität zur Verminderung der aufsteigenden Feuchtigkeit unter Einsatz der Simulation evaluiert.

Die Resultate der Untersuchung besagen, dass aufsteigende Feuchtigkeit infolge der Kapillarwirkung der Hauptverursacher von Feuchtigkeitsschäden auf den Oberflächen der Innenwände ist. Die visuelle Inspektion und die Ergebnisse der Simulation deuten darauf hin, dass Innenwände größere Schäden und einen höheren Wassergehalt als Außenwände haben.

Die Effektivität der mechanischen Horizontalsperre, einer bekannten Methode zur Bauwerksabdichtung, wird hinsichtlich ihres Potentials zur Verringerung aufsteigender Feuchtigkeit, analysiert und die Resultate der hygrothermischen Analyse der sanierten Wände werden präsentiert. Die Erkenntnisse dieser Arbeit legen nahe, dass die mechanische Horizontalsperre eine effektive Methode zur Verringerung aufsteigender Feuchtigkeit in historischen Gebäuden ist, wobei aber auch das Innenklima und das Wetter potentiell eine

Rolle spielen können. Des Weiteren hat sich herausgestellt, dass die mechanische Horizontalsperre bei Innenwänden effektiver wirkt als bei Außenwänden, wobei die Trocknungszeit der sanierten Innenwand auch deutlich kürzer war.

Da diese Arbeit hauptsächlich auf Simulationsergebnissen beruht, hat sie von den Resultaten einer Simulationskalibrierung an der TU Wien profitiert. Die Simulationsergebnisse für eine sanierte Wand am TU Campus wurden mit Messdaten von den verschiedenen Schichten der existierenden Wand verglichen, um die Zuverlässigkeit der eingesetzten Simulationssoftware zu evaluieren. Die Ergebnisse zeigen eine merkbare Verbesserung der Simulationsresultate durch Setzen der Eingabeparameter auf Messwerte. Da das Wissen über materialspezifische Parameter essentiell für die Erstellung einer zuverlässigen Simulation ist, untersucht diese Arbeit auch den Grad der Sensitivität der hygrothermischen Analyse hinsichtlich der Wahl der materialspezifischen Eingabeparameter. Um jene Variablen zu identifizieren, welche signifikanten Einfluss auf die Simulationsergebnisse haben, wurde am Mauerwerk eines historischen Tempels in tropischem Klima (Thailand) eine Sensitivitätsanalyse durchgeführt.

# Summary

Presence of water in historical masonry wall construction is one of the most pervasive problems that adversely affects architectural heritage, causing various considerable building surface and structural damages, subsequently could lead to indoor air quality problems. Capillary rise of ground water, so-called rising damp, through masonry brick wall is the most widespread phenomenon leading to moisture presence in historical buildings. Due to the complexity of rising damp mechanisms and the number of unknown factors involved in rising damp finding appropriate solutions for rising damp mitigation has been a challenge for decades.

The focus of this dissertation is placed on historical buildings and their pertinent building components constructed with traditional techniques in 19th-century Thailand, a Southeast Asian nation governed by a tropical climate where lack of effective retrofit options persists despite the wide range of rising damp problems. A historical church with severe moisture-related deteriorations from the respective era serves as the case study. Hence, on-site visual inspection of the affected wall constructions along with numerical hygro-thermal performance simulation tools are integrated as a two-step procedure, which is used to investigate the dampness occurrence and the causes of moisture-related deteriorations. The hygro-thermal simulation was conducted using actual dimensions of the interior wall and the four exterior walls of the historical church facing four different cardinal directions. Furthermore, retrofit options for these historical walls were considered and evaluated for its effectiveness in rising damp mitigation by deploying the aforementioned hygro-thermal simulation software.

The results of the investigation suggest that capillary moisture rise is the main agent that exacerbates existing moisture-related deteriorations, which can be found on the surfaces of the interior wall. Consistent with the simulation results, further findings from visual inspection also indicate that there are more severe problems on the interior wall surfaces compared to those on the exterior wall surfaces. The findings conclude that more water content exists in the interior wall than in the exterior walls. The effectiveness of wall cutting, a well-known mechanical intervention method, was then evaluated in light of its potential as a rising damp mitigation measure. The results of the hygro-thermal analysis of the post-retrofit walls are presented. The main findings of the study can be summarized that in historical buildings, the wall cutting method appears to be an effective rising damp mitigation measure. Nevertheless, there still exists potential impact from humidity due to indoor climate and outdoor weather conditions. Moreover, the cutting wall method was found to be more

effective for retrofitting the interior wall compared to the exterior cases. A shorter notable drying out time also appeared in the retrofitted interior wall.

Since this dissertation relies mainly on simulation results, it benefited from the results of a simulation calibration effort at TU Wien, Austria. The simulation results for a retrofitted wall at TU Campus were compared with data measured at the positions within the different layers of the existing wall construction in order to evaluate the reliability of the employed simulation tool. The results show a noticeable improvement of the predictive potency of the simulation model when input variables were adjusted based on measurements.

Moreover, since the reliable knowledge of material-specific parameters is essential to generating dependable simulation models, this dissertation also investigated the degree of sensitivity of hygro-thermal analysis with respect to the choice of material-specific model input data. In order to identify a subset of input variables with significant influence on the simulation results, the wall construction of a historical building located in a hot-humid climate in Thailand (Thai temple wall) is subjected to a sensitivity analysis. The results illustrating as the sensitivity degree classification (i.e., low, medium, high) of the influential input parameters were presented.

# Acknowledgments

First and foremost, my deepest gratitude goes to Professor Ardeshir Mahdavi for his continual support during the entire period of my study at TU Wien. His professional attitude inspires me not only in the academic field but also in my work and personal life. Under his guidance, he has vastly broadened my experience and knowledge by encouraging me to contribute to the scientific works and participate in international conferences, whenever possible.

I would also like to express my gratitude to Samira Aien among others for our collaboration and the publication, which has been adopted and integrated into a part of this dissertation. I would also like to give special thanks to another colleague, Mahnameh Taheri, with regard to her doctoral thesis guidance and her support, especially at the beginning of the dissertation where I felt was the most difficult stage. Moreover, my thanks also go to Dr. Matthias Schuss for his advice on my research direction. To my friends and colleagues with whom I have come into contact at the Department of Building Physics and Building Ecology, thank you for your kindness and generous support along my journey at TU Wien.

Last but not least, I am deeply grateful to my family, my parents and my brother who constantly provide me with unconditional and moral support, both physically and emotionally, and for always believing in me that I could achieve what I have intended to. My sincere thanks also goes to my cousin, Surachate Pinich, who has given me enormous linguistic support and elaborate feedback during the drafting and revising stages of the dissertation. Lastly, I also would like to express my warmest appreciation to my fiancée, Benjamin Van den Nest, who has been a true supporter from the very first time we met and specifically during this time of uncertainty and the duration of this ongoing pandemic.

# Contents

Zusammenfassung .....	1
Summary .....	3
Acknowledgments .....	5
Contents .....	6
<b>Chapter 1</b> Introduction .....	9
1.1 Motivation.....	9
1.2 Background.....	10
1.3 Structure of work .....	11
<b>Chapter 2</b> Predictive performance of hygro-thermal simulation models .....	13
2.1 Background.....	13
2.1.1 Moisture in building materials .....	13
2.1.1.1 Moisture storage.....	13
2.1.1.2 Moisture transport mechanisms .....	16
2.1.2 Hygric effect on heat storage and transport .....	20
2.1.3 Hygro-thermal analysis using simulation software (WUFI) ..	22
2.1.3.1 Numerical calculation model .....	23
2.1.3.2 Schematic diagram of the numerical calculation method ..	24
2.1.3.3 Accuracy of the numerical solution .....	25
2.1.4 Hygro-thermal simulation (WUFI) inputs and settings .....	26
2.1.4.1 Assembly and monitoring positions.....	26
2.1.4.2 Orientation, inclination, and building component position	27
2.1.4.3 Surface transfer conditions.....	28
2.1.4.4 Climate and initial conditions .....	30
2.1.4.5 Calculation period and options .....	33
2.1.5 Hygro-thermal properties in building materials.....	34
2.1.5.1 Basics values .....	34
2.1.5.2 Hygro-thermal functions .....	37
2.1.6 Validation of hygro-thermal simulation model.....	40
2.2 Method .....	41

2.2.1	Overview.....	41
2.2.2	Building case study and monitoring positions .....	41
2.2.3	Hygro-thermal simulation (1D) .....	43
2.2.3.1	Simulation software (1D).....	43
2.2.3.2	Geometry modelling .....	44
2.2.3.3	Simulation inputs and settings .....	44
2.2.3.3	Hygro-thermal simulation outcomes.....	46
2.2.4	Simulation scenarios .....	47
2.2.5	Evaluation criteria.....	49
2.3	Results and discussion .....	50
2.3.1	Results.....	50
2.3.2	Conclusion .....	53
<b>Chapter 3</b> Sensitivity Analysis of hygro-thermal simulation models of a historical building in tropical climate .....		54
3.1	Background.....	54
3.1.1	Tropical climate (Thailand) .....	54
3.1.2	Sensitivity analysis.....	57
3.1.3	Meteonorm software for generating Thai weather file .....	59
3.2	Method.....	60
3.2.1	Overview.....	60
3.2.2	Building case study .....	60
3.2.3	Hygro-thermal simulation (1D) .....	64
3.2.3.1	Geometry modelling .....	64
3.2.3.2	Simulation inputs and settings .....	66
3.2.3.3	Hygro-thermal simulation outcomes.....	68
3.2.4	Evaluation criteria.....	68
3.3	Results and discussion .....	71
3.3.1	Results.....	71
3.3.2	Conclusion .....	78
<b>Chapter 4</b> Hygro-thermal analysis of a historical building in tropical climate and the presence of moisture problems.....		79
4.1	Background.....	79
4.1.1	Efflorescence: A Moisture-Related Deterioration in Masonry Construction.....	79
4.1.2	Building defects and diagnosis .....	81
4.1.3	Capillary rise in historical wall .....	82
4.1.4	Thai historical wall and foundation construction.....	86
4.2	Method.....	91

4.2.1	Overview.....	91
4.2.2	Building case study.....	92
4.2.3	Hygro-thermal simulation (2D) .....	96
4.2.3.1	Geometry modelling .....	96
4.2.3.2	Simulation inputs and settings .....	97
4.2.3.3	Hygro-thermal simulation outcomes.....	100
4.2.4	Evaluation criteria.....	100
4.3	Results and discussion .....	102
4.3.1	Results.....	102
4.3.1.1	The visual inspection of moisture problems .....	102
4.3.1.1	Simulation outputs .....	106
4.3.2	Conclusion .....	109
<b>Chapter 5</b>	<b>Evaluation of historical building retrofit options.....</b>	<b>110</b>
5.1	Background.....	110
5.1.1	Intervention Methods against rising damp: Wall cutting or insertion of impermeable layer method .....	110
5.2	Method.....	119
5.2.1	Overview.....	119
5.2.2	Retrofit options for the case-study building.....	120
5.2.3	Hygro-thermal simulation (2D) .....	121
5.2.3.1	Geometry modelling .....	121
5.2.3.2	Simulation inputs and settings .....	122
5.2.3.3	Hygro-thermal simulation outcomes.....	124
5.2.4	Evaluation criteria.....	124
5.3	Results and discussion .....	125
5.3.1	Results.....	125
5.3.2	Conclusion .....	129
<b>Chapter 6</b>	<b>Conclusion .....</b>	<b>130</b>
6.1	Contributions .....	130
6.2	Future research.....	132
	References.....	134
	List of Figures.....	143
	List of Tables .....	147
	Curriculum vitae .....	149

## Chapter 1

# Introduction

### 1.1 Motivation

The presence of water in historical brick walls is one of the most prominent problems affecting architectural heritage. The accumulation of water in the wall is caused by different sources, including air humidity, condensation of water vapor in the air, precipitation, and capillary rise of water from the ground in both liquid and vapor phase (supplied by agricultural irrigation, poor drainage, rainfall, or underground water currents). Capillary rise of ground water through masonry brick wall is the most widespread phenomenon leading to moisture presence in historical buildings. It can cause various moisture-related problems such as building component decay, structural failure, degradation of materials, and mold growth (Ibrahim et al. 2014) which can lead to indoor air quality problems.

Whereas related studies have been conducted in different locations, less attention has been paid to this problem in hot-humid climates, even though there exist considerable moisture-related problems in historical buildings in these areas. Tropical or hot-humid climate contains enormous amounts of moisture in the air as vapor and plenty of precipitation as rain water, which both can accumulate in the building components and later cause moisture-related problems.

The selected historical building in this study serves as Thai religious historical buildings, which were constructed with traditional techniques of the respective era (Bunjerdskul 2014). Given their importance to the country and surrounding community, historical buildings must be maintained and renovated by using effective methods. However, related reliable studies about retrofit options are rare.

To address the moisture presence and find suitable refurbishment options in historical masonry, numerical hygro-thermal performance simulation tools can be useful (see, for example, Holm and Künzle 2003, Torres and Freitas 2007). In this context, this dissertation presents the results of the hygro-thermal analysis of historical building walls in hot-humid climate (Bangkok, Thailand). Moisture-related problems are studied using a state-of-the-art numerical simulation tool. Furthermore, retrofit options for these historical instances are considered and examined.

## 1.2 Background

Because of various harmful consequences of excessive moisture concentration, it is important to keep water out of building components or to lower their water content to a point where its deleterious effect is minimized (Künzel 1995). Moisture can affect a building component in both liquid form, as rain or rising damp, and vapor form as water vapor condensing on the surface or inside the component (Künzel 1995). Figure 1.1 schematically shows the main mechanisms which contribute to moisture entering the building components.

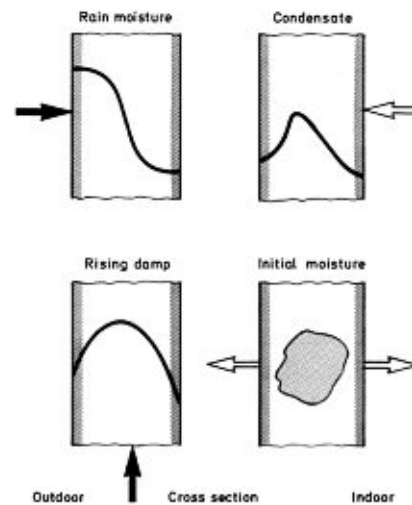


Figure 1.1 Schematic diagrams showing the effect and distribution of moisture inside and outside wall (source: Künzel 1995)

Capillary rise of ground water through building components is a well-known phenomenon leading to moisture presence in historical buildings. The phenomenon of rising damp is more recurrent in the ancient than the modern-day constructions, due to the facts that the old buildings commonly have masonry brick foundations without damp-proofing procedures (EMERISDA 2014). Moreover, they have been affected by the source of incoming water over longer periods of time.

Water capillary rise is especially relevant in case of porous building materials, such as bricks, stones, and mortar, given their wettability in presence of water. However, water rise height will reach a static level referred to as equilibrium line (Franzoni 2014). A balance between water uptake from capillary rise and water loss from evaporation leads to a dynamic equilibrium (Guimaraes et al. 2012a, Franzoni 2014, Falchi et al. 2018).

Historical buildings frequently experience physical impairment, owing to dampness. If maintenance is neglected or is done improperly for related problems, damages will become more serious due to obsolescence of materials from climate and environment (Halim et al. 2012). Especially in a hot-humid

climate, the environment contains more moisture such as high-humidity air and a high rate of rainfall. Historical buildings in Thailand, such as those studied in this dissertation, are commonly constructed with a load bearing masonry construction using solid clay brick (Jungsiriarrak 1997, Issarathumnoon 2018), which has a direct contact to moisture under the ground. Given their construction, underground water can easily spread through the whole building components.

For decades, finding appropriate solutions for the refurbishment of the affected historical building façade has been a challenge. For instance, the rising damp problem has been treated via a variety of methods such as mechanical interruption, chemical interruption (i.e., injection with pressure) and electro kinetic methods (i.e., electro-osmosis) (EMERISDA 2014). Mechanical intervention method, consisting of the insertion of a water impermeable layer or wall cutting (Sandrolini and Franzoni 2007), is considered to be amongst the more effective measures to stop the migration of capillary water from the ground. The cut is executed by means of different technologies. A wide range of materials can be used for the sheets, such as steel or lead plates, bitumen-based membranes, polyethylene or polyester-based, or PVC membranes (Freitas and Torres 2003, EMERISDA 2014).

For the analysis of the moisture situation and the selection of potential retrofit solutions, numeric simulation tools can provide useful support to study hygro-thermal performance of building components. Several numerical tools are quoted in various publications for prediction of combined heat, air, and moisture transport in building envelopes (see, for example, Othmen et al. 2014, Mundt-Petersen and Harderup 2013, Mundt-Petersen 2012, Künzel 1995, Mendes et al. 2002, Qinru et al. 2009, Woloszyn and Rode 2008). In this study, a commercially available hygro-thermal simulation application has been used as the main calculation tool. This tool can simulate the transient heat and moisture transport to analyze cases of rising damp from ground water.

### 1.3 Structure of work

This dissertation consists of the following six chapters:

- Chapter 1 discusses the motivation for and the background of the dissertation. The structure of work in this dissertation is also presented.
- Chapter 2 presents a literature review as well as a summary of the background information regarding moisture occurrence in building materials. Additionally, a description of a hygro-thermal prediction tool is provided. In evaluating its predictive potency and its suitability for hygro-thermal analysis of other existing buildings, the simulation outcomes, specifically relative humidity and temperature, were compared with measure data at four different positions along the layers of the wall construction of a historical building at TU Wien in Austria. The various input settings were also adjusted and investigated for their influence on the simulation results.
- Chapter 3 further investigates the degree of sensitivity of hygro-thermal analysis with respect to the choice of model input data. Reliable

knowledge especially of material properties and material-related parameters is essential to generating dependable simulation models. In order to identify a subset of input variables with significant influence on the simulation results, the wall construction of a historical building located in a hot-humid climate in Thailand (Thai temple wall) is subjected to a sensitivity analysis.

- Chapter 4 proposes the integrated application of on-site visual inspection and the hygro-thermal prediction tool as a method for investigating the mechanisms of rising dampness as well as examining the causes of moisture-related deteriorations. A historical church with severe moisture-related deteriorations located in Thailand serves as a case study in this chapter. Wall conditions affected by capillary moisture rise undergo a preliminary assessment by means of visual inspection. A hygro-thermal analysis is then conducted in two-dimensional numeric simulation using actual dimensions of the interior and exterior wall constructions facing four different cardinal directions.

- Chapter 5 presents a review of retrofit options used to treat historical buildings affected by rising damp. In particular, a mechanical intervention method known commonly as wall cutting is considered for its potential as an effective measure in preventing the migration of groundwater via capillary action. The historical church, which serves as a case study in Chapter 4, also serves as a case study in this chapter. The evaluation of the post-retrofit hygro-thermal performance results is then compared to that of the pre-retrofit results.

- The final chapter 6 entails the conclusions and suggestions regarding future research.

## Chapter 2

# Predictive performance of hygro-thermal simulation models

## 2.1 Background

### 2.1.1 Moisture in building materials

The presence of water in building materials is known as one of the most prominent problems affecting not only building component surfaces but also building structures. Three states of water, included solid state (ice), liquid state, and gaseous state (water vapor), can exist in building materials, specifically, porous ones, such as brick, stone, and mortar. There are various sources of moisture in building materials (Hagentoft 2001). Humidity in the air as water vapor, from both indoor and outdoor, can cause moisture accumulation in building materials. Various construction materials already contain a large amount of moisture at their initial state before the building is constructed (Hagentoft 2001). Precipitation is also one of the sources of moisture in building materials occurring in different forms, such as rain, snow, and hail (Bakri and Mydin 2014). Moreover, water leakage, for example from bursting pipes, and moisture from the ground in both liquid and vapor form, can also result in severe moisture problems (Hagentoft 2001, Bakri and Mydin 2014).

To ensure accurate and reliable results from any given hygro-thermal analysis of building components, a basic understanding of moisture is required. The occurrence of moisture can be described in terms of its capacity to be stored as well as its ability to transport from one point to another. In particular, proper simulation settings can be adjusted accordingly to minimize any potential errors and misinterpretations of the data. Moisture storage ability and moisture transport mechanism will be discussed in the following section.

#### 2.1.1.1 Moisture storage

Künzel (1995) contends that “a building material is called dry when it contains no water or only chemically bonded water”

(p.6). According to DIN-standard 52620 (DIN 1991) stated by Künzle (1995) “this state is reached by drying the material to constant weight” (p.6). There are two categories regarding the ability of porous building materials to store and transport moisture: (1) hygroscopic material, and (2) non-hygroscopic material. Non-hygroscopic building materials will remain dry when it has contact with moisture in the air. While hygroscopic building materials will capture and localize water molecules at the inner surfaces of their pore walls until a water content at equilibrium with the humidity of the surrounding air is reached (Künzel 1995). The moisture content of the material will be given at an equilibrium state for each given relative humidity (Hagentoft 2001). Figure 2.1a presents a unit of porous material that stays in an environment containing air with water vapor of a certain temperature and relative humidity. The pore structure of a porous building material (i.e., cellular concrete) is illustrated in Figure 2.1b. In terms of the interaction of porous building material with liquid water, some materials absorb water through capillary forces, while others contain molecules that repel water, regarded as hydrophobic (Künzel 1995, Biology dictionary 2020).

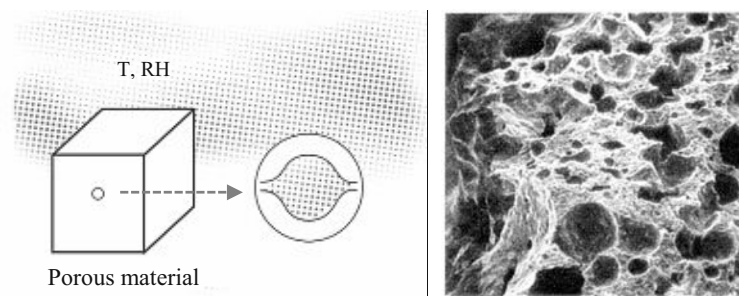


Figure 2.1 (a) A material surrounded by humid air with a part of the pore structure absorbing moisture (source: Hagentoft 2001), and (b) a scanning electron micrograph of cellular concrete with 22x magnification, showing its pore structure (source: Künzel 1995)

Theoretically, at a very high relative humidity level, close to saturation, a building material can take moisture until all its pores are filled with water (Künzel 1995). In order to perform a hygro-thermal analysis of building components, it is important to understand the connection between the water content of building material and the ambient conditions. The moisture storage function describes the moisture storage capacity of a building material as a function of water content in relation to the relevant climatic parameter, namely the relative humidity (Künzel 1995). The moisture storage function is also one of the main input parameters in order to perform a numeric hygro-thermal calculation, which will be mentioned also in section 2.1.6 (Hygro-thermal properties in building materials). According to Künzel

(1995), “[there are] three moisture regions which may occur in building materials due to increasingly intensive moisture conditions.” (p.6). The three moisture regions comprise region: A; B; and C (see Figure 2.3).

Region A is named as the sorption moisture or hygroscopic region. This is a region covered from the dry state of material to moisture of around 95% relative humidity mentioned by Künzle (1995), and around 98% relative humidity mentioned by Hagentoft (2001). This region can be described by sorption isotherms (Künzel 1995) (see Figure 2.2).

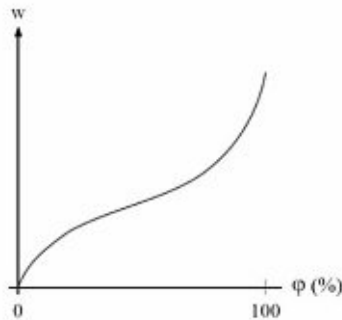


Figure 2.2 Sorption isotherm (source: Hagentoft 2001)

Region B is the capillary water region. It is the region that occurs after the sorption moisture region until it reaches the moisture level at 100% relative humidity. The upper limit for this region can be called capillary saturation ( $W_{cap}$ ) (Künzel 1995, Hagentoft 2001), or free water saturation ( $W_f$ ) (WUFI 2020b). This condition will occur when a material is in contact with liquid water and a considerable amount of water is taken up by material pores (Hagentoft 2001).

Region C is called the supersaturated region. This region cannot be reached by normal suction. Practically, this region occurs either when the conditions in the laboratory are set under high pressure for the suction, or when the diffusion is driven by thermal gradient (Künzel 1995, WUFI-Wiki 2020a). Region C is positioned above the free water saturation and ranges to the complete filling of all cavities by liquid water, called maximum water saturation ( $W_{max}$ ). The maximum water saturation can represent the porosity of the material (WUFI 2020b).

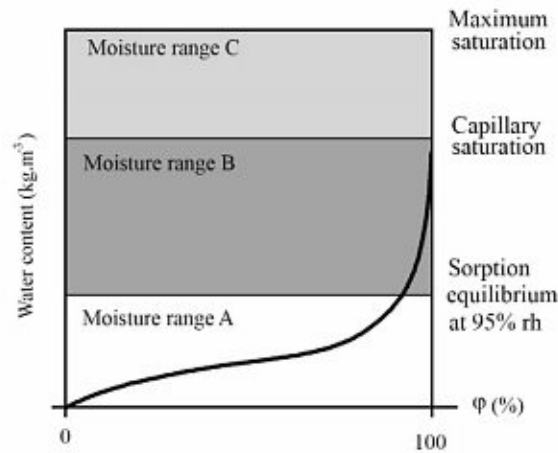


Figure 2.3 Schematic diagram of the moisture storage function of a hygroscopic capillary-active building material (source: Künzle 1995)

In hygroscopic, capillary-active building materials, for example, mortar, bricks, and stones, the three regions categorizing the moisture storage behavior exist as shown in Figure 2.3. In non-hygroscopic, non-capillary-active materials, for instance, wetted insulation materials (e.g., fiberglass, mineral wool), only region C occurs. This indicates that liquid water can be found in these materials only in the condition under dew point which leads to water vapor condensation (Künzel 1995). In a particular situation that hygroscopic, capillary-active building materials such as mortar or building stones are made to be water-resistant (hydrophobic) by a water repellent agent, a direct transition from region A to region C can occur. These materials (e.g., water-resistant brick or mortar) are still hygroscopic, but no longer capillary-active (Künzel 1995).

### 2.1.1.2 Moisture transport mechanisms

This dissertation focuses on the transient heat and moisture transfer calculation as the main method for analyzing the hygro-thermal performance of the historical building façades. Moisture transport mechanisms relevant to calculation, including water vapor diffusion and liquid transport through capillary forces, will be discussed in this section.

The water vapor diffusion will be discussed as the first moisture transport mechanism. According to Künzle (1995), “the kinetic gas theory describes the diffusion of molecules in multi-component gas mixtures by means of equations which basically contain three diffusion potentials, the mass fraction, the temperature and the total pressure” (p.14). Fick’s diffusion law is often used to explain the vapor diffusion phenomenon caused by differences in the mass fraction (Künzel 1995). In case of vapor

diffusion in building components, the thermodiffusion due to temperature gradient is commonly negligible (Künzel 1995).

Regarding porous building materials, only in large pores vapor diffusion can be comparable to the vapor diffusion in the air. With ambient pressure, Fick's diffusion predominates in pore with a radius which is larger than  $10^{-6}$  m (Künzel 1995). In smaller pores, the collision between vapor molecules and pore walls, known as effusion transport, happens more often compared to the collision between vapor molecules themselves (Künzel 1995). The vapor pressure is the driving gradient for both circumstances, Fick's diffusion and effusion (Künzel 1995).

According to Hagentoft (2001), the vapor diffusion in a porous material (see Figure 2.4) can be explained by the following equation:

$$g = \delta v \frac{v_1 - v_2}{d} \quad (\text{Eq. 2.1})$$

Here,  $d$  is the width of the material layer and  $g$  is steady-state diffusive flux ( $\text{kg}\cdot\text{m}^{-2}\cdot\text{s}^{-1}$ ). The humidity by volume ( $v$ ) is kept at  $v_1$  at one side of the layer and at  $v_2$  on the other side.  $\delta v$  ( $\text{m}^2\cdot\text{s}^{-1}$ ) is the vapor permeability of the material. Fick's law, for water vapor diffusion through a material can be stated as follows (Hagentoft 2001):

$$g = -\delta v \frac{dv}{dx} \quad (\text{Eq. 2.2})$$

Since the rate of diffusion (the vapor permeability of the material;  $\delta v$ ;  $\text{m}^2\cdot\text{s}^{-1}$ ) can be compared with the one obtained in stagnant air ( $D$ ), the following ratio applies:

$$\mu = \frac{D}{\delta v} \quad (\text{Eq. 2.3})$$

Here,  $\mu$  is water vapor diffusion resistance factor (-), and  $D$  is the diffusivity of water vapor in air ( $25\cdot 10^{-6} \text{m}^2\cdot\text{s}^{-1}$  at  $20^\circ\text{C}$ ).

As mentioned above, the water vapor transport through porous materials can be identified and applied for the hygro-thermal calculation, by introducing a water vapor diffusion resistance factor ( $\mu$ ) which is a specific property for each building material. A more detailed explanation can be found in section 2.1.6

(Hygro-thermal properties in building materials). The equation can be written as follows (Hagentoft 2001):

$$g = - \frac{D}{\mu} \frac{dv}{dx} \quad (\text{Eq. 2.4})$$

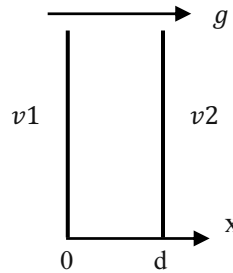


Figure 2.4 Diffusion of water vapor through a porous material layer (source: Hagentoft 2001)

Another moisture transport mechanism which is relevant to the hygrothermal calculation is liquid transport through capillary forces, known as “capillary conduction” or “capillary suction”. Only capillary conduction at water contents above the critical moisture content (Künzel 1995) is mentioned in this discussion. In cases of capillary-active building materials, the critical moisture content represents the moisture condition at the last point before capillary conduction starts (Künzel 1995). However, in micro-capillary pores, capillary conduction already happens in the circumstance which is significantly below the critical moisture content (Künzel 1995). In the pore system of building materials, depending on the pore’s size, vapor transport occurs in the form of effusion or Fick’s diffusion, while capillary conduction and surface diffusion also occur simultaneously in liquid transport (Künzel 1995).

Concerning the Hagen-Poiseuille law, capillary conduction is explained by a formula which is used for calculating a capillary conduction in a cylindrical capillary (Künzel 1995). On the other hand, Künzel (1995) states that “capillary suction is clearly a “flow”, the diffusion equation used by many authors,” (p.17). According to WUFI (2020b), “although it is basically a convective phenomenon, in the context of building physics it is sufficiently accurate to regard the liquid transport in the pore spaces as a diffusion phenomenon” (topic 15, paragraph 1). Based on these arguments, it can be concluded that liquid transport through capillary forces can be identified by the diffusion equation in the hygro-thermal calculation. The capillary conduction, defined by the diffusion phenomena, is explained by the formula below:

$$g = -D(w) \nabla w \quad (\text{Eq. 2.5})$$

Here,  $g$  is liquid flux density ( $\text{kg}\cdot\text{m}^{-2}\cdot\text{s}^{-1}$ ),  $w$  is water content ( $\text{kg}\cdot\text{m}^{-3}$ ), and  $D$  is capillary transport coefficient ( $\text{m}^2\cdot\text{s}^{-1}$ ). Since the capillary transport coefficient strongly depends on the water content, it can lead to a good approximation of suction process under certain conditions (Künzel 1995).

Due to the fact that there are two phases of water (i.e., vapor and liquid phases) contained in porous building materials, the moisture is also transported in both phases. Subsequently, the moisture transport mechanism when diffusion and capillary suction occur combined or simultaneously must be discussed in order to have a clearer understanding of the moisture transport phenomenon in building components.

According to Hagentoft (2001), the transportation of both liquid water and water vapor can be described by means of a schematic diagram of moisture flow through a chain of material pores in Figure 2.5. In completely dry pores (see figure 2.5a), the moisture is transported only by vapor diffusion, while capillary suction fully dominates when the pore system is totally filled with liquid water (see figure 2.5b). In the case shown in Figure 2.5c and Figure 2.6, there is a mixture of two mechanisms: (1) diffusion in the open part of the system; and (2) capillary suction in the systems filled with liquid water. At the same time, surface migration, known as surface diffusion (Künzel 1995), of the absorbed water at the pore walls can also occur (Figure 2.5d).

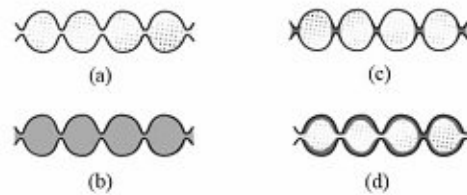


Figure 2.5 Chain of pores inside the material  
(source: Hagentoft 2001)

Under conditions in which relative humidity is relatively low or is not high enough to start the water vapor condensation process, the diffusion of water vapor is greater than the capillary suction of liquid water in pores. On the other hand, when relative humidity rises and condensation starts to occur, the water vapor diffusion process becomes slower and in turn, the capillary suction of liquid water is much more rapid (Hagentoft 2001). The transportation rate of both vapor and liquid water can be increased by water evaporation at the end of the chain pores at the material surfaces (Hagentoft 2001) (see Figure 2.6a).

Regarding the situation when the relative humidity of the material becomes higher than the status of pure water vapor but not as high as above a critical moisture content (the end of the water vapor state before capillary conduction starts), surface diffusion occurs in the pore systems. At that point, the water vapor molecule starts to adsorb at the pore walls, and are subsequently formed as layers on the pore surfaces and start to migrate (Künzel 1995). The adsorbed water vapor molecules at the pore walls or a film is transported from areas with thicker films towards thinner films. These will become thicker when relative humidity increases (WUFI 2020b). According to Künzel (1995), “in contrast to capillary conduction, which normally is observed only at water contents above the critical moisture, surface diffusion in paper products begins to be noticed already at 30% relative humidity and in sandstone at about 60% relative humidity” (p.16). As mentioned above by Künzel (1995), surface diffusion mechanism begins from different levels of relative humidity depending on the type and the size of the material’s pore structure.

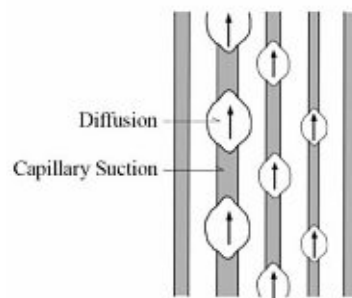


Figure 2.6 Transport of water in a partially filled pore system  
(source: Hagentoft 2001)

### 2.1.2 Hygric effect on heat storage and transport

Thermal conduction and specific heat of melting and evaporation are some of the principles of calculating the thermal behavior of building components in dry conditions (Künzel 1995). However, there are other conditions that these parameters significantly depend on moisture presence in building materials. In order to gain a better understanding of heat and moisture transfer mechanisms and relevant hygro-thermal properties of building materials, a brief discussion is provided.

In physics, a type of thermodynamic process under the condition that the pressure of the system stays constant is called an isobaric process (Lyu 2017). Under the isobaric condition, the heat content of a material is known as the enthalpy (Künzel 1995). There is an approximately linear relationship between material temperature and its enthalpy, in the range of temperature which is of concern in building physics. In the case of material with moisture, the enthalpy of the water contained in the

material has to be included in the enthalpy of material (Künzel 1995). However, it is difficult to define the enthalpy of the water contained in the material since it depends on the existing physical states of water which are hard to exactly defined in the material pores (Künzel 1995).

According to the thermal conduction in moist building materials, it describes only the influence of thermal conduction of localized water on heat transport (Künzel 1995, WUFI-Wiki 2020a). According to Künzel (1995), the moisture-dependent thermal conductivity ( $\lambda$ ;  $\text{W}\cdot\text{m}^{-1}\text{K}^{-1}$ ) of the mineral building materials (e.g., concrete, limestone) can be calculated by the following equation:

$$\lambda(w) = \lambda_0 (1 + b \cdot w / \rho_s) \quad (\text{Eq. 2.6})$$

Here,  $\lambda(w)$  is the thermal conductivity of moist building material ( $\text{W}\cdot\text{m}^{-1}\text{K}^{-1}$ ),  $\lambda_0$  is the thermal conductivity of dry building material ( $\text{W}\cdot\text{m}^{-1}\text{K}^{-1}$ ),  $\rho_s$  is bulk density of dry building material ( $\text{kg}\cdot\text{m}^{-3}$ ), and  $b$  is thermal conductivity supplement ( $\%$ . ( $\text{M}\cdot\%$ ) $^{-1}$ ). The thermal conductivity supplement ( $b$ ) provides the fractional increase (in  $\%$ ) of the heat conductivity per moisture content (in mass  $\%$ ) (WUFI-Wiki 2020a). The thermal conductivity supplement ( $b$ ) of some building materials are presented in Table 2.1 (Künzel 1995). These  $b$  values can be applied for the purpose of estimating moisture-dependent thermal conductivity function for the hygrothermal calculation.

Table 2.1 Thermal conductivity supplement ( $b$ ) of building materials (Künzel 1995)

Material	Bulk Density ( $\text{W}\cdot\text{m}^{-3}$ )	$\lambda$ ( $\text{W}\cdot\text{m}^{-1}\text{K}^{-1}$ )	$b$ ( $\%$ . ( $\text{M}\cdot\%$ ) $^{-1}$ )
lime silica brick	1800	0.7	8
cellular concrete	400-800	0.09-0.19	4
normal concrete	2300	1.3-1.5	8
wood	400-700	0.08-0.15	1.5

Since water vapor diffusion with phase change (i.e., evaporation and condensation of water) also contributes to heat transport, they cannot be identified in practical terms in accordance with the thermal conduction equation (Künzel 1995, WUFI-Wiki 2020a). Künzel (1995) states that “enthalpy flows as the result of liquid transport play a negligible role in comparison with other thermal flows, while vapor diffusion flows connected with phase changes, such as drying processes, can be of great importance in terms of the heat balance” (p.28). Hence, a separate term in the transport equation allows for the phase change mechanism in water vapor diffusion (WUFI-Wiki 2020a).

### 2.1.3 Hygro-thermal analysis using simulation software (WUFI)

Hygro-thermal analysis investigates the intrinsic transfer of heat and moisture flow through building components (such as walls, floors, and roofs), as well as, the ability of building components to store heat and moisture (WUFI 2020a). For decades, hygro-thermal calculation has been known as an iterative process to simulate the performance of building assemblies in order to evaluate the future durability and risk associated with different assembly designs or environmental conditions (Holm and Künzle 2003, Franzoni 2018).

In order to perform hygro-thermal analysis on historical building façade and finding potential retrofit strategies, numerical simulation tools can provide useful support (see, for example, Othmen et al. 2014, Mundt-Petersen and Harderup 2013). The hygro-thermal simulation software applied in this dissertation is WUFI, which is an acronym for “Wärme und Feuchte instationär” in German with the direct translation of “heat and moisture transiency” in English (WUFI 2020a). WUFI software has been developed by the Fraunhofer Institute for Building Physics (IBP). It complies with the requirements of BS EN 15026:2007 (BSI 2007).

There are two versions applied in this study, included: (1) WUFI Pro 5.3 (one-dimensional simulation), and (2) WUFI 2D-3.4 (two-dimensional simulation). According to Browne (2012) “their conformity within the tolerances set out in BS 15026 show that they are capable of good accuracy and WUFI is considered to be one of the most advanced of the commercially available programs, having been validated against full-scale field tests over many years” (p.20). WUFI (2020a) contends that “The software has been validated by detailed comparison with measurements obtained in the laboratory and on IBP’s outdoor testing field” (page 1<sup>st</sup>, paragraph 1). Based on these considerations, WUFI is assumed here to be a proper tool to study the hygro-thermal performance of building components. Moreover, many software validation reports are provided by, for example, Hägerstedt and Arfvidsson (2010), Mundt-Petersen and Harderup (2013), and Alev et al. (2014).

WUFI works based on the discretization of the Künzle model by means of an implicit finite volume scheme (Ibrahim et al. 2014). For the numerical solution, WUFI uses the finite volume technique for the spatial discretization of the transport equations, and the fully implicit scheme for the discretization in time (Künzle 1995, Ibrahim et al. 2014). Simulation provides hourly values of temperature, relative humidity, and water content (detailed explanation see section 2.2.3.3 Hygro-thermal simulation outcomes).

In the following sections, the numerical calculation model, the schematic diagram of the numerical calculation method, and the accuracy of the numerical solution are discussed.

### 2.1.3.1 Numerical calculation model

There have been numerous efforts to develop hygrothermal simulation models in order to obtain reliable results (Hens 1996). The following section will describe the hygro-thermal calculation model which forms the basis for the WUFI software. The dynamic coupled heat and moisture transfer processes in building components exhibited in this calculation model are described by the following respective heat and mass balance equations (Künzel 1995, Künzel 1998, Othmen et al. 2014, WUFI-Wiki 2020a):

$$\frac{\partial H}{\partial \vartheta} \frac{\partial \vartheta}{\partial t} = \frac{\partial}{\partial x} \left( \lambda \frac{\partial \vartheta}{\partial x} \right) + h_v \frac{\partial}{\partial x} \left( \frac{\delta}{\mu} \frac{\partial p}{\partial x} \right) \quad \text{Heat Transport} \quad (\text{Eq. 2.7})$$

$$\rho_w \frac{\partial u}{\partial \varphi} \frac{\partial \varphi}{\partial t} = \frac{\partial}{\partial x} \left( \rho_w D_w \frac{\partial u}{\partial \varphi} \frac{\partial \varphi}{\partial x} \right) + \frac{\partial}{\partial x} \left( \frac{\delta}{\mu} \frac{\partial p}{\partial x} \right) \quad \text{Moisture Transport} \quad (\text{Eq. 2.8})$$

in which:

$D_w$ [ $\text{m}^2 \cdot \text{s}^{-1}$ ]	is	Liquid transport coefficient
$H$ [ $\text{J} \cdot \text{m}^{-3}$ ]	is	Enthalpy of moist building material
$h_v$ [ $\text{J} \cdot \text{kg}^{-1}$ ]	is	Evaporation enthalpy of water
$p$ [ $\text{Pa}$ ]	is	Water vapor partial pressure
$u$ [ $\text{m}^3 \cdot \text{m}^{-3}$ ]	is	Water content
$\delta$ [ $\text{kg} \cdot \text{m}^{-1} \cdot \text{s}^{-1} \cdot \text{Pa}^{-1}$ ]	is	Water vapor diffusion coefficient in air
$\vartheta$ [ $^{\circ}\text{C}$ ]	is	Temperature
$\lambda$ [ $\text{W} \cdot \text{m}^{-1} \cdot \text{K}^{-1}$ ]	is	Heat conductivity of moist material
$\mu$ [-]	is	Vapor diffusion resistance factor of dry material
$\rho_w$ [ $\text{kg} \cdot \text{m}^{-3}$ ]	is	Density of water
$\varphi$ [-]	is	Relative humidity

The first equation expresses the heat transfer by a temperature gradient, and the second equation presents the moisture transfer due to relative humidity and water vapor pressure gradient (Künzel 1998, Othmen et al. 2014). The heat and moisture storage terms are presented on the left-handed side of both equations. On the right-hand side of both equations, the transport terms are found (WUFI-Wiki 2020a). Heat transport is the combination of moisture-dependent thermal conductivity and vapor enthalpy flow, while liquid transport occurs through surface diffusion and capillary conduction in which both are mainly influenced by a gradient of relative humidity (WUFI-Wiki 2020a, Künzel 1995).

### 2.1.3.2 Schematic diagram of the numerical calculation method

In order to explain the main steps in solving the coupled heat and moisture transport equations, the following flow chart can be helpful (see Figure 2.7) for both cases of one-dimensional and two-dimensional calculations. For the purpose of performing the transient heat and moisture transfer calculation, it is important to provide the set of input data as follows. A more detailed discussion of these input data set will be presented in section 2.1.4:

- The design of the building component to be calculated and the numerical grid of that model
- Material properties (both thermal and hygric), such as the bulk density, the porosity, moisture storage function, and liquid transportation coefficient.
- Climatic boundary conditions and initial calculation values included temperature, and relative humidity (or water content)
- Transitional conditions at the building component boundaries
- Simulation control parameter used for adjusting the calculation resolution and other calculation-specific parameters.

After the above-mentioned input sets of data are considered, the steady-state initial distributions of moisture and temperature is calculated. Alternatively, any initial states, such as distributions from measurements or other calculations can be entered. The transient calculation of the temperature and moisture fields is then established. According to Künzel (1995), “For every new time increment, the coupled heat and moisture transport equations are solved in alternation until the predetermined termination criterion is reached” (p. 44). It is maintained that the termination criterion has to be set before the calculation begins. All relative thermal storage and transport coefficients are updated before every iterative solution of the heat transfer equation. Similarly, before the solution of the moisture transport equation, the same process is applied to the calculation of the hygric coefficients (Künzel 1995). At the end of the calculation period, the software provides the simulation outputs of the required temperature and moisture field (heat and moisture flows) and the evaluation in time of these variables (e.g., water content, relative humidity, and temperature). Regarding further calculations, the moisture and temperature fields can serve as the initial conditions (Künzel 1995).

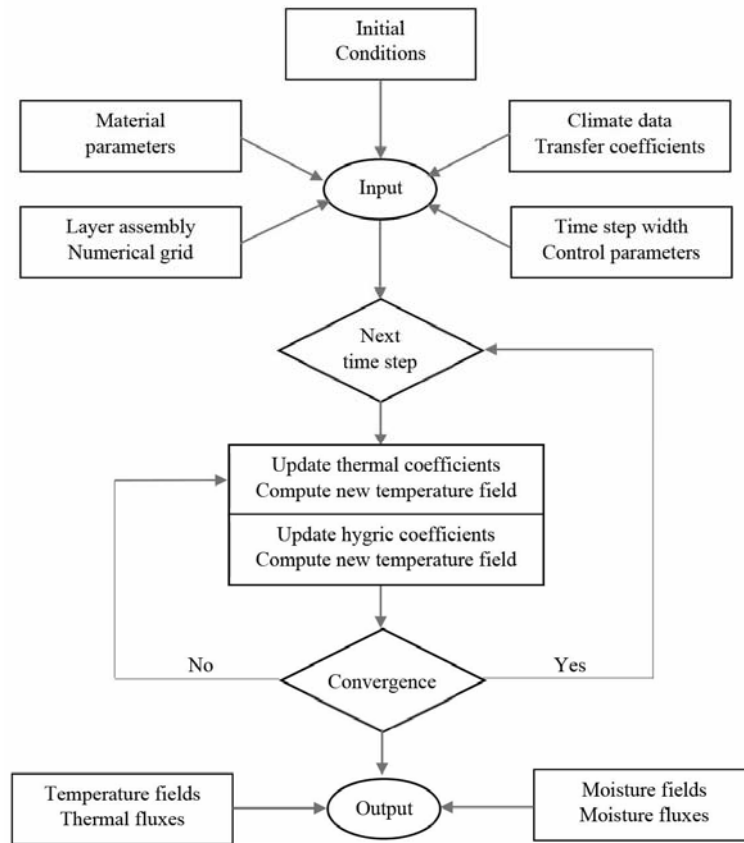


Figure 2.7 The flow chart for the WUFI model  
(source: WUFI-Wiki 2020a)

### 2.1.3.3 Accuracy of the numerical solution

The choice of termination criteria, the length of time increment, and the mesh sized of the numerical grid determine the accuracy of the numerical solution technique in WUFI (Künzel 1995, WUFI 2020b).

According to Künzel (1995), “to establish termination criteria for the numerical iteration, in most cases, it is sufficient when the maximum change of variables in the calculation area during two successive iteration steps falls below one-thousandth of one percent in relative humidity and one-thousandth of one degree centigrade in temperature” (p.45). The time structure of the boundary conditions (time intervals, such as hourly or monthly weather data) and the expected temperature and moisture transients in the building component influence the length of the time increments (Künzel 1995). For example, the time increment of one hour is sufficient when hourly climatic data are employed (Künzel 1995). The desired moisture and temperature field in the building component lead to the mesh sizes of the numerical grid definition (WUFI 2020b, Künzel 1995). In the simulation model area with a high range of moisture and temperature gradient, such as the area at the model layer boundaries, small mesh sizes (e.g., a

few millimeters) are required. On the other hand, the larger grid size is adequate, when the range of low moisture and temperature gradient is found at those material layers (Künzel 1995). Moreover, in case a lower level of resolution is acceptable, the grid distances can be several centimeters. Producing a numerical grid with variable mesh sizes is found to be useful in order to save storage capacity and computing time without losing accuracy (Künzel 1995). In addition, WUFI-Wiki (2020b) states that “usually the numerical solution is sufficiently accurate so that the effect of numerical parameters can be ignored in comparison with the effects of the physical parameters such as material and climate data” (paragraph 4). Based on this statement, it can be inferred that the physical input parameters such as material properties and climatological data require more detailed and careful attention before incorporated in the model.

### **2.1.4 Hygro-thermal simulation (WUFI) inputs and settings**

For building component simulations, there are five main input and setting categories (WUFI 2020d, WUFI 2020e): (1) assembly and monitoring positions; (2) orientation, inclination, and height; (3) surface transfer coefficients; (4) climate and initial conditions; and (5) calculation period and options.

#### **2.1.4.1 Assembly and monitoring positions**

As a first category, the determination of a graphical model of a part of the studied building component is required for creating the assembly of the component in the simulation software. Regarding the simulation of a one-dimensional version of WUFI (WUFI Pro 5), the layers of the studied component and the desired material properties are needed. Commonly, the left side of the model is defined as the exterior boundary, and the right side is defined as the interior boundary. Material properties can be assigned by using the WUFI material database (WUFI 2020d). A typical thickness of the material layer is automatically displayed for some materials, however, a manually defined option is also possible. In case of two-dimensional modeling, there is a drawing area to define the building construction in a graphical way as rectangular elements. While the model elements are being drawn, a graphic script is automatically created which can be later adjusted in order to modify the size and the position of the model (WUFI 2020e). In both versions, a numerical grid across the component is automatically generated simultaneously (WUFI 2020d, WUFI 2020e). The monitoring position is necessary to be provided only in the one-dimensional model simulation. The hygrothermal conditions (e.g., temperature and water content) at the concerned points can be assessed. For the 2D simulation, the

hygro-thermal conditions at each interest point can be selected after running the simulation.

#### 2.1.4.2 Orientation, inclination, and building component position

The second category is to define the orientation, inclination, and positioning (the height) of the building component. These definitions are related to the exterior boundary conditions which are read from the weather file. The orientation (the direction the building component is facing) is the compass direction comprising north (N), northeast (NE), east (E), southeast (SE), south (S), southwest (SW), west (W), and northwest (NW). The inclination is the angle at which the surface is tilted in relation to the horizontal. The inclination is used to calculate solar radiation and precipitation loads incident on the component surface, which can be chosen between 90° (vertical wall) and 0° (flat roof).

The positioning or the height of the building component influences the driving rain coefficients which are used to calculate the driving rain load on the building component. There are two calculation methods offered by WUFI (2020b, 2020c): (1) The driving rain coefficients R1 and R2; and (2) ASHRAE Standard 160P (ASHRAE 2006). For the first calculation method, the driving rain coefficients (i.e., R1 and R2) serve to calculate the driving rain load on a surface of arbitrary orientation and inclination. Moreover, the data on normal rain, wind velocity, and mean wind direction are employed in the calculation using the following relation:

$$\text{Driving rain load} = \text{rain} \cdot (R1 + R2 \cdot \text{wind velocity}) \quad (\text{Eq. 2.9})$$

Here, 'rain' denotes the rainfall intensity on a horizontal surface in mm/h (normal rain) and 'wind velocity' is the wind speed measured at the height of 10 m in an open area. The selected weather file provides the data on normal rain, wind velocity, and wind direction. The values of R1 and R2, as rain coefficients, are strongly dependent on the specific location of the concerned building component surface on the building facade. There are some predefined rain coefficients. In the case of a vertical surface, R1 is zero and R2 is 0.2 s.m<sup>-1</sup> at the surface conditions of free-standing locations without influence from surrounding buildings or a very top part of a high-rise building, defined by WUFI (2020b, 2020c) as an option referred to as “the building part which is higher than 20 m”.

Optionally, the driving rain load on a vertical wall can be estimated by means of ASHRAE Standard 160P method (ASHRAE 2006). This method provides the equation as follows:

$$\text{Driving rain load} = \text{rain} \cdot \text{FE} \cdot \text{FD} \cdot 0.2 \text{ s.m}^{-1} \cdot \text{wind velocity} \text{ (Eq. 2.10)}$$

Here, 'rain' denotes the rainfall intensity on a horizontal surface in  $\text{mm.h}^{-1}$  (normal rain) and 'wind velocity' is the wind speed measured at the height of 10 m in an open area. The selected weather file provides the data on normal rain, wind velocity, and wind direction. The rain exposure factor (FE), recommended by ASHRAE Standard 160P (ASHRAE 2006), depends on the surrounding terrain and the height of the building. In terms of the rain deposition factor (FD), it describes the influences of the building itself on the rain coefficient values. The FD estimated values are provided by ASHRAE Standard 160P (2006).

### 2.1.4.3 Surface transfer conditions

Thirdly, surface transfer conditions are another category of inputs and settings which is essentially defined for the simulation run. Theoretically, the building component surfaces are affected by the outdoor and indoor climate, for example, the outdoor temperature and the outdoor air relative humidity, except the underground condition. Right at the surface a boundary air layer exists and acts as an intermediary which represents a resistance for heat and moisture transport (WUFI-Wiki 2020a). The heat and moisture transport resistances are quantified by the respective surface transfer coefficients (see Table 2.2).

Ignoring the effects of convection and its flow patterns at the component surface, the average values for the exterior and interior heat transfer listed in Table 2.2. These are appropriate for most hygro-thermal simulation cases (Künzel 1995, WUFI-Wiki 2020a). Alternatively, the heat transfer resistance at the exterior component surface can be defined by employing a wind-dependent resistance. In the situation that the convective and the radiative heat flows go in the same direction at the component surface, long-wave radiation exchange is considered in the heat transfer coefficients (WUFI-Wiki 2020a). This is not valid if the temperature of the surface of a building component drops below the surrounding air temperature during the night due to radiative cooling (WUFI-Wiki 2020a).

Table 2.2 Average surface transfer coefficients for calculating the heat and moisture exchange between exterior or interior component surfaces and the environment (WUFI-Wiki 2020a)

<b>Component Surface</b>	<b>Heat transfer <math>\alpha</math> [W.m<sup>-2</sup>K<sup>-1</sup>]</b>	<b>Water Vapor Transfer <math>\beta_p</math> [kg.m<sup>-2</sup>s<sup>-1</sup>Pa<sup>-1</sup>]</b>
Exterior	17	75 x 10 <sup>-9</sup>
Interior	8	25 x 10 <sup>-9</sup>

In terms of defining the energy absorption factor, known as short-wave radiation absorptivity, the factor value depends on the surface color of the building component which accounts for the fact that the short-wave radiation incident on the component is partially converted into heat (Künzel 1995, WUFI-Wiki 2020a). WUFI (2020b) suggests that the values of short wave radiation absorptivity for bright surfaces (for white exterior rendering such as plasters or paint colors) should be around 0.4. For dark surfaces, such as painted wood and bituminous sheeting, the value should be between 0.6 and 0.8. A list of short-wave absorptivity and brightness reference value for various building material surfaces is given in Table 2.3.

Table 2.3 Short-wave absorptivity and brightness reference value of various building material surfaces (source: Künzel 1995)

<b>Building material</b>	<b>Short-wave absorptivity [-]</b>	<b>Brightness reference value [%]</b>
Roof tile, red-brown	0.6 0.8	20 10
Bituminous roof covering	0.9	10
Plaster, white (aged)	0.4	60
Klinker brick dark red	0.7	15
Lime silica brick, dry-wet	0.45 0.6	55 40
Schilf sandstone, dry-wet	0.7 0.85	30 15
Red Main sandstone	0.75	19
Sandstone with patina	0.9	10
Wood (spruce) untreated	0.4	50
Weathered (silver-gray)	0.7	20
Painted brown	0.8	10

Naturally, only some amount of the incident rainwater can stay at the component surface and be absorbed. As a result, a rain water absorption factor, known as the adhering fraction of rain in WUFI software (WUFI 2020b), may be applied for driving rain

calculation. The rain water absorption factor depends on the inclination of the component. Commonly, the case of a 90-degree vertical wall requires 0.7 as a value of the rain water absorption factor (WUFI-Wiki 2020a). However, if the component is not exposed to the rain at all, for example, the interior wall, the rain water absorption factor must not be provided (the rain water absorption factor is 0).

Moreover, when the building component surface is treated with a coating, such as paint coats, laminations, vapor retarders, and wallpapers, the coating will impede the water vapor diffusion ability of the surface. However, since the coating is applied as a very thin layer, it will not affect the thermal behavior of the building component (WUFI-Wiki 2020a). Instead of creating a new layer for the coating, WUFI (2020b) allows this resistance to be defined as the thickness of a stagnant air layer with the same diffusion resistance, which is known as vapor diffusion thickness (Sd-value). Nevertheless, apart from vapor diffusion resistance as requiring Sd-value, there is always some surface transfer resistance to the water vapor diffusion flow due to the existence of the boundary air layer at every wall surface (WUFI-Wiki 2020a).

#### 2.1.4.4 Climate and initial conditions

Fourthly, climate and initial conditions are very important to be assigned as simulation inputs and settings in order to gain reliable results. In every building component, through its surface, a component is undergoing hygro-thermal interaction with its surrounding (WUFI-Wiki 2020a). Building components and their surroundings influence each other, for example, by absorbing indoor air humidity or by releasing stored heat.

Principally, boundary conditions can be classified into three types: (1) the exterior ambient conditions above the ground, (2) the indoor conditions, and (3) the exterior conditions below the ground (WUFI-Wiki 2020a). Under all these three circumstances, different surface transfer conditions are employed due to the different heat and moisture exchange processes including diffusion, conduction, convection, and radiation (WUFI-Wiki 2020a). When performing a simulation with WUFI (2020d, 2020e), it is required to assign climate conditions on all surfaces of the building component model in two-dimensional cases and on two sides (i.e., left and right) in one-dimensional cases. In this dissertation, in order to perform the simulation in Chapter 3 and 4, the deployed software programs, WUFI pro 5.3 (1-D) and WUFI 2D 3.4 (2-D), contain climate files from many places around the world except Southeast Asia (Thailand), therefore synthetic data had to be generated in an external program. Moreover, since the prediction of the hygro-thermal performance of brick wall constructions in the existing building in TU Vienna is carried out in this chapter, the weather file had to be created following the in-

situ monitored data by using also a weather data generator. Among various sources of international climate data, Meteororm software (Meteororm 2020), the so-call weather data generator, is one of the easily accessible sources (Browne 2012). It will be introduced in Chapter 3. The obtained climate files from the software consist of hourly weather data in one year in which is repeatedly deployed in the course of a multi-year simulation.

With respect to the exterior climate conditions, there are mainly four factors acting on the building component surface, included air temperature, relative humidity, solar radiation, and precipitation. The solar radiation and precipitation loads depend on the inclination and orientation of building components which mostly are walls (Künzel 1995, WUFI-Wiki 2020a). Both the radiation and precipitation loads have to be computed accordingly for the specific component. Künzel (1995) contends that “the solar radiation vertical to the building component surface can be calculated from direct (or global) and diffuse solar radiation to a horizontal surface” (p.32). Regarding the estimation of precipitation loads, wind speed and wind direction are given for driving rain calculation. Alternatively, the exposition of the building to wind flow (rain exposure factor; FE) and local wind flow patterns (rain deposition factor; FD) can be employed to determine driving rain in compliance with ASHRAE Standard 160 (ASHRAE 2006). Without the driving rain calculation, the driving rain measurement throughout the calculation period directly on the component surface is required (Künzel 1995). In the circumstance with the horizontal component surface, the normal rain data acquired from the weather station can be used directly (Künzel 1995). For hygro-thermal simulations, hourly climate data (e.g., temperature, humidity, radiation) have been shown to be sufficient (WUFI-Wiki 2020a).

Concerning the interior climate conditions, DIN 4108-3 (2001) specifies interior climate conditions for the dew point period (20°C, 50% RH) and for the evaporation period (12°C, 70% RH) for the general assessment of diffusion processes in building components. However, these boundaries conditions are not suited for simulations that span over a year (WUFI-Wiki 2020a). According to Künzel (1997) explained by WUFI-Wiki (2020a), regarding measurements in residential buildings, the results exhibit that the monthly indoor moisture load (i.e., the difference between the moisture contents of the indoor and the outdoor air) decreases almost linearly related to the outdoor temperature. This circumstance results from the building occupants' activity by keeping the windows open more frequently during the warmer seasons. Moreover, the airtightness of the building envelope also affects indoor moisture value (WUFI-Wiki 2020a). Based on these considerations, it can be concluded that constant indoor climate input for each period per year (e.g., the dew point period and the evaporation period) is found not to be

sufficient since there are various factors influencing the indoor condition.

In order to perform a hygro-thermal simulation with a reliable indoor condition, WUFI (2020b) provides four options for creating a suitable condition for each specific case as follows:

Option (1) Sine curves – As a simplified option, the mean indoor air temperature and relative humidity can be defined manually to create predefined curves as Sine curves. The amplitude can also be set to represent the deviation from the mean values during summer or winter conditions.

Option (2) EN 13788 (ISO 2001) – The indoor air temperature can be manually set and it will remain constant through the simulation run period. In terms of relative humidity value setting, humidity class can be also selected from four different classes depending on moisture loads in a minus-degree outdoor temperature period (wintertime).

Option (3) EN 15026 (BSI 2007) – The indoor air temperature remains constant at 20 °C during the heating season (when the outdoor air temperature is below 10 °C), and at 25 °C during the cooling season (when the outdoor air temperature is greater than 20 °C onwards). Moreover, BS 15026 (BSI 2007) provides the algorithm using in the condition when the outdoor temperature is varying between 10 °C and 20 °C. The indoor relative humidity is derived from the outdoor temperature also using the algorithm in BS 15026 (BSI 2007), by selecting moisture load options between normal and high.

Option (4) ASHRAE 160P (ASHRAE 2006) – During the summertime, the indoor air temperature is derived from the outdoor climate file using the algorithm defined in ASHRAE 160P (Browne 2012, ASHRAE 2006). During the wintertime, the software provides options to set the indoor air temperature, as a set point for the building heating system and a floating temperature shift. The indoor relative humidity can be calculated by defining occupancy numbers, building volume, and the number of air changes per hour at normal pressure.

Under the hygro-thermal conditions below ground, the temperature typically remains constant. At the depth of around 1.00 m from the ground level, the temperature of underground soils has already eliminated the influence of daily temperature variations (WUFI-Wiki 2020a) (see Figure 2.8). The underground conditions usually have relative humidity at around 99%-100%, especially in the areas with presences of plants (WUFI-Wiki 2020a).

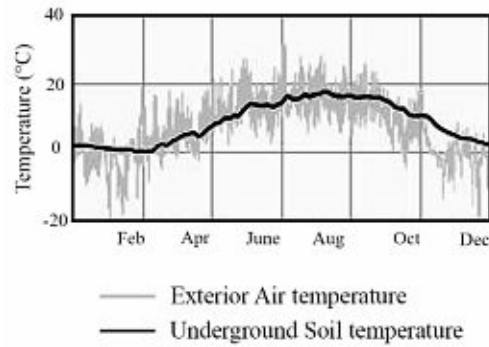


Figure 2.8 Temperatures of the exterior air compared with temperatures of the ground at a depth of 1 m (source: WUFI-Wiki 2020a)

At the beginning of the calculation, temperature and moisture content is essential to be specified for all the different material layers of the studied component. Afterward, the temperature field and the moisture field of the component will be initialized with the respective values by defining one of each in every grid element (WUFI-Wiki 2020a). The simulation will start with these initial values and subsequently determine their development in time. In order to define the initial temperature and moisture content, there are two options included: (1) setting a constant initial value across the component, and (2) uploading a file with an arbitrary initial moisture profile, specifying different initial water contents for different grid elements. For identifying the initial moisture content, there is another alternative setting in which a different initial moisture content can be defined in each material layer. WUFI (2020b) allows specifying either the initial moisture content ( $\text{kg}\cdot\text{m}^{-3}$ ) or the corresponding relative humidity (from 0 to 1) since the moisture storage function of each material is employed automatically to convert from the respective other values.

#### 2.1.4.5 Calculation period and options

Lastly, in order to define the simulation period, the starting date and time for the calculation is required. This starting point in the weather file will be searched by WUFI (2020b) and the calculation will start there. The weather file contains the climate data representing either the typical year climate or the individual year. WUFI (2020b) will read the same weather file repeatedly when the calculation period extends more than one year.

Regarding the modes of calculation, it is possible to adjust which heat and/or moisture transport is suitable for the calculation. Generally, both modes (i.e., heat transport and moisture transport) are activated. However, switching one of them off may be suitable

for some cases. Moreover, there are four hygro-thermal special options related to heat and moisture transfer mechanisms, which are capillary conduction, latent heat of evaporation, latent heat of fusion, and temperature dependency in latent heat of evaporation, where they can be switched off (WUFI 2020b).

As a result of the calculation suffering from numerical problems, apart from numerical grid revision, there are two numerical parameter options, including increased accuracy and adapted convergence, considered to be helpful to improve the calculation. Commonly, increased accuracy is more effective than adapted convergence (WUFI-Wiki 2020a). The numerical grid should be well adapted before using these options and a smaller time step may be also helpful (WUFI-Wiki 2020a).

### **2.1.5 Hygro-thermal properties in building materials**

The material properties as input parameters have a great impact on the results (Othmen et al. 2014). The reliability of the calculation results depends on the difference between the material property values defined in the software and the actual material properties (Browne 2012). Material properties required to be specified regarding the hygro-thermal calculation can be categorized into two groups: (1) basics values; and (2) hygro-thermal functions. Several material properties required for the calculation are provided by WUFI material database (2020b). Since the lack of reliable material data has been known as a notable problem for building performance simulation method, the relevant input material parameters will be discussed in terms of the purpose of their usage in the different kinds of investigation and their accuracy requirements. Moreover, their descriptions related to the use in WUFI will also be explained.

#### **2.1.5.1 Basics values**

There are five basic values of material properties including: (1) bulk density; (2) porosity; (3) specific heat capacity; (4) thermal conductivity; and (5) water vapor diffusion factor (see Table 2.4).

Table 2.4 Lists of the material basic properties

Basic properties	Symbol	Unit
Bulk density	$\rho$	$\text{kg.m}^{-3}$
Porosity	$n$	$\text{m}^3.\text{m}^{-3}$
Specific heat capacity	$C_p$	$\text{J.kg}^{-1}.\text{K}^{-1}$
Thermal conductivity (dry material at 10°C)	$A$	$\text{W.m}^{-1}.\text{K}^{-1}$
Water vapor diffusion resistance factor	$\mu$	[-]

Generally, three of those five parameters, comprising bulk density, specific heat capacity, and thermal conductivity are essential for the non-steady computation of the temperature fields (WUFI-Wiki 2020a).

Bulk density is defined as the mass of the material over its total volume. It is different from true density which is defined as the mass of the material over the volume after deducting the volume of its pore (Browne 2012). According to Browne (2012) “density does not need to be exactly defined as it only affects the specific heat capacity, which does not depend on very precise values”. This sentiment is echoed by WUFI (2020b) which explained that “since it only affects the specific heat value entering into the calculation, and hygrothermal simulations usually don’t depend very sensitively on this value, it need not be known with great precision” (topic 13 paragraph 2). Based on these considerations, it can be concluded that bulk density has little influence on the simulation results.

Thermal conductivity is defined by the measurement of heat flow being conducted across a material sample (Browne 2012). Browne (2012) states that “when studying the moisture contents and distributions, the hygrothermal simulations do not normally depend very sensitively on a precise value for thermal conductivity” (p.23). Therefore, the thermal conductivity, measured in the material in the dry condition at 10°C, is normally relevant for heat flow studies including U-value in the calculation (Browne 2012). If the moisture in the material affects the U-value, the thermal conductivity has to be given as a function of moisture content. Moreover, if the temperature-dependent thermal conductivity is taken into consideration, WUFI (2020b) can optionally provide either a table with the relevant data or the estimation option. The material property data related to the thermal conductivity can be found in WUFI’s material database (WUFI 2020b).

The specific heat capacity used in WUFI (2020) is defined by the mass of the dry material, given the benefit that the value does not depend on its porosity but only rely upon its chemical composition. For example, the same material such as cellular concrete bricks with different bulk densities has the same specific heat capacity by mass (WUFI-Wiki 2020a). The rough estimations

of the specific heat capacity value of mineral materials, with  $850 \text{ J.kg}^{-1}.\text{K}^{-1}$ , and organic materials, with  $850 \text{ J.kg}^{-1}.\text{K}^{-1}$ , are sufficient for the calculation since the value only slightly influences the hygro-thermal simulation results, particularly the resulting moisture contents and distributions (WUFI-Wiki 2020a). Moreover, in the case of wet materials, the heat capacity of the additional water content is automatically included in the heat capacity of the dry materials (WUFI-Wiki 2020a).

The hygric properties which are mandatory to be known for all materials to perform hygro-thermal simulation are porosity and water vapor diffusion resistance factor ( $\mu$ -value). Porosity is a material property expresses as a ratio of the volume of the material pores in relation to the total volume of the material. Bulk density and true density of materials are used to determine its porosity (WUFI-Wiki 2020a). In addition, the porosity can also be determined from maximum water saturation ( $W_{\max}$ ) (Browne 2012). The porosity value can be applied only when the material pore has the ability to take up liquid water or water vapor (hygroscopic, capillary-active building materials). In order to define the porosity by the maximum water content of a material, the water-saturated situation can only be achieved when it is under high pressure or through water vapor diffusion in a temperature gradient (Künzel 1995). Since water contents above free saturation rarely occur, most calculation results are not sensitive to the exact value of the maximum water content (WUFI-Wiki 2020a).

According to Browne (2012), “[Water vapor diffusion resistance factor] describes how a material impedes the diffusion of water vapor compared to diffusion through stagnant air” (p.23). The diffusion resistance factor known as  $\mu$ -value of the material is defined as a material property in dry conditions. Alternatively,  $\mu$ -value can be defined as a moisture-dependent value. However, in WUFI (2020b) simulation circumstances when moisture contents are above free water saturation ( $W_f$ ), moisture content at 100% relative humidity, a moisture-dependent  $\mu$ -value will be automatically employed. Afterward, it will be reduced proportionally to the moisture excess over  $W_f$  until it reaches  $\mu=0$  at the maximum water content ( $W_{\max}$ ) (WUFI 2020b). This statement explains that not only small pores, but also large ones can be blocked by liquid water leading to vapor transport interruption in the condition of a very high-level moisture content.

Regarding vapor diffusion thickness known as Sd-value, it is commonly used for defining diffusion resistance in a very thin material layer where its  $\mu$ -value and its thickness do not separately play any roles in the calculation, such as coating, paint, and particularly water vapor retarder. The Sd-value of material (m) expresses the thickness which a stagnant air layer would require in order to have the same diffusion resistance as the relevant material (WUFI 2020b). Their relation is explained in the following equation:

$$S_d\text{-value} = \mu * s \quad (\text{Eq. 2.11})$$

Here,  $\mu$  is water vapor diffusion resistance factor (-) of the relevant material and its thickness (m).

With respect to the aforementioned material properties specified as basic values in the hygro-thermal calculation, they only allow simulation computing without the effects of sorption or liquid transport. Since sorption and liquid transport in material, so-called by WUFI (2020b) as hygro-thermal functions, are the important phenomena involving in the hygro-thermal calculation, they will be discussed in the following section.

### 2.1.5.2 Hygro-thermal functions

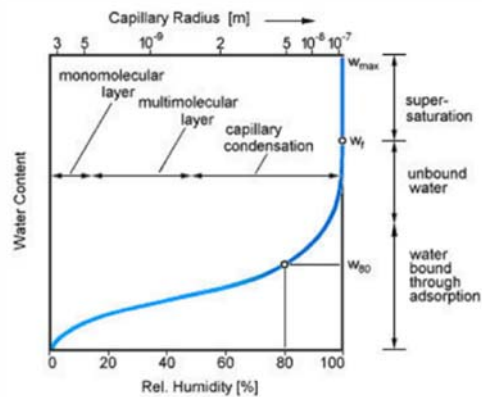
In order to precisely simulate the behavior of hygroscopic capillary-active materials, hygro-thermal functions such as moisture storage function and moisture-dependent liquid transportation coefficients are required. Various relevant sources, such as the WUFI database (WUFI 2020b), currently provide the hygroscopic and the capillary properties for a large number of building materials. The lists of the hygro-thermal functions of material regarding WUFI software simulation are presented in Table 2.5. The discussion will focus more on moisture storage function and liquid transport coefficient (both suction and redistribution), since water vapor diffusion resistance factor and thermal conductivity were already mentioned in the previous section and enthalpy is not relevant in this study. In the occurrence of phase change material investigation, enthalpy is required.

Table 2.5 Lists of the hygro-thermal functions of material regarding WUFI software simulation.

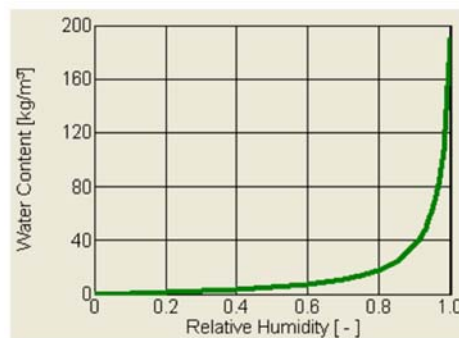
<b>Basic properties</b>
Moisture storage function
Liquid transport coefficient, suction
Liquid transport coefficient, redistribution
Water vapor diffusion resistance factor, moisture-dependent
Thermal conductivity, moisture-dependent
Thermal conductivity, temperature-dependent
Enthalpy, temperature-dependent

Moisture storage function is a material property which indicates the moisture content of a material at a given relative humidity (WUFI 2020b, Browne 2012). WUFI (2020b) states that “since this function depends only weakly on temperature, the temperature-dependence can be ignored for many proposes” (topic

14, paragraph 3). Based on this statement it can be inferred that the relative humidity is the only variable affecting the moisture storage function. This function is a line curve generated from 0% relative humidity, and then it goes through the reference water content (the moisture content of the material at 80% relative humidity;  $W_{80}$ ) and free water saturation (the moisture content of the material at 100% relative humidity under normal saturated pressure;  $W_f$ ), until it reaches the maximum water content (the moisture content of the material at 100% relative humidity under high pressure or condensation conditions;  $W_{max}$ ) (WUFI 2020b, Browne 2012) as shown in Figure 2.8. Note that in the supersaturated region, WUFI (2020b) allows moisture contents between  $W_f$  and  $W_{max}$  to be associated with relative humidity between 1 and 0.01, only as fictitious values, in order to assign a unique relative humidity to each water content as required by the moisture transport equations. Due to the limitations of the respective measuring procedures of the moisture storage function, the function has to be composed of sorption isotherms (from 0% RH to around 0.9% RH) and pressure plate measurements (above 0.95% RH) (Krus 1996).



(a)



(b)

Figure 2.9 Moisture storage function, and (b) the moisture storage function of solid brick masonry provided in WUFI database (source: WUFI 2020b)

The capillary liquid transport is the predominant moisture transport mechanism in capillary porous materials (WUFI 2020b). In the building physics framework, it is sufficiently precise to define liquid transport in the pore spaces as a diffusion phenomenon (WUFI 2020b). The line graph employed in WUFI (2020b) (see Figure 2.9) shows the liquid transportation coefficient ( $\text{m}^2 \cdot \text{s}^{-1}$ ) plotted against the normalized water content. The normalized water content is the water content divided by the maximum water content ( $W_{\text{max}}$ ). Moreover, the liquid transport coefficient can be classified into two types which are the liquid transport coefficient for: (1) suction ( $D_{\text{ws}}$ ); (2) redistribution ( $D_{\text{ww}}$ ). Concerning the situation that the material surface is submerged, the capillary water absorption mechanism is defined by the liquid transport coefficient for suction. The suction transport is dominated by the larger capillaries due to their greater suction velocity (Künzel 1995). The liquid transport coefficient for redistribution describes the transporting of the absorbed water at the material pore where the material surface is dry and there is no more water uptake to the surface (WUFI 2020b). The smaller capillaries dominate the water redistribution circumstances since their tension is higher and able to draws the water out of the larger capillaries (WUFI 2020b). The redistribution process is relatively slow compared to the suction (Künzel 1995).

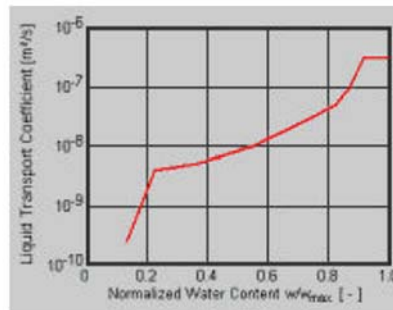


Figure 2.10 Liquid transportation function provided in the software (source: WUFI 2020b)

Due to the complexity and the high price of the moisture storage function and the liquid transport coefficients measurement, there are approximation methods, implemented in WUFI (2020b) used to estimate the material properties from known data. In order to approximate the moisture storage function, if there is no data provided by the laboratory measurement, reference moisture content ( $W_{80}$ ) and free water saturation ( $W_f$ ) are required. Similarly, the liquid transport coefficients can also be estimated from the water absorption coefficient (A-value), as defined in DIN 52617 (DIN 1987), by the algorithm in WUFI (2020b).

Establishing accurate material properties is very essential in order to obtain reliable simulation outcomes (BSI 2007). WUFI (2020b) offers a large database of predefined properties of conventional materials in modern constructions from reliable sources. However, a certain material has to be selected prudently due to the sensitivity of the software and the various specific purposes of investigations (Browne 2012).

### 2.1.6 Validation of hygro-thermal simulation model

Currently there are several tools available that could be used to predict the hygrothermal performance such as WUFI, DELPHIN and, HAM tool (Mundt-Petersen 2012). Specifically, two calculation tools, WUFI and DELPHIN, are commercially available and seen as user-friendly (Mundt-Petersen and Harderup 2013). WUFI is the one selected to perform hygrothermal analysis in this dissertation.

According to hygro-thermal simulation model validation studies, using the WUFI software model, some studies in northern European climates are found in which measured and calculated values are comparable, such as Geving and Holme (2010), and Geving et al. (2011). Mundt-Petersen (2013a, 2013b and 2015) conducted several studies with blind evaluations of the hygrothermal calculation tool (WUFI) by using field measurements in Swedish wooden houses under real conditions. There are some studies found with explicit blind comparisons focus on moisture control by allowing a high airflow in the air gap between the cladding and exterior mold-resistant insulation boards (Hägerstedt and Arfvidsson 2010, Hägerstedt and Harderup 2011a, and 2011b). There is also a software validation study conducted with an internally insulated log house as a case study, concerning air leakage rate (Alev et al. 2014). Based on this large amount of interests in the software validation study, it can be inferred that the validation is one of the essential processes in hygro-thermal performance study.

Therefore, since a central objective of this dissertation was to predict the hygro-thermal performance of historical brick wall constructions using WUFI simulation software as the transient heat and moisture calculation tool, the predictive potency of the simulation software was evaluated. The results of the evaluation are presented in this chapter.

## 2.2 Method

### 2.2.1 Overview

Through a collaborative research study (Aien et al. 2017), hygro-thermal simulations were performed to support a better understanding of moisture and heat transfer phenomenon in building components and evaluate the predictive performance of hygro-thermal simulation models. To present relevant data and references, the current chapter thus describe the key points of this study (Aien et al. 2017).

The study aimed at the evaluation of the predictive performance of the transient heat and moisture calculation tool, WUFI (WUFI 2020a), as a tool for the historical building refurbishment regarding moisture-related damage assessment and retrofit design decision making. WUFI Pro 5.3, used specifically in one-dimensional calculations, was applied for this purpose. A historical building of TU Wien used as an office area served as a case study.

In order to evaluate the hygro-thermal prediction, simulated temperature and relative humidity values were compared with measured data at different locations in the wall material layers. This was done to identify those factors that highly affect the relationship between measured and calculated values. This effort benefited from the use of observational data in an existing building component monitored in another research project described in Schuss et al. (2017). To achieve better agreement between measured and calculated data, some simulation settings and inputs were adjusted. The adjustment scenarios of the simulation model calibration were based on literature reviews. The results of the comparisons between calculated and measured values were analyzed.

### 2.2.2 Building case study and monitoring positions

This case study concerns a historical building of TU Wien, which is used as an office area. The original wall construction has three layers: gypsum plaster, hollow brick masonry, and lime cement plaster. The old paint on top of the lime cement plaster had to be removed since it is not a proper surface for the aerogel plaster. Additionally, an adhesive primer was applied after removing the paint to have a better connection and reduce the soaking effect of the wall.

The construction was retrofitted by applying aerogel plaster (FIXIT F222) (Fixit group 2017). The applied aerogel plaster (FIXIT F222) needed to dry for one month. The drying period was during the hot summer time, so the aerogel plaster had to be watered daily to ensure a slow drying out. Next a mineral based undercoat stabilizer (Röfix 380) (Fixit group 2017) was sprayed on the fully dried out aerogel plaster to get a harder surface and more grip for the finishing layers (Schuss et al. 2017) (see Figure 2.11). To prevent cracks in the wall and make a more resistant surface, a fabric mesh in an embedding mortar was added on

the undercoat stabilizer. As the last finishing layer Röfix PE 819 Sesco, lime wash was applied.

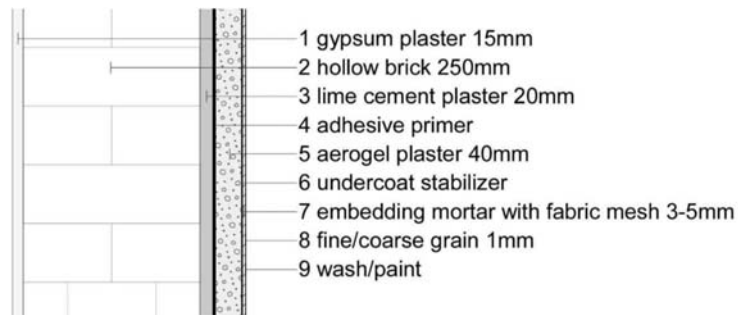


Figure 2.11 Section of the layers of the tasted façade  
(source: Schuss et al. 2017)

A set of sensors were installed within different layers of the construction, which enabled the in-situ measurement of temperature and relative humidity levels (Figure 2.12). The tested wall was located at the southern façade, which was equipped with five sensors to measure the temperature and the humidity in different positions. The first sensor position is directly under the exterior finishing layer. Position 0 is the heat flow sensor and Positions 1 to 5 are sensors measuring temperature and humidity.

Indoor and outdoor environmental conditions were monitored for the duration of the experiments (Schuss et al. 2017). This study utilizes the monitored data from 2015 for a period of one year (2015). See Schuss et al. (2017) for more details about the data and the experimental setup.

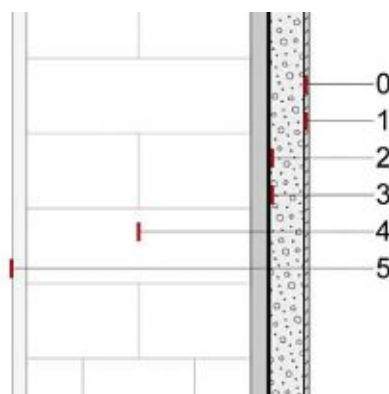


Figure 2.12 Position of the Sensors in a façade  
(source: Schuss et al. 2017)



Figure 2.13 View of installed sensors on the existing wall; temperature and humidity sensors as well as the heat flow plates of the test areas on the south façade (source: Schuss et al. 2017)



Figure 2.14 External surface after retrofit (source: Schuss et al. 2017)

## 2.2.3 Hygro-thermal simulation (1D)

### 2.2.3.1 Simulation software (1D)

The case study wall construction was simulated in WUFI Pro version 5.3 (WUFI 2020a, Künzle 1998). WUFI, Wärme Und Feuchte Instationär, works based on the discretization of the Künzle model by means of an implicit finite volume scheme. WUFI is a transient coupled heat and moisture calculation tool used to analyze the hygrothermal performance of building envelope designs. For the numerical solution, WUFI uses the finite volume technique for the spatial discretization of the transport

equations, and the fully implicit scheme for the discretization in time. In the calculation, the driving potentials for moisture movement are relative humidity and temperature, and the potential for energy flow is temperature difference (Mundt-Petersen 2012). The tool has been developed in both one and two-dimensional versions (WUFI 2020a). However, one-dimensional software was deployed in the present case study. Simulation provides hourly values of temperature, relative humidity, and water content as outcomes. However, only temperature and relative humidity were analyzed in this chapter.

### 2.2.3.2 Geometry modelling

As mentioned in section 2.2.2 (Building case study and monitoring positions), five sensors were installed within different layers of the construction (see Figure 2.12). Figure 2.15 presents the positions of sensors in different layers of simulation model construction (01, 02, 04, and 05) following the actual monitoring positions in the wall. On the left side of the model, the finishing layer is exposed to interior boundary conditions and on the right faces the exterior boundary conditions.

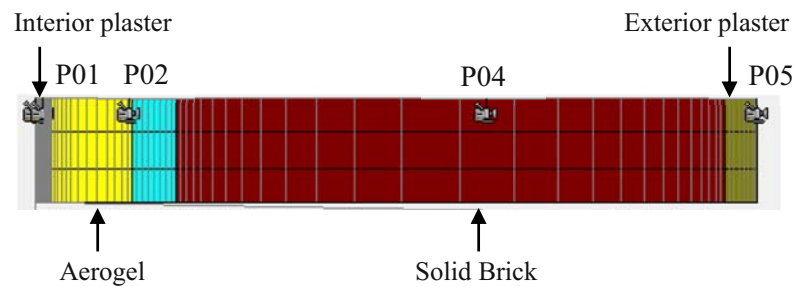


Figure 2.15 Position of sensors in different layers of construction (01, 02, 04, and 05)

### 2.2.3.3 Simulation inputs and settings

The design of the generated building model requires several input data and program settings. The model inputs and settings in this chapter are shown in Table 2.6. The hygro-thermal and physical characteristics of the materials required for the simulations in WUFI are presented in Table 2.7 and Table 2.8.

The properties of the materials were defined based on available information (e.g., material catalogs), measurements, and observations. In case of the missing information, the material data library of WUFI (2020b) was used. The boundary condition required for the simulations includes the outdoor climate and indoor environmental conditions (hourly temperature and humidity values). In addition, the initial condition (see Table 2.9)

(i.e., the temperature and water content) of each layer at the beginning of the simulations, must be specified.

Table 2.6 Inputs and settings of WUFI (source: Aien et al. 2017)

<b>Settings and inputs</b>		<b>Value</b>
Orientation/	Orientation	South
Height/	Height [m]	> 20
Inclination	Inclination [°]	90
Building height-driven rain coefficient	Rain load= $\text{Rain} \times \text{FE} + \text{FD} + 0.2$ [s.m <sup>-1</sup> ] *wind velocity (According to the ASHRAE Standard 160)	FD=1.5 FE=1
Surface transfer coefficient	Thermal resistance of exterior surface [m <sup>2</sup> .k.W <sup>-1</sup> ]	0.0588
	Sd-Value of exterior surface [m]	0.0002
	Short wave radiation absorptivity	0.2
	Ground short wave reflectivity	0.2
	Adhering fraction of rain absorption	No
	Thermal resistance of interior surface [m <sup>2</sup> .k.W <sup>-1</sup> ]	0.125
	Sd-Value of interior surface [m]	0.1

Table 2.7 Material basic properties input data (source: Aien et al. 2017)

<b>Basic properties</b>	<b>Röfix 380</b>	<b>Aerogel</b>	<b>Old plaster</b>	<b>Brick</b>	<b>Interior plaster</b>
Layer thickness [m]	0.002	0.04	0.02	0.25	0.02
Bulk density [kg.m <sup>-3</sup> ]	1000	220	1900	1560	1721
Porosity [m <sup>3</sup> .m <sup>-3</sup> ]	0.24	0.92	0.24	0.38	0.31
Specific heat capacity [J.kg <sup>-1</sup> .K <sup>-1</sup> ]	1000	1000	850	850	850
Thermal conductivity (dry material at 10°C) [W.m <sup>-1</sup> .K <sup>-1</sup> ]	0.47	0.029	0.8	0.4	0.2
Water vapor diffusion resistance factor [-]	12	4	19	14.93	13

Table 2.8 Material hygro-thermal properties input data (source: Aien et al. 2017)

<b>Basic properties</b>	<b>Röfix 380</b>	<b>Aerogel</b>	<b>Old plaster</b>	<b>Brick</b>	<b>Interior plaster</b>
Reference water content (RH 80%) [kg.m <sup>-3</sup> ]	45	6.6	45	11.80	1.77
Free water saturation (RH 100%) [kg.m <sup>-3</sup> ]	210	213	210	368.96	264.27
Water absorption coefficient (A-value) [kg.m <sup>-2</sup> .s <sup>-0.5</sup> ]	0.02	0.0004	0.02	0.51	0.30
Moisture-dependent thermal conductivity supplement [%.M <sup>-1</sup> % <sup>-1</sup> ]	8	0.5	8	8.51	3.23
Temperature-dependent thermal conductivity [W.m <sup>-1</sup> K <sup>-2</sup> ]	0.0002	0.0002	0.0002	0.0002	0.0002

Table 2.9 Initial conditions assumptions in the initial simulation model (source: Aien et al. 2017)

<b>Initial conditions</b>	<b>Exterior plaster</b>	<b>Aerogel layer</b>	<b>Middle of the wall</b>	<b>Interior plaster</b>
Temperature [°C]	-1.88	13.37	17.05	19.18
Relative humidity [%]	72.09	31.64	41	22.37
Water content [kg.m <sup>-3</sup> ]	31.679	0.796	2.120	0.408

### 2.2.3.3 Hygro-thermal simulation outcomes

Following the hygro-thermal simulation, water content, relative humidity and temperature were computed. The detailed descriptions of the results are listed below.

#### *Water content*

Due to the complexity of the nature of hygroscopic porous materials, there is no perfectly clear distinction between water vapor and liquid water (WUFI 2020b). For example, the water

molecules temporarily absorbed at the pore walls and absorbed multi-molecular layers at the pore walls cannot be easily classified as vapor or liquid. Since WUFI is a simplified simulation tool, it simply assumes that the “water content” indicated by the moisture storage function is liquid water. Since WUFI is a simplified simulation tool, it can be assumed that the “water content” indicated by the moisture storage function is liquid water with properties such as capillary transport and heat capacity, to name a few. (WUFI 2020b). WUFI gives the water content as water density in the unit of  $\text{kg}\cdot\text{m}^{-3}$ .

#### *Relative humidity*

Ignoring of the complication of water state in porous materials, WUFI defines the relative humidity within the bulk of a porous material as the relative humidity of the pore air (WUFI-Wiki 2020a). However, in the real situation, the relative humidity of the pore air has a strong influence on the water content of the material as a result of the intense interaction between air in the material pore and the material pore’s wall. It is possible that water content of the material is much larger than the water vapor content of the pore air.

#### *Temperature*

WUFI gives the temperature as a simulation outcome in the unit of degree Celsius ( $^{\circ}\text{C}$ ) (WUFI 2020a). The software provides the temperature of the material in the selected positions or an area in the material layer.

### 2.2.4 Simulation scenarios

For the evaluation of reliability of the simulation, alternative configurations of input data (i.e., initial condition, as well as indoor and outdoor climate, and some material properties) were considered. Four scenarios with different conditions were set up (see Table 2.10). Note that all scenarios used the same inputs and settings, as well as further material properties as listed in Table 2.6, Table 2.7 and Table 2.8.

Table 2.10 Simulation scenarios (source: Aien et al. 2017)

<b>Simulation scenarios</b>	<b>Initial conditions</b>	<b>Indoor conditions</b>	<b>Outdoor climate</b>	<b>Brick</b>
Initial model	Constant software default values equal for all layers	Calculated by software using EN15026	Reference Vienna weather file	Solid

Scenario 1	Measured values for each layer	Calculated by software using EN15026	Reference Vienna weather file	Solid
Scenario 2	Measured values for each layer	Measured indoor climate	Reference Vienna weather file	Solid
Scenario 3	Measured values for each layer	Measured indoor climate	Local Vienna weather file	Solid
Scenario 4	Measured values for each layer	Measured indoor climate	Local Vienna weather file	Extruded

- Initial model: The initial conditions for each material layer were defined as 20°C for the temperature and 80% for the relative humidity. For the outdoor condition setting, the hourly weather data from the database of WUFI (WUFI 2020a) for the city of Vienna, Austria, was used. The indoor climate condition was derived in the program based on outdoor climate, using standard EN 15026 (WUFI 2020b, BSI 2007). Commonly, this standard is recommended to be used when actual indoor environmental data is not available.
- Scenario 1: This scenario differs from the initial model by using the measured values as initial values for each wall layers, (see Table 2.4). The initial condition was imported as a text file containing hourly data of the first hour for both temperature and relative humidity.
- Scenario 2: Similar to Scenario 1, with the imported actual indoor environmental conditions (Measured indoor temperature and humidity), instead of calculated indoor conditions based on EN15026 standard (BSI 2007).
- Scenario 3: Compared to scenario 2, the measured weather values (temperature, relative humidity and global radiation) from a locally installed weather station were used. The measurement results provided the basis to create an hourly data file. To create an epw file (.epw) that can be imported to WUFI, the software Meteororm 7 (Meteororm 2020) was used.
- Scenario 4: In this scenario an extruded brick (9.5 water vapor diffusion resistance factor, 8.7 kg.m<sup>-3</sup> reference water content) was used for the simulation instead of the solid brick. The information was based on the WUFI materials database (WUFI 2020b).

### 2.2.5 Evaluation criteria

To evaluate the predictive performance of the hygro-thermal simulation tool, the simulated temperature and relative humidity at each monitoring position in each material layer was compared to the corresponding measured values at each time step. Error of the calculation can be calculated as the difference between the predicted values, i.e. simulation results, and the measured values.

Four statistical indicators were used as a model evaluation index. CV (RMSD), the coefficient of variation with the RMSD (Root-mean-square deviation), which aggregates time step errors over the runtime into a single dimensionless number. The second measure is  $R^2$ , which describes the proportion of the variance in measured data explained by the model (Tahmasebi and Mahdavi 2013).

In addition, the absolute and relative errors, denoted by  $E_{abs}$  and  $E_{rel}$  were calculated for each scenario in this study. The difference between the measured value and actual value is calculated as absolute error.

Moreover, the minimum, maximum, mean and range of the whole year hourly data are presented by means of the “Box and Whiskers Plot” or “Quartile Boxes” or simply called as “Box plot” in this study (see Figure 2.15). The box contains quartiles and includes an additional character to represent the mean of the data (Othmen et al. 2014). The first quartile  $Q_1$  is the lower quartile and it means that 25% of the data are lower than this value. The second quartile  $Q_2$  is also called the median and it divides the data set in two equal populations. The third quartile  $Q_3$  is the upper quartile and it represents 75% of the data (Othmen et al. 2014). The minimum and maximum of all of the data are presented at the ends of the whiskers.  $Q_2$  or median is focused more, comparing to  $Q_1$  and  $Q_3$ , in this study.

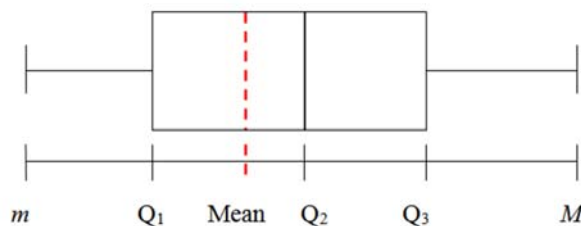


Figure 2.16 An example of Box plot with whiskers.  
(source: Othmen et al. 2014)

## 2.3 Results and discussion

### 2.3.1 Results

Figure 2.17 (Left) and Figure 2.17 (Right) include boxplots that illustrate the temperature and relative humidity distributions in different nodes (node 01, 02, 04 and 05), presenting the minimum, maximum, mean and range of the whole year hourly data in different scenarios, as well as measured and initial model. It can be seen that the relative humidity of the simulation scenarios, especially scenario 02, 03 and 04, in nodes 2, 4, and 5 improved significantly and became closer to the measurements, as compared to the initial model. The temperature results demonstrate some improvement in all nodes, which is clearly seen in scenario 02, 03 and 04.

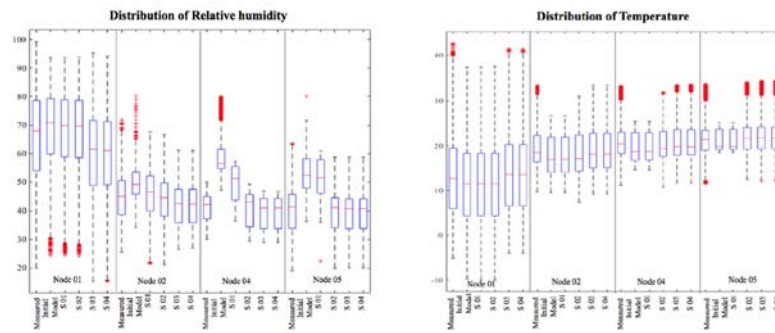


Figure 2.17 Distribution of relative humidity (Left) and temperature (Right) of measured values, initial model values and values from all scenarios in each node (source: Aien et al. 2017)

As it can be seen from Figure 2.18 on the left side and on the right side, the model in Scenario 03 generated outputs with reasonable  $R^2$  values, for both temperature (more than 0.9) and relative humidity (more than 0.8) in all nodes. This improvement is clearly visible for humidity predictions in node 2 (Aerogel layer) after feeding in the actual initial conditions (Scenario 1). However, the  $R^2$  value is still not reasonable (around 0.2). Moreover, the accurate definition of indoor environment led to significant improvements in all nodes, except the exterior layer for both relative humidity and temperature. Therefore, indoor conditions have no significant effects on the exterior layer. Similarly, the outdoor conditions have no significant impact on the interior layer since applying the in-situ weather data hardly affects the simulation results regarding interior layer (see Figure 2.7). Particularly, for the internal layer, the use of accurate indoor conditions greatly improved the  $R^2$  (from 0.23 to 0.98 for relative humidity and from 0.43 to 0.99 for temperature) (see Figure 2.18).

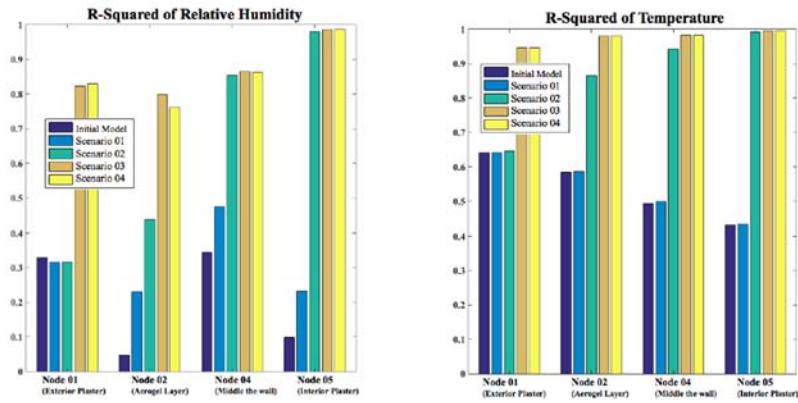


Figure 2.18  $R^2$  of relative humidity (Left) and temperature (Right) of measured values, initial model values and values from all scenarios in each node (source: Aien et al. 2017)

The calculated CV (RMSD) for each node in the initial model and the corresponding scenarios are shown in Figure 2.19. The left figure is for relative humidity and the right is for temperature. It can be seen that in the scenario 3 and 4 the errors are dramatically decreased in both relative humidity and temperature. In the last two scenarios (scenario 3 and 4), the calculated errors are below 5% for temperature in all nodes, except in node 01, which shows higher corresponding errors (around 15%). For relative humidity, the errors are around 12% and 10% for node 01 and 02, respectively, and the rest (node 4 and 5) are less than 5%.

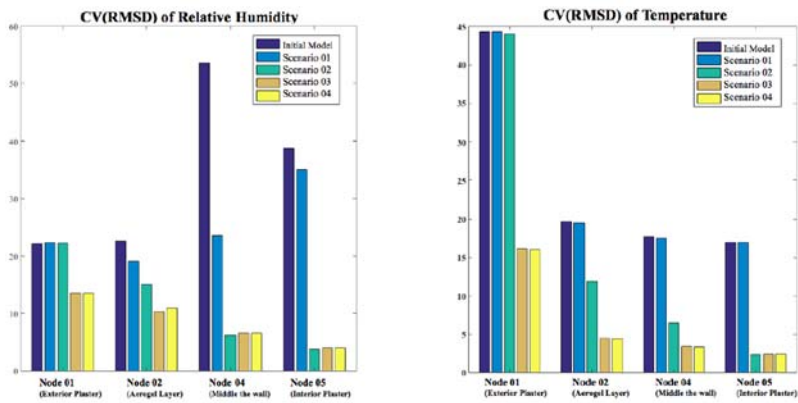


Figure 2.19 (CV)RMSD of relative humidity (Left) and temperature (Right) of measured values, initial model values and values from all scenarios in each node (source: Aien et al. 2017)

The absolute and relative errors illustrated in Figure 2.20, 2.21 and 2.22 confirm the results presented above. Boxplot of the absolute errors (Figure 2.20) demonstrates a higher rate of improvement for the brick layer and the internal layer (node 4 and node 5) in both relative humidity and temperature from scenario 2 on. The mean errors are less than 5%

for relative humidity and less than 2 K for temperature. The external layer (node 01) has the highest error values (mean value), which is about 2.5 K for the temperature and 5% for the relative humidity in scenario 3 and 4.

The same pattern of improvement can be seen in Figure 2.21 and Figure 2.22. It is noted that due to the higher errors in case of relative humidity calculations, only the cumulative percentage of relative errors for relative humidity is shown in Figure 2.21 and Figure 2.22. It can be seen in these graphs that in node 5 (Interior plaster) the prediction shows the best results (The least errors) in scenario 3 and 4, comparing with others.

Based on the results presented in this study, Scenario 4 does not generally perform better than Scenario 3. However, as shown in Figure 2.23, changing the solid brick to extruded brick can slightly improve relative humidity predictions. A more detailed model of the layer geometry (for instance, using WUFI 2D to correctly model hollow bricks) may have the potential to improve predictions.

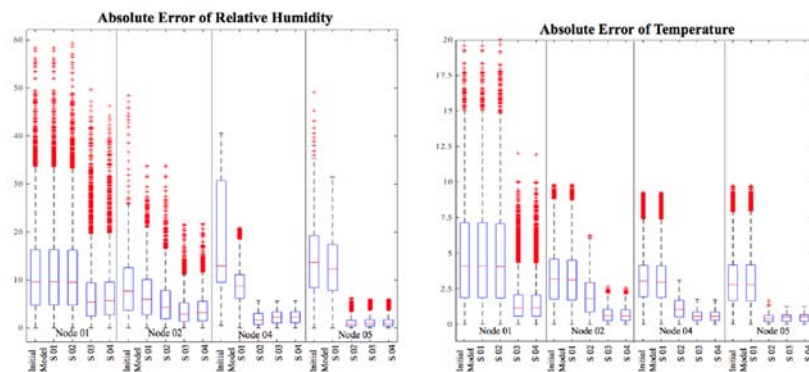


Figure 2.20 Absolute error of relative humidity (Left) and temperature (Right) of measured values, initial model values and values from all scenarios in each node (source: Aien et al. 2017)

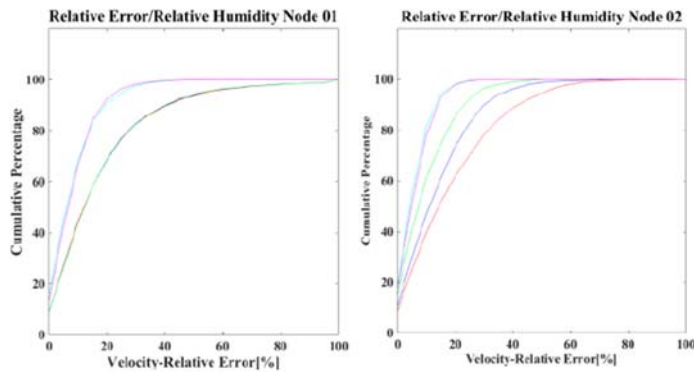


Figure 2.21 Relative error of relative humidity of measured values, initial model values and values from all scenarios in node 01 (Left) and node 02 (Right). (source: Aien et al. 2017)

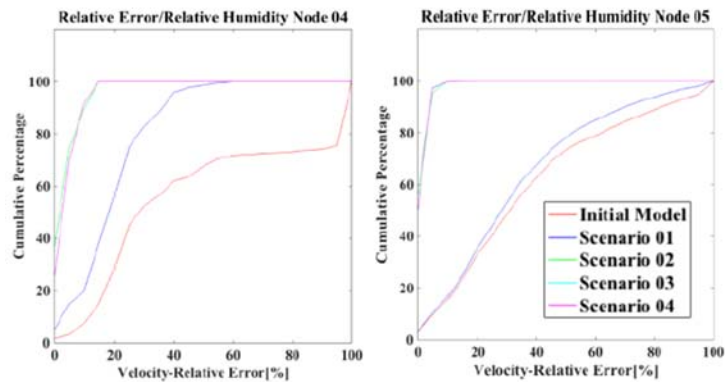


Figure 2.22 Relative error of relative humidity of measured values, initial model values and values from all scenarios in node 04 (Left) and node 05 (Right). (source: Aien et al. 2017)

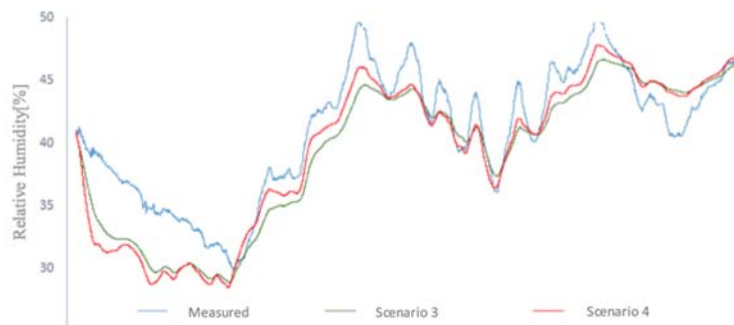


Figure 2.23 Trend of relative humidity in middle of the wall (node 04) comparing between the measured data, the calculated data in scenario 3 and scenario 4 (source: Aien et al. 2017)

### 2.3.2 Conclusion

The results of a case study on the predictive performance of hygro-thermal simulations of an existing wall retrofitted with an Aerogel-based plater layer were presented. Measured data was used to both create a more accurate initial model and to evaluate the accuracy of the simulation outcomes. The results show a noticeable improvement of the predictive potency of the simulation model by adjusting the input variables based on measurements. A key implication of this study is that it is of great importance to apply a local indoor and outdoor climate. Additionally, accurate initial conditions (i.e., starting values of layer temperatures and humidities) can contribute to more reliable simulation results.

## Chapter 3

# Sensitivity Analysis of hygro-thermal simulation models of a historical building in tropical climate

### 3.1 Background

#### 3.1.1 Tropical climate (Thailand)

Tropical countries are countries that are located in the region called the tropics, confined as the zone between the Tropic of Cancer, the parallel of latitude at 23° North, and the Tropic of Capricorn, the parallel of latitude at 23° South (Morgan 2011).

Thailand is located in the center of Southeast Asia, on the tropical zone, between latitudes 5° 37' N - 20° 27' N and longitudes 97° 22' E - 105° 37' E) (TMD 2020) (see Figure 3.1). The country is approximately 513,115 km<sup>2</sup> in size and shares a border with Myanmar, Cambodia, Laos and Malaysia (TMD 2020) (see Figure 3.2). It consists of six regions, namely, Northern, North-eastern, Central, Western, Eastern and Southern Thailand (see Figure 3.2).

Corresponding to the Köppen climate classification system, Thailand is partially classified as a tropical monsoon climate and a tropical savanna climate (Phumkokrux 2020).



Figure 3.1 Thailand location map  
(source: Mapsofworld 2020)



Figure 3.2 Regions of Thailand and surrounding countries  
(source: Stevenandrewmartin 2020)

Weather conditions in Thailand are generally hot and humid throughout the year. The average annual temperature is approximately 27 °C (TMD 2020). Typically, seasons in Thailand are divided into three periods, which are hot (from the middle of February to the middle of May), rainy (from the middle of May to the middle of October) and cool

(from the middle of October to the middle of February) (TMD 2020, Climatemps 2020). Although temperatures are moderately hot for the whole course of a year, average monthly temperatures vary by 4.1 K (Climatemps 2020).

Geographical location and seasonal characteristics influence thermal conditions in each region in the country (see Table 3.1). For example, during the cool season, the average minimum temperature in the central region is higher than the northern region by around 4 K and in terms of the average temperatures, this difference is around 3 K (TMD 2020). Comparing thermal conditions within each season in the central region, in summer, temperature becomes the highest in April (the hottest month of the year) with almost 40 °C, and in cool season it becomes the lowest in December (the coolest month of the year) at around 17.5 °C (TMD 2020).

Table 3.1 Thermal conditions in each region in Thailand during 1981-2010 (30 years) (source: TMD 2020)

		Temperature (°C)		
		Cool season	Hot season	Rainy season
<b>Northern Region</b>	Average monthly	23.4	28.1	27.3
	Average monthly maximum	31.1	36.1	32.4
	Average monthly minimum	17.5	21.8	23.8
<b>Northeastern Region</b>	Average monthly	24.2	28.6	27.6
	Average monthly maximum	30.6	35.2	32.6
	Average monthly minimum	18.7	23.2	24.4
<b>Central Region</b>	Average monthly	26.2	29.7	28.2
	Average monthly maximum	32.3	36.2	33.4
	Average monthly minimum	21.2	24.6	24.8
<b>Eastern Region</b>	Average monthly	26.7	29.1	28.3
	Average monthly maximum	32	34.1	32.3
	Average monthly minimum	22.3	25.2	25.2
<b>Southern Region</b>	Average monthly	26.65	28.3	27.65
	Average monthly maximum	31.2	33.55	32.15
	Average monthly minimum	23	24.05	24.35

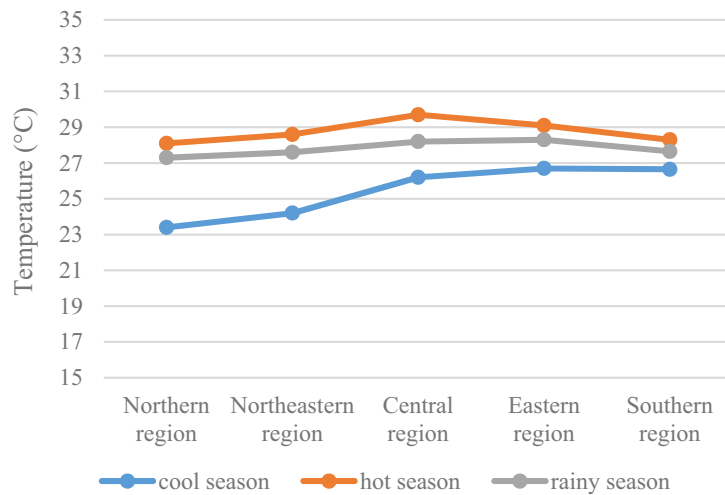


Figure 3.3 Average monthly temperature in each region in Thailand during 1981-2010 (30 years) (source: TMD 2020)

Average annual rainfall throughout the country is approximately 1,587.7 mm (TMD 2020). The amount of rainfall in each region varies depending on seasonal conditions as well as terrain characteristics. The northern part of Thailand is generally arid with less precipitation during the cool season, whereas during the rainy season, the amount of rainfall significantly increases. In the central region the total amount of annual rainfall is around 1,200 mm (TMD 2020). On the other hand, the southern region experiences abundant rainfall all year round except the hot season, which is more than 4,000 mm per year (TMD 2020).

As Thailand is located in a tropical region near the equator, it mostly experiences hot and humid weather conditions throughout the year. Except the continental areas, from the central region to the northern region, relative humidity decreases during the cool and summer seasons. For example, the average relative humidity in the central region can drop from 78% (rainy season) to 68% (hot season) (TMD 2020).

This dissertation focuses on the central region as two selected case studies are located in Ayutthaya and in Bangkok (Figure 3.2). The case-study building in Ayutthaya is investigated in detail in the following sections of this chapter through sensitivity analysis. And the case study in Bangkok is explored in the fourth chapter.

### 3.1.2 Sensitivity analysis

For the selection of potential refurbishment solutions, numeric simulation tools can provide useful support to study hygro-thermal performance of the building facade. Consequently, good knowledge of material related parameters is essential to generate dependable models. It is therefore important to determine the sensitivity of hygro-thermal

analysis to identify the most suitable choice of model input data, for instance, material properties. While some of the material properties can be obtained through simple measurements, others require tremendous efforts and great financial expenses to be obtained with reliable outcomes. Browne (2012) contends that “The cost of measuring a material’s full range of hygrothermal properties in a specialist laboratory is prohibitively expensive” (p.1). This sentiment is echoed by Othmen et al. (2014) who explained that “it may be useless to seek high accuracy of a parameter if the heat and moisture transfer model is weakly sensitive to this parameter” (p.2). Based on these considerations, it can be concluded that sensitivity analysis (SA) is an important part of a hygrothermal study.

According to Pannell (1997), “sensitivity analysis (SA), broadly defined, is the investigation of these potential changes and errors and their impacts on outcomes to be drawn from the model.” (p. 139). Furthermore, SA can be used for many purposes, for example, increasing understanding of the system, decision support, model development and enhancing communication (Pannell 1997). SA has been used in many previous studies for the purpose of improving model performances in various disciplines, for example, finance, lift science and environmental engineering (Othmen et al. 2014). SA is a well-known requirement of any scientific fields. Hence, SA should be a fundamental part of any solution methodology (Fiacco 1983).

In hygro-thermal analysis study, SA allows the identification of essential model input parameters, especially the material properties, which is one of the most significant impact on the results (Stephan et al. 2013). There are many different SA approaches. Overall, they can be categorized into two groups: local SA and global SA (Othmen et al. 2014). To put it simply, the local SA explores the changes of model reaction by changing one parameter, while keeping other parameters constant. Global SA considers the changes of model response by varying all input parameters at once. In this chapter, local SA was conducted on a selected historical building model as a case study.

Theoretically, SA approaches follow a simple procedure: change the model and observe its behavior (Pannell 1997). Practically, there are many different ways to change the model inputs and observe the outcomes. For an overall concept of how to conduct SA, it can be concisely explained as three steps: (1) to specify what to vary, (2) to clarify what to observe and (3) design an experiment (Pannell 1997). For a parameter levels selection, which will be applied in SA, values commonly specify in advance with equal sized intervals between the levels (Pannell 1997, Othmen et al. 2014).

### 3.1.3 Meteonorm software for generating Thai weather file

In this chapter, Meteonorm software was used to generate the weather file as outdoor climate conditions for the simulation model.

Meteonorm is a meteorological database containing climatological data of many locations on Earth. The software stochastically generates typical years from interpolated long-term monthly means (Meteonorm 2020). It offers monthly climatological data. Since numerous simulation processes require hourly values, Meteonorm can additionally calculate synthetic hourly values for a typical meteorological year from the monthly values using stochastic model (Meteonorm 2020, PVsyst 2020). An average year of the selected climatological time period is presented based on the user's setting. Fundamentally, the results do not represent a real historic year but a hypothetical year. The hypothetical climatological year data statistically represents a typical year at a selected location (Meteonorm 2020). Apart from obtaining weather data provided by the software database, Meteonorm allows users to import their own monthly and hourly climate data to generate their own data records. In Meteonorm version 7, CSV (Character Separated Value) file format is required for the importing. Meteonorm can then generate various file types including “.epw” (EnergyPlus file type), which can be applied to selected hygro-thermal simulation (WUFI).

In this study, hourly measured weather data was provided by the Thai Meteorological Department. The data set is from the year 2016 from the weather station in Bangkok, named Don Muang District (TMD 2020). Acquired data comprises of air temperature (°C), air humidity (%), wind speed (knot), wind direction (angle; turn clockwise starting from the north), precipitation (mm) and global solar radiation ( $\text{W}\cdot\text{m}^{-2}$ ) (Meteonorm 2020). In order to generate the weather file by using Meteonorm software, measurements that belong to three main parameters, which are outdoor temperature (°C), global solar radiation ( $\text{W}\cdot\text{m}^{-2}$ ), and dew point temperature (°C), are uploaded. Afterward, generated file (.epw file) was edited by replacing the created data with the remaining measurement data (wind speed, wind direction, precipitation).

## 3.2 Method

### 3.2.1 Overview

The presence of moisture-related problems in historical buildings caused by poor retrofit methods can lead to substantial structural and surface damages. Finding appropriate solutions for the refurbishment of the historic building façade has been a challenge (see, for example, EMERISDA 2014, Franzoni 2014, Torres and Freitas 2007). In order to select potential retrofit strategies, numeric simulation tools can provide useful support in studying the hygro-thermal performance of building façades (see, for example, Othmen et al. 2014, Mundt-Petersen and Harderup 2013, Kunzel 1995).

Therefore, in this chapter a sensitivity analysis (SA) is performed to determine the choice of model input data for hygro-thermal simulation. Since the material properties as input parameters have great impact on the results, they were selected to be used in the sensitivity analysis (Othmen et al. 2014). The material-related input parameters selected in this chapter are the following six properties, porosity ( $n$ ), density ( $\rho$ ), thermal conductivity ( $\lambda$ ), specific heat capacity ( $C_p$ ), water vapor diffusion resistance factor ( $\mu$ ) and water absorption coefficient ( $A$ ).

Since relatively few studies in this area concentrate on the specific circumstances of tropical climates where the occurrence of moisture problems is widespread, a historical building constructed in the tropical climate of Thailand was selected as a case study. Located in the central region in the province of Ayutthaya, the building was constructed using traditional techniques of the respective era. Generally, the construction of this and other similar buildings from such period was influenced by the location and availability of the materials on the site, as well as the importance of the building (Stephan et al. 2013, Bunjerdskul 2014). A hygro-thermal performance model of the exterior brick wall was generated and subjected to a SA to identify a subset of the input variables (material properties) with significant influence on the simulation results.

### 3.2.2 Building case study

The case-study building is a Buddhist temple named Wat-Niwet-Thammaprawat (Figure 3.5 and 3.6), designed by Joachim Grassi, an Italian architect of Austrian/French nationality working for the Siamese government in the late nineteenth century (Issarathumnoon 2018). In the style of an English Gothic church with a load-bearing wall construction, the temple was constructed in 1878 on a riverine island in Ayutthaya, Thailand (Figure 3.4). The building was last refurbished in 2015 (Figure 3.7 and 3.10). However, the post-retrofit moisture problems on the middle and lower parts of the exterior walls (Figure 3.8) are clearly visible.

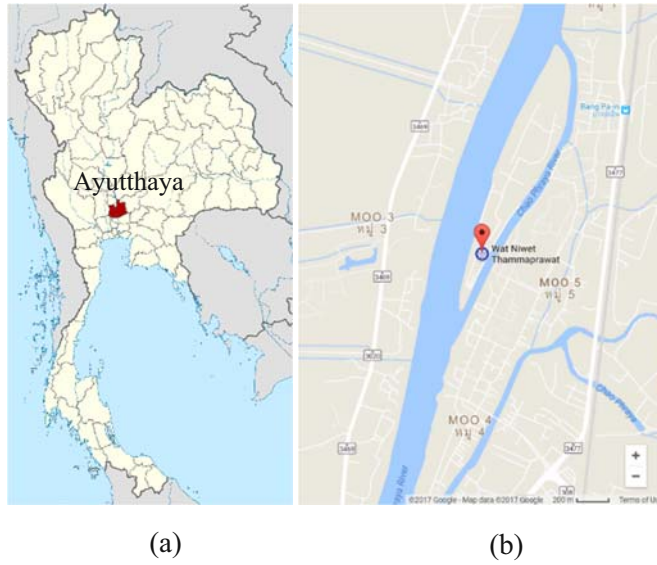


Figure 3.4 The location of (a) Wat-Niwet-Thammaprawat temple (source: Googlemap 2020a), (b) Ayutthaya, Thailand (source: Wikipedia 2020a)



Figure 3.5 Wat-Niwet-Thammaprawat temple, Ayutthaya, Thailand (source: Pinich 2018)



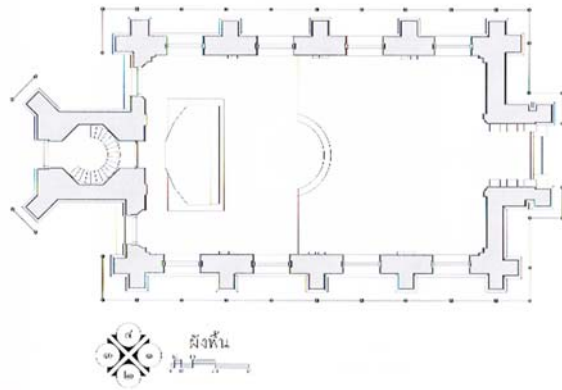
Figure 3.6 Interior perspective of Wat-Niwet-Thammaprawat temple, Ayutthaya, Thailand



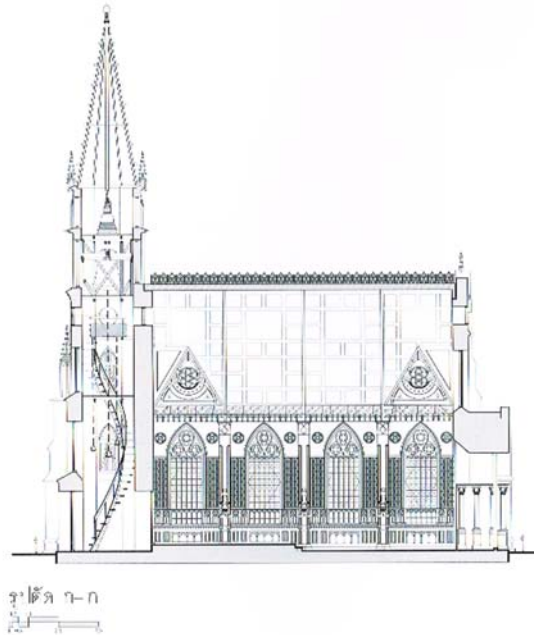
Figure 3.7 Last refurbishment of the temple's exterior wall in 2015 (source: Pinich 2018)



Figure 3.8 Signs of post-retrofit moisture problems on the middle and lower parts of the walls (photo taken in 2017) (source: Pinich 2018)



(a) plan



(b) section

Figure 3.9 Architectural drawings of the building  
(i.e., (a) plan and (b) section) (source: Wongchaturaphat 2011)

The outside wall of this temple - a typical Thai traditional temple wall construction from the 19<sup>th</sup> century - is selected for this study (Watsantachad 2006, Bunjerdskul 2014). The wall construction consists of three main layers, namely lime stucco (0.005 m), lime plaster (0.045 m), and solid clay brick (0.7 m) (see Figure 3.10b and 3.11). The material properties are presented in the following section.



(a)



(b)

Figure 3.10 Photographs (a) and (b) from the renovation in 2015 with the Massari method (EMERISDA 2014)

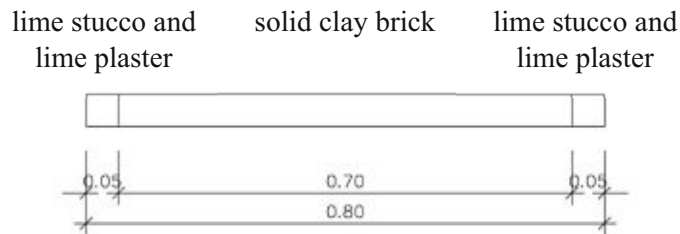


Figure 3.11 The wall construction in cross-section details.

### 3.2.3 Hygro-thermal simulation (1D)

The material properties of the wall construction in the case study was simulated using WUFI Pro version 5.3. A detailed overview of the software is given in Chapter 2.

#### 3.2.3.1 Geometry modelling

As illustrated in figure 3.11, there are three layers inside the building wall construction, comprising of lime stucco (0.005 m), lime plaster (0.045 m), and solid clay brick (0.7 m). Figure 3.12 presents the simulation model of the building as a typical historical Thai wall construction and the three main positions analyzed in

this chapter: external plaster (P1); solid brick (P2); and internal plaster (P3). On the left side of the model, the finishing layer (lime stucco) is exposed to an interior boundary condition and on the right the innermost wall layer (lime plaster) faces an exterior boundary condition.

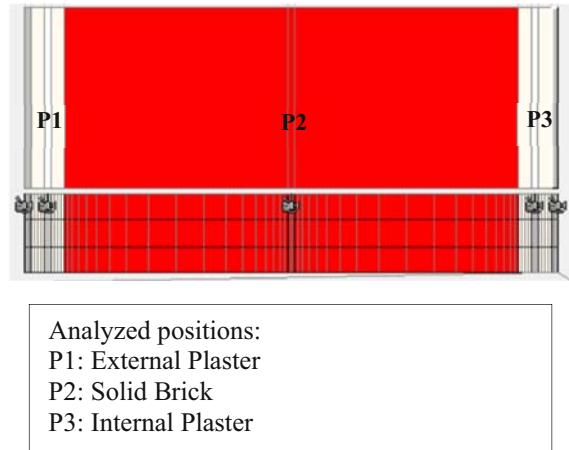


Figure 3.12 The simulation model of the case-study building (typical historical Thai wall construction) (source: Pinich 2018)

Material properties were assigned based on the material databases of WUFI using the sources of Fraunhofer (IBP) (Germany), North America Database (Germany), and TU Wien (Austria) (WUFI 2020b). Details regarding the used materials are presented in Table 3.2.

Table 3.2 Information regarding the used materials in the model.

	<b>Layers of wall component</b>	<b>Source</b>	<b>Thickness (m)</b>
<b>1</b>	Regular Lime Stucco	North America Database	0.005
<b>2</b>	Lime Plaster (Stucco, A-value:3.0 kg/m <sup>2</sup> h <sup>0.5</sup> )	Fraunhofer-IBP – Holzkirchen, Germany	0.045
<b>3</b>	Solid Brick, historical	TU Wien, Austria	0.700

### 3.2.3.2 Simulation inputs and settings

The building model was generated with the following input data and program settings. The outdoor heat transfer coefficient is calculated by WUFI as a function of wind speed. The wind-dependent heat transfer resistance parameter was calculated by using the climate data from the weather file. For the indoor heat transfer coefficient, a constant (default) value is used. The value of short-wave radiation absorptivity corresponds to a bright-colored surface. Ground short-wave reflectivity was set to 0.2 and the adhering fraction of rain to 0.7 (function of the wall inclination). To ensure unidirectional heat and moisture transfer along the x axis (vertical direction), the lower and upper boundaries were defined as perfectly insulated and impermeable. The input information and settings, including the rain coefficient and surface transfer properties, together with their initial values are shown in Table 3.3.

Material properties were assigned based on WUFI material databases (see Table 3.2). The hygro-thermal and physical characteristics of the materials required for the simulations in WUFI are presented in Table 3.4 and Table 3.5.

Table 3.3 Inputs and settings of WUFI

Settings and inputs		Value
Orientation/	Orientation	South
Height/	Height [m]	<10
Inclination		Short building
	Inclination [°]	90
Building height-driven rain coefficient	Rain load	$R1[-] = 0$
	$=\text{Rain} \cdot (R1 + R2 \cdot \text{Wind velocity})$	$R2[\text{s/m}] = 0.07$
Surface transfer coefficient	Thermal resistance of exterior surface [ $\text{m}^2 \cdot \text{k} \cdot \text{W}^{-1}$ ]	Function of wind speed
	Sd-Value of exterior surface [m]	0 (No coating)
	Short wave radiation absorptivity	0.2
	Ground short wave reflectivity	0.2
	Adhering fraction of rain	0.7
	Thermal resistance of interior surface [ $\text{m}^2 \cdot \text{k} \cdot \text{W}^{-1}$ ]	0.125
	Sd-Value of Interior surface [m]	0 (No coating)

Table 3.4 Material basic properties input data

<b>Basic properties</b>	<b>Lime stucco</b>	<b>Lime plaster</b>	<b>Solid brick</b>
Layer thickness [m]	0.005	0.045	0.70
Bulk density [kg.m <sup>-3</sup> ]	1769	1600	1800
Porosity [m <sup>3</sup> .m <sup>-3</sup> ]	0.274	0.3	0.31
Specific heat capacity [J.kg <sup>-1</sup> .K <sup>-1</sup> ]	840	850	850
Thermal conductivity (dry material at 10°C) [W.m <sup>-1</sup> .K <sup>-1</sup> ]	0.343	0.7	0.6
Water vapor diffusion resistance factor [-]	310.6	7	15

Table 3.5 Material hygro-thermal properties input data

<b>Hygro-thermal properties</b>	<b>Lime stucco</b>	<b>Lime plaster</b>	<b>Solid brick</b>
Reference water content (RH 80%) [kg.m <sup>-3</sup> ]	Hygrothermal function	Hygrothermal function	4.5
Free water saturation (RH 100%) [kg.m <sup>-3</sup> ]	Hygrothermal function	Hygrothermal function	230
Water absorption coefficient (A-value) [kg.m <sup>-2</sup> .s <sup>-0.5</sup> ]	Hygrothermal function	Hygrothermal function	0.36
Moisture-dependent thermal conductivity supplement [%.M <sup>-1</sup> % <sup>-1</sup> ]	Hygrothermal function	8.0	15
Temperature-dependent thermal conductivity [W.m <sup>-1</sup> .K <sup>-2</sup> ]	0.0002	0.0002	0.0002

The indoor climate condition was created using a function of sine curve (Arena and Mantha 2013) provided by WUFI, according to the WTA guideline 6-2-01/E (WTA 2004). The temperature and humidity values required for the indoor climate condition calculations were defined based on the actual measured data from a similar building (i.e., The Holy Rosary Church Kalawar, Bangkok, Thailand which is selected as a case-study building in Chapter 4) in 2016 (see Table 3.6). Initial conditions in this model included a layer temperature of 25°C and a relative humidity of 80% (see Table 3.7).

The outdoor climate file generation was based on the measured data from the Thai Meteorological Department, using Meteororm software version 7.1.5 (Meteororm 2020). It is available in one-hour steps and sufficient to repeat the same year reaching the end of the simulation period (see Table 3.7).

Table 3.6 The temperature and humidity values required for the indoor climate condition calculations

	Temperature	Relative humidity
Mean Value (°C)	25	55
Amplitude (°C)	5	25
Day of Maximum	27/04/2016	16/10/2016

Table 3.7 Initial conditions in this model as well as calculation period

Duration (hour)	Initial conditions in component (Constant across component)	
	T (°C)	φ (%)
35,064	25	80

### 3.2.3.3 Hygro-thermal simulation outcomes

The outcomes of hygro-thermal simulation presented in this chapter are water content, relative humidity and temperature. The detailed definitions of each outcome are listed in Chapter 2, section 2.2.3.3.

### 3.2.4 Evaluation criteria

As previously mentioned, model input parameters and assumptions of any model input are known with uncertainty. Consequently, the goal in this chapter is to determine the change in model output data as the result of variations in the model input data by using sensitivity analysis (SA). It should be noted that in this study one parameter is changed at a time (local sensitivity analysis). The local sensitivity analysis (LSA) was applied to identify the choice of material properties that have noticeable impact on the main model outcomes including water content (%), temperature (°C) and relative humidity (%) at different positions along the wall (see, Figure 3.12, P1 to P3). To perform the analysis, the material properties (solid brick properties) were varied in 6 steps (i.e., ±10%, ±20%, and ±30%) (see Table 3.9) from the initial values (see Table 3.8). In total 37 simulation runs (initial model, plus six varying cases for six input parameters) were carried out with the assumption that these parameters can be varied independently.

Table 3.8 The properties of lime stucco, lime plaster and solid clay brick serving as the model input parameters (the model initial values) (source: Pinich 2018)

Input variable	Units	Stucco	Plaster	Solid brick
Water absorption coefficient [A]	kg.m <sup>-2</sup> .s <sup>-0.5</sup>	0.005	0.05	0.36
Porosity [n]	m <sup>3</sup> .m <sup>-3</sup>	0.274	0.3	0.31
Density [ρ]	kg.m <sup>-3</sup>	1769	1600	1800
Thermal conductivity [λ]	W.m <sup>-1</sup> .K <sup>-1</sup>	0.343	0.7	0.6
Specific heat capacity [Cp]	J.kg <sup>-1</sup> .K <sup>-1</sup>	840	850	850
Water vapor diffusion resistance factor [μ]	-	310.6	7	15

Table 3.9 The properties of solid clay brick with 6-step varied values

Input variable	-10%	+10%	-20%	+20%	-30%	+30%
Water absorption coefficient [A]	0.05	0.36	0.32	0.40	0.29	0.44
Porosity [n]	0.3	0.31	0.28	0.34	0.25	0.37
Density [ρ]	1600	1800	1620	1980	1440	2160
Thermal conductivity [λ]	0.7	0.6	0.54	0.66	0.48	0.72
Specific heat capacity [Cp]	850	850	765	935	680	1020
Water vapor diffusion resistance factor [μ]	7	15	13.50	16.50	12.00	18.00

Two statistical indicators, which are relative error (Othmen et al. 2014), particularly called in this study as relative deviation, and coefficient of variation (CV), were used as indicators of sensitivity analysis. For the purpose of the analysis, the calculated performance indicators were compared to those of the initial model. The relative deviation, represented by  $\delta y$ , was calculated by the formula below (Othmen et al. 2014):

$$\delta y(\%) = 100 \frac{|y_{sim} - y_{ref}|}{y_{ref}} \quad (\text{Eq. 3.1})$$

Where,  $\delta y$  is the relative deviation,  $y_{sim}$  is the output value determined with varied parameter ( $\Delta = \pm 10\%, \pm 20\%, \pm 30\%$ ) and  $y_{ref}$  is the initial output value ( $\Delta = 0\%$ ). The relative deviation ( $\delta y$ ) is calculated from the time evolution of water content, relative humidity and temperature during the simulation period. Statistical calculation of the

relative deviation was performed for the different parameters and presented the results by means of the “Box and Whiskers Plot” or “Quartile Boxes” (see Chapter 2 for the definition). In addition, the mean value of relative deviation was calculated to establish sensitivity classification.

Another selected measure is the coefficient of variation (CV), which is a statistical measure of the distribution of data points in a data series around the mean. It represents the ratio of the standard deviation to the mean so that it is possible to compare the degree of variation from one data series to another.

The input variables were subsequently classified in three groups with low, medium, and high influence on the simulation outcomes. The categorization was done based on i) the mean value of relative deviation, and ii) the CV. The threshold for the classifications is presented in Table 3.10.

Table 3.10 Threshold of the sensitivity classification based on mean relative deviation and coefficient of variation (CV) values (source: Pinich 2018)

Sensitivity class	Thresholds for the sensitivity classification	
	Mean	CV
<b>Low</b>	Mean $\leq$ 0.3	CV $\leq$ 0.7
<b>Medium</b>	0.3 < Mean $\leq$ 0.6	0.7 < CV $\leq$ 1.4
<b>High</b>	0.6 < Mean	1.4 < CV

## 3.3 Results and discussion

### 3.3.1 Results

The results presented in this section are obtained by performing 37 simulation runs, varying 6 model input parameters in terms of 6 steps (from -30% to +30%, with intervals of 10%).

To illustrate the influence of material-related input parameters on the main simulation outcomes (i.e., water content, relative humidity, and temperature), the mean relative deviations (from the initial model) of calculated hourly water content, relative humidity, and temperature were computed at three positions in the middle of each layer in the construction (Figure 3.12, P1 to P3). The results are presented in Figure 3.13 for calculated water content, in Figure 3.14 for calculated relative humidity and in Figure 3.15 for calculated temperature, which are the outcomes of varying water absorption coefficient ( $A$ ), porosity ( $n$ ), density ( $\rho$ ), thermal conductivity ( $\lambda$ ), specific heat capacity ( $C_p$ ) and water vapor diffusion resistance factor ( $\mu$ ), respectively.

The findings from the water content and relative humidity analyses indicate that these parameters are more sensitive to two of the investigated material properties, namely water absorption coefficient ( $A$ ) and water vapor diffusion resistance ( $\mu$ ) (see Figure 3.13 and 3.14).

According to the outputs derived from the temperature analysis (see Figure 3.15), thermal conductivity ( $\lambda$ ) is the most influential parameter, followed by density and specific heat capacity. As a contrast, thermal conductivity has a moderate influence on relative humidity.

Overall, P2 (Figure 3.12, solid brick layer) is identified as the most sensitive position to all the material parameters except thermal conductivity with respect to the mean relative deviation of the calculated relative humidity and temperature. P3 (Figure 3.12, internal plaster layer) is more sensitive to thermal conductivity than the second position in those two calculated outcomes (relative humidity and temperature).

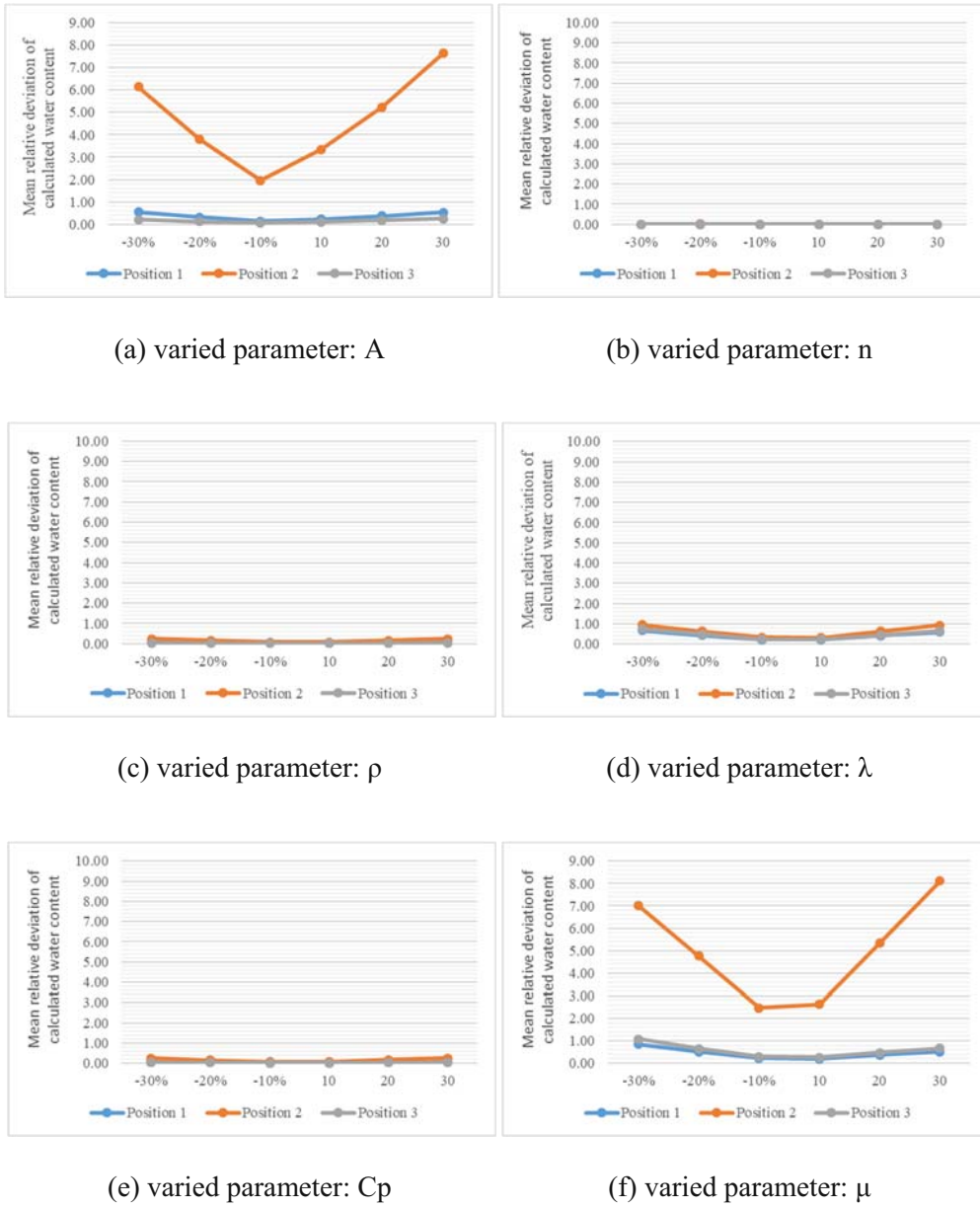


Figure 3.13 Mean relative deviations (from the initial model) of calculated hourly water content values in the three layers as a result of varying (a)  $A$ , (b)  $n$ , (c)  $\rho$ , (d)  $\lambda$ , (e)  $C_p$ , (f)  $\mu$

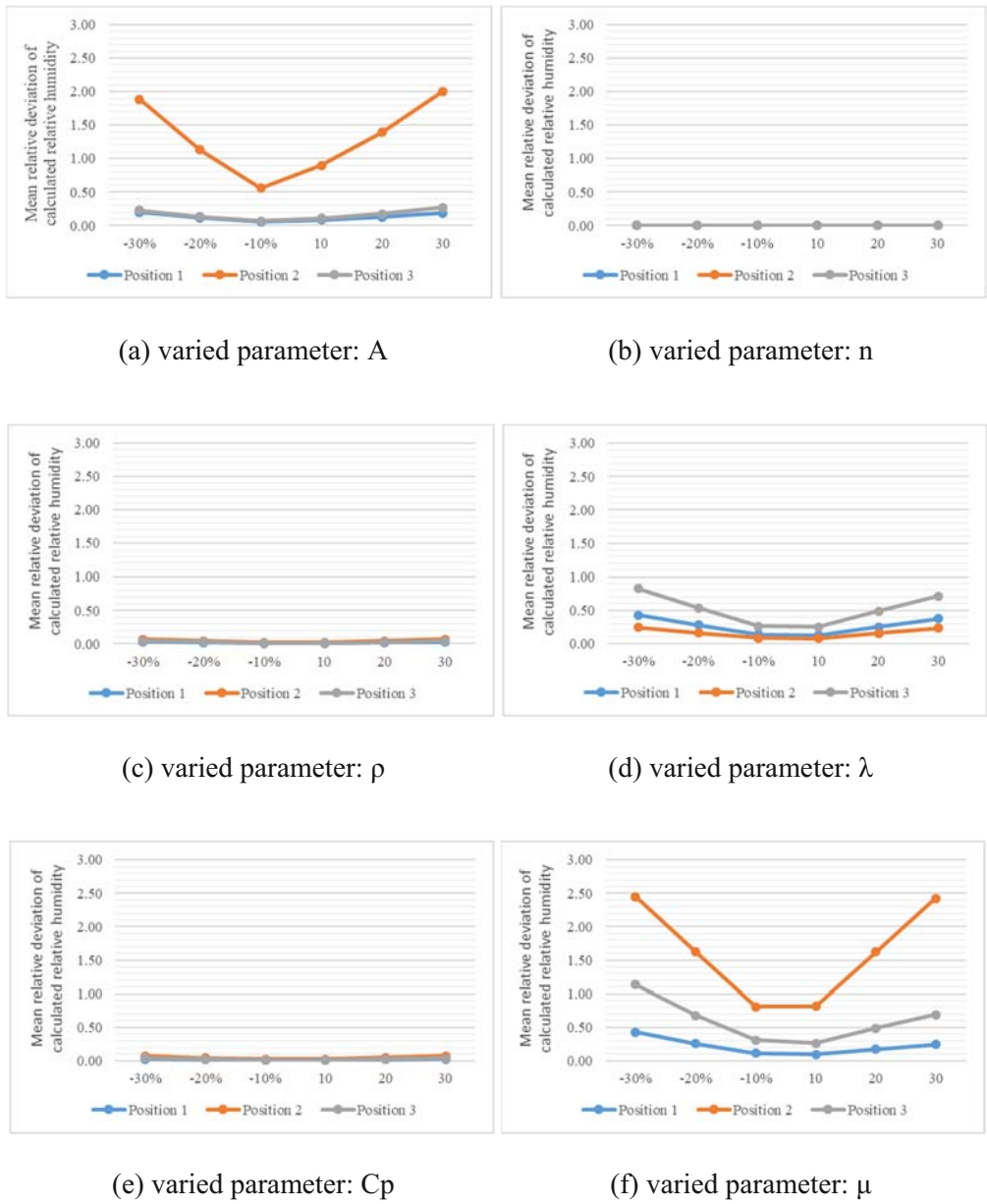


Figure 3.14 Mean relative deviations (from the initial model) of calculated hourly relative humidity values in the three layers as a result of varying (a)  $A$ , (b)  $n$ , (c)  $\rho$ , (d)  $\lambda$ , (e)  $C_p$ , (f)  $\mu$

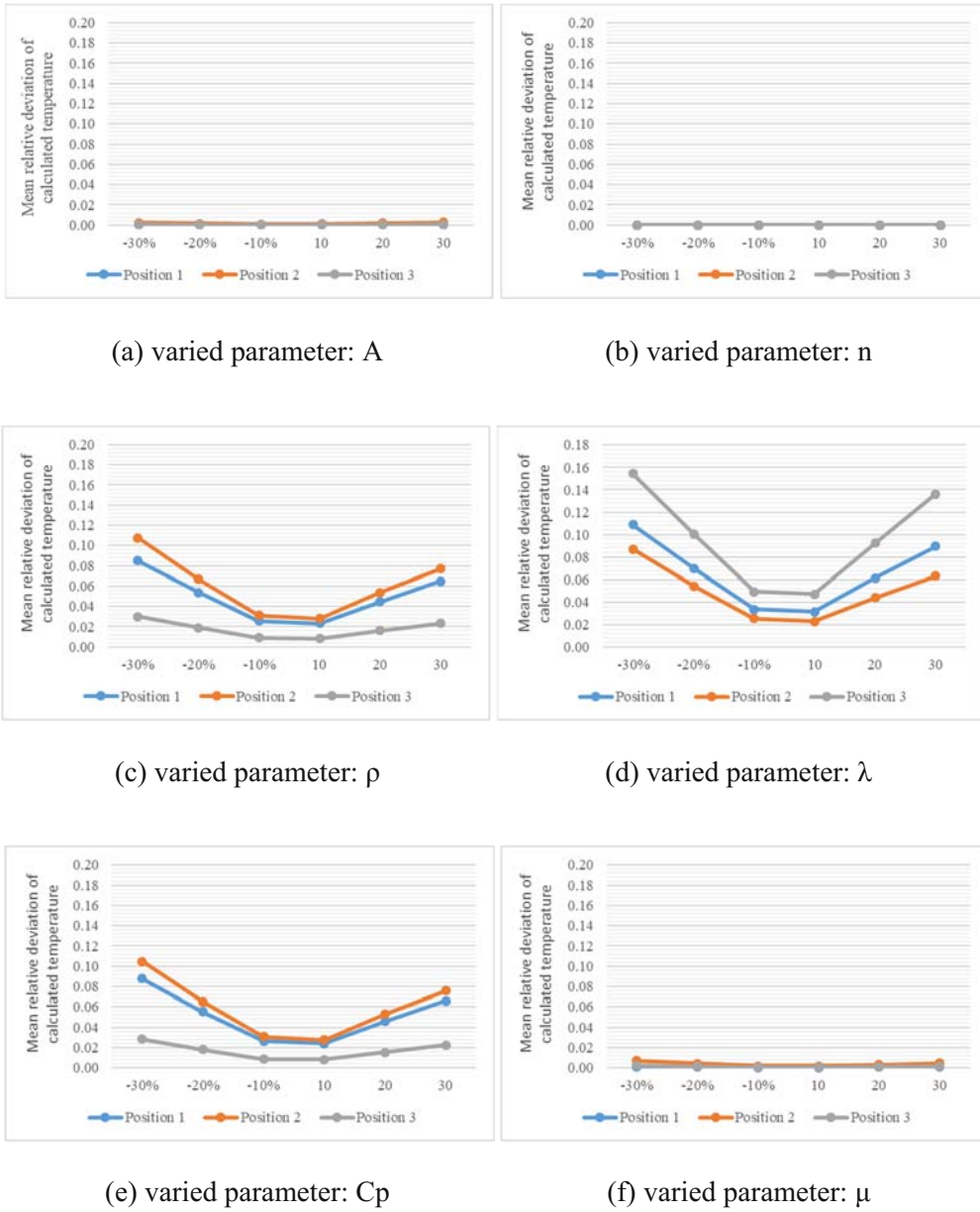


Figure 3.15 Mean relative deviations (from the initial model) of calculated hourly temperature values in the three layers as a result of varying (a)  $A$ , (b)  $n$ , (c)  $\rho$ , (d)  $\lambda$ , (e)  $C_p$ , (f)  $\mu$

In order to classify the parameters into three categories (i.e., low sensitivity, medium sensitivity and high sensitivity) with respect to their influence on the simulation outputs, the calculated statistical indicators (i.e., mean relative deviation and coefficient of variation) are averaged over the three positions (Figure 3.12, P1 to P3).

Table 3.11 Calculated mean relative deviation and coefficient of variation (CV) values over the 6 steps of respective input variable alteration averaged over the three positions (source: Pinich 2018)

Input variable	Water content		Temperature		Relative humidity	
	Mean	CV	Mean	CV	Mean	CV
Water absorption coefficient [A]	1.73	1.03	0.06	0.87	0.53	0.82
Porosity [n]	0.00	1.91	0.00	2.1	0.00	1.49
Density [ $\rho$ ]	0.07	0.65	0.04	0.90	0.03	0.57
Thermal conductivity [ $\lambda$ ]	0.50	0.87	0.07	0.75	0.31	0.80
Specific heat capacity [Cp]	0.07	0.67	0.04	0.91	0.03	0.63
Water vapor diffusion resistance factor [ $\mu$ ]	0.02	0.86	0.00	0.65	0.81	0.83

Tables 3.12 and 3.13 categorize the input variables with low, medium and high sensitivities, with respect to the mean relative deviation and CV values calculated in Table 3.11.

Based on the classification shown in Tables 3.12 and 3.13 the observation can be made as follows.

- Porosity (n), has a strong impact on all three performance indicators in view of CV with less significance in relation to the mean relative deviations.
- The water absorption coefficient (A) and thermal conductivity ( $\lambda$ ), are classified into the medium and high sensitivity categories based on both statistical indicators, namely mean deviations and CV.
- With respect to the mean relative deviations of the results, calculated temperatures are the least sensitive to all of the above-mentioned material properties. By looking at the detailed results in each position (Figure 3.12, P1 to P3), the maximum calculated mean relative deviations in temperature is 0.15 K in interior plaster (Figure 3.12, P3), when the thermal conductivity ( $\lambda$ ) is varied for  $\pm 30\%$ .

- Considering the mean relative deviations, water vapor diffusion resistance ( $\mu$ ) falls into the high sensitivity category, exhibiting substantial impact on water content and relative humidity. Based on the CV classification,  $\mu$  falls in the medium sensitivity class. However, for temperature calculations, it has little consequence.
- Density ( $\rho$ ) and specific heat capacity ( $C_p$ ) fall in the low-sensitivity class for all performance indicators, except for the temperature with respect to the calculated CVs.

Table 3.12 Classification of six input parameters with respect to the mean relative deviation (source: Pinich 2018)

Sensitivity	Parameter		
	Water Content	Temperature	Relative humidity
Low	n, $\rho$ , $C_p$	n, $\rho$ , $C_p$ , $\lambda$ , A, $\mu$	n, $\rho$ , $C_p$ , $\lambda$
Medium	$\lambda$	-	$\lambda$ , A
High	A, $\mu$	-	$\mu$

Table 3.13 Classification of six input parameters with respect to the coefficient of variation, CV (source: Pinich 2018)

Sensitivity	Parameter		
	Water Content	Temperature	Relative humidity
Low	$C_p$ , $\rho$	$\mu$	$C_p$ , $\rho$
Medium	A, $\lambda$ , $\mu$	$C_p$ , $\rho$ , A, $\lambda$	A, $\lambda$ , $\mu$
High	n	n	n

In general, based on the mean relative deviations, it can be seen from the above-mentioned results that the most influential parameters are the water vapor diffusion resistance factor ( $\mu$ ), the water absorption coefficient (A), and the thermal conductivity ( $\lambda$ ).

Considering the CV of deviations, the most influential parameter is porosity (n), followed by water vapor diffusion resistance factor ( $\mu$ ), water absorption coefficient (A), thermal conductivity ( $\lambda$ ), specific heat capacity ( $C_p$ ), and density ( $\rho$ ).

To provide an example for the distribution of the deviations, Figures 3.16 and 3.17 present box plots of the calculated relative deviations of the parameters classified as highly influential with respect to water content (i.e., A and  $\mu$ ), and relative humidity (i.e.,  $\mu$ ) in the brick layer (Figure 3.12, P2).

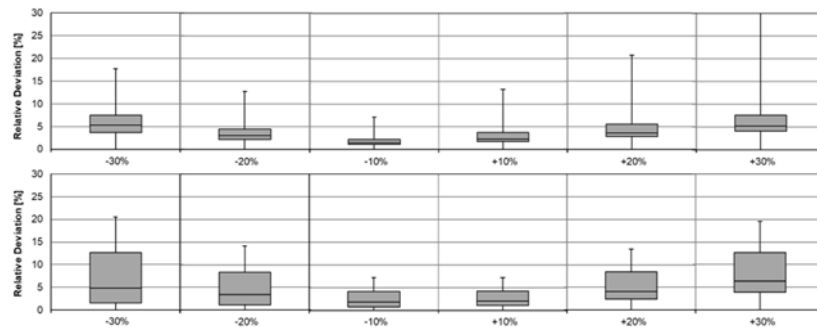


Figure 3.16 Box plots of relative deviations (from the initial model) of calculated hourly water content values in the brick layer as a result of varying A (Upper chart) and  $\mu$  (Lower chart) (source: Pinich 2018)

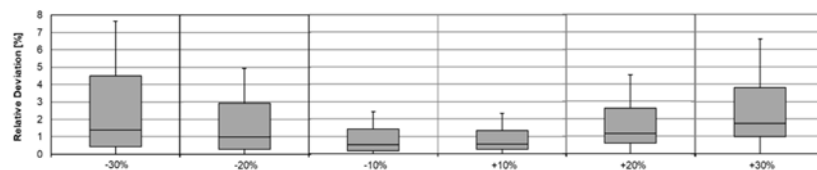


Figure 3.17 Box plot of relative deviations (from the initial model) of calculated hourly relative humidity in the brick layer as a result of varying  $\mu$  (source: Pinich 2018)

Moreover, an additional observation can be made directly from raw simulation outputs (i.e., water content, relative humidity and temperature). Figure 3.18 presents the water content time evolution at solid brick layer (Figure 3.12, P2) in the wall. The figures (3.18) is related to different values of water vapor diffusion resistance ( $\mu$ ) (reference value and 6-varying values from -30% to +30%, with intervals of 10%). The results of water vapor diffusion resistance ( $\mu$ ) was chosen to be presented due to its great impact on the simulation outcome (i.e., water content). As is illustrated by the graph (Figure 3.18), the impact of varying the input parameters on the simulation results gradually decrease with time.

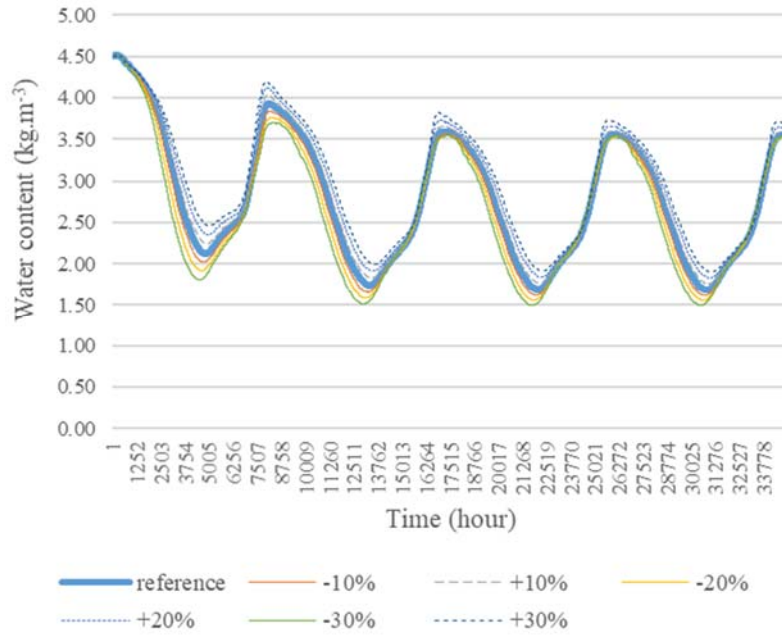


Figure 3.18 Time evolution of the water content for water vapor diffusion resistance ( $\mu$ )

### 3.3.2 Conclusion

This chapter reported on a case study concerning the hygro-thermal performance of the exterior brick wall of a historical building in Thailand (Thai temple). The hygro-thermal simulation model of the wall was subjected to a systematic sensitivity analysis to classify a subset of the material-related input variables, which significantly influence the simulation outcomes, comprising material water content, temperature and the relative humidity of the air pores in the material.

The simulations were carried out for a multilayer Thai historical wall in the tropical climate. Needless to say, the same model used in a different climate conditions could result in a different sensitivity classification. In addition, the results obtained in this chapter are relative to 0.8 m thick solid wall (i.e., clay brick, lime plaster and lime stucco). Therefore, for future research, other construction types and configurations should be studied. Moreover, additional efforts are required to evaluate the sensitivity of the hygro-thermal performance indicators to other material properties, such as water absorption isotherm or other model input variables, such as Sd-value of exterior surface.

## Chapter 4

# Hygro-thermal analysis of a historical building in tropical climate and the presence of moisture problems

## 4.1 Background

### 4.1.1 Efflorescence: A Moisture-Related Deterioration in Masonry Construction

Understanding of the various properties of construction materials is beneficial not only in terms of suitability but also in terms of preventing future deteriorations. Furthermore, understanding the mechanisms of potential material deterioration can lead to more evidence-based assessments of the surrounding conditions and the causes. Acquiring these insights can facilitate architects and engineers in determining as well as mitigating or eliminating altogether the unfavorable conditions for the materials.

According to Beall (1999), temperature, ultraviolet radiation, wind, moisture, ozone, carbon dioxide, pollution and freeze-thaw represent the various factors that can contribute to material degradation. In a publication by the American Society of Civil Engineers, Nicastro (1997) defines the durability of a material as “the quality of maintaining satisfactory aesthetic, economic, and functional performance for the useful life of a material or system.” Considering moisture-related damage as the most pervasive problem, Beall (1999) further emphasizes the need for selecting the right materials to suit the right environment: “Durability results from choosing a material with the right physical characteristics for its environment” (p. 5).” In fact, building materials can suffer from moisture-related deteriorations in many ways: expansion and contraction, mold and mildew growth, corrosion, decay, freeze-thaw damage, delamination and adhesion loss, thermal resistance reduction, efflorescence and insect infestation (Beall 1999). When it comes to porous materials like masonry bricks used in wall construction, however,

efflorescence and its effects on the wall construction constitute a major concern.

Efflorescence is a physical process in which salt or other minerals essentially held in solution migrate from within a porous material to the surface, leaving clearly visible residues, as “water-soluble salts brought to the surface of masonry in solution of water and deposited there by evaporation” (Wilson 1984, p. 109) (see Figure 4.1). Beall (1999) states that three conditions must happen simultaneously in order for efflorescence to occur: (1) soluble salt must be present; (2) water must be present and in contact with the salt in a duration long enough to move them into solution; and (3) the pore structure must allow the salt solution to migrate to a surface where evaporation can take place. Efflorescence, a natural occurrence, is commonly white in color; however, green deposit (normally referred to as green stain) can also be found in some ceramic units. Occasionally, brown stain occurs when manganese compounds are present (Wilson 1984).



Figure 4.1 Efflorescence on the wall surface  
(source: Iaqsolutions 2020)

Identifying the sources of efflorescence is made complicated by the many available sources of soluble compounds (Wilson 1984). Commonly found salts in efflorescence are sulfate and carbonate compounds of sodium, potassium, calcium, magnesium, and aluminum. Chlorides rarely occur as efflorescence, but there is an increased likelihood when masonry units or mortar sand is contaminated by sea water or runoff from alkaline soils (Wilson 1984). Decomposition of subterranean organic compounds can also add acidity to the soil and the forming of salt substrate can subsequently effect efflorescence in masonry brick construction situated on or within the very soil (Aranyanak 1983).

In maintaining the satisfactory aesthetic of a construction, efflorescence therefore poses as a significant hindrance. At the same time, the potential damage beyond the surface of the porous materials poses a serious threat as substantial growth of salt or other mineral deposits within the pores can accelerate cracks and the eventual disintegration of the material (Wilson 1984, Watsantachad 2006). As the case study building illustrates in the following sections, accumulation of

moisture in the wall construction proves to be a strong factor that indicates the impact of rising damp problems.

#### 4.1.2 Building defects and diagnosis

The majority of building defects are caused by dampness or high moisture content in building components. Visually identifiable, building defects typically occur in both new-design buildings and old ones, but are more common in older structures such as historical ones (Bakri and Mydin 2014, Ramsom 1981). According to Bakri and Mydin (2014), “as in BS 3811 (Code of Practice, British Standard 1984), defects are defined as “the deterioration of building features and services to unsatisfactory quality levels of requirement of the users.” (p.4).

Building defects can be categorized either as (1) structural or (2) non-structural defects. Bakri and Mydin (2014) argue that “any defect in a structural element of a building that is attributable to defective design, defective or faulty workmanship or defective material and sometimes any combination of these” can be identified as structural defects (p.5). Bakri and Mydin (2014) also argue that non-structural defects, on the other hand, signify defect in brick work, dampness in old structures and defects in plaster work.” (p.5). Regardless of the types of defects, various symptoms of defects can be commonly found in historical building materials. Such defects may include decay, blister, rotten timber, rusty steel, deformation, erosion, cracking, staining of water or soluble mineral, and plaster peeling (Halim et a. 2012, Bakri and Mydin 2014).

Dampness problems can be identified as physical defects on building surfaces (Halim et a. 2012). Caused by dampness on masonry constructions, the specific characteristics of the defects that can be visually identified include symptoms such as surface cracks, stains (e.g., black, gray, or green water-soluble mineral stains), crystal deposits (i.e., water-soluble salts) on the building surface, and biological plants (e.g., fungi, mosses, and creeping plants). Moisture-related defects commonly affecting the wall paint include paint flaking, paint peeling and blistering of paint (Halim et a. 2012).

As a part of the investigation process, the study of building defects is a necessary tool for gaining valuable insights into the damaged conditions of historical buildings. In terms of diagnosis and identifying retrofit solutions, three types of procedures can be applied in the dampness study: (1) visual inspection; (2) non-destructive method; and (3) destructive method. Whereas the non-destructive method requires the use of moisture measuring instruments (e.g., protimeter), which essentially leaves the construction intact, the latter is the least commonly used procedure since different tools (e.g., drills) and techniques (e.g., ion test, oven drying) involved may ultimately damage the building elements.

When measurement devices are not available, visual inspection is a viable option and can be performed as a preliminary assessment. With

regard to dampness problems caused by leakage, condensation or rising damp, a careful observation of the physical defects on the surfaces can provide insights into the contributing factors (Halim et al. 2012).

Nevertheless, this procedure is highly subjective in nature, specifically for complex systems, its accuracy will depend largely on the experience of the surveyor (Halim et al. 2012). Moreover, using this procedure to determine appropriate retrofit options may not be strategically effective for long-term refurbishment decisions. As the contributing factors and the surrounding conditions vary on a daily basis, integrating this procedure with prediction tools such as simulation software can help increase the accuracy of the findings and enhance retrofit decision making. In circumstances where provisions of measurement tools are limited, using calculation tools is a useful alternative. In this study, a hygro-thermal simulation software known as WUFI (2020a) is deployed.

#### 4.1.3 Capillary rise in historical wall

The accumulation of water, specifically in terms of rising damp, in historical building components is caused by a number of factors ranging from condensation, precipitation to capillary rise of water through the ground (e.g., agricultural irrigation, poor drainage, rainfall, and underground water currents). In fact, capillary rise of groundwater through masonry brick wall is a worldwide phenomenon leading to moisture presence in historical buildings which may cause degradation of materials, building component decay, structural failure, and mold growth (Ibrahim et al. 2014). The latter can lead to indoor air quality problems and negatively affect the inhabitants' health (Franzoni 2014).

Water capillary rise is a phenomenon defined by the prevalence of the adhesive forces, between water and capillary surfaces, compared with the cohesive forces, between the water molecules itself (Franzoni 2014). An ideal of water rise phenomenon presents as a cylindrical tube of radius  $r$  (see Figure 4.2a) which was primarily investigated by Laplace (Dullien and Batra 1970) and later by Jurin (Alfano et al. 2005). According to Jurin's law, the capillary suction is greatest in small capillaries and inversely proportional to the pore radius (Rirsch and Zhang 2010). The water rise height  $h$  can be expressed by Jurin in the following equation (Sandrolini and Franzoni 2007, Franzoni 2014, Rirsch and Zhang 2010):

$$h = (2\tau \cos \theta) / (\rho g r) \quad (\text{Eq. 4.1})$$

Where,  $\theta$  is the contact angle between water and capillary surfaces,  $T$  the surface tension,  $\rho$  the liquid density, and  $g$  the gravity acceleration. This equation explains the relationship between height of water rise and pore size. Given their porous nature, capillary rise is a prevalent concern in building materials, such as brick, stone, and mortar (Franzoni 2014). The pore size of brick and mortar can be as small as 0.001 mm. Hence,

there is significant potential for rising damp (Reimondo et al. 2009). The water capillarity is governed by the above equation (Eq. 4.1); however, in reality there are more factors that should be taken into consideration.

There are many in-situ building observation studies about rising damp in terms of water rise height. According to Franzoni (2014), “the rise height is usually around 0.5-0.15 m, up to about 4 m, but it actually depends on the thickness of the wall and the evaporation conditions” (p.125). Massari G. and Massari I. (1985) argued that in the church of San Bernado in Rome, where wall thickness is 4 m, rising damp reaches 5.3 m. In Venetian buildings, Falchi et al. (2018) observed that “the moisture front in Venice reaches in average the 1.5-3 m” (p.118). Moreover, Sandrolini and Franzoni (2007) expressed that “rising dampness is certainly the most frequent and severe problem, as it can reach the height of up to 2-3 m (or even more in particular cases)” (p.162). Regarding these discussions, it can be concluded that in reality there are additional parameters that may affect the water rise height.

Water rise height will reach a static level referred to as equilibrium line, the so-called maximum water rise height. A dynamic equilibrium can be reached by a balance between water uptake from capillary rise and water loss from evaporation (Guimaraes et al. 2012a, Franzoni 2014, Falchi et al. 2018) (see Figure 4.2b). The maximum water rise height is a result of the dynamic interactions among the following variables: the rate of water ingress in the wall, the rate of evaporation and the pore structure of materials in terms of pore size, porosity or amount of pores, discontinuities, to name a few (Franzoni 2014). Due to the occurrence of evaporation of water at the wall surface and pore tortuosity, the maximum water rise height is lower in actual masonry in the wall than in an ideal capillary presented cylindrical tube inferred by Jurin (Sandrolini and Franzoni 2007, Franzoni 2014). The base of walls affected by rising damp is commonly near saturation (Massari and Massari 1985).

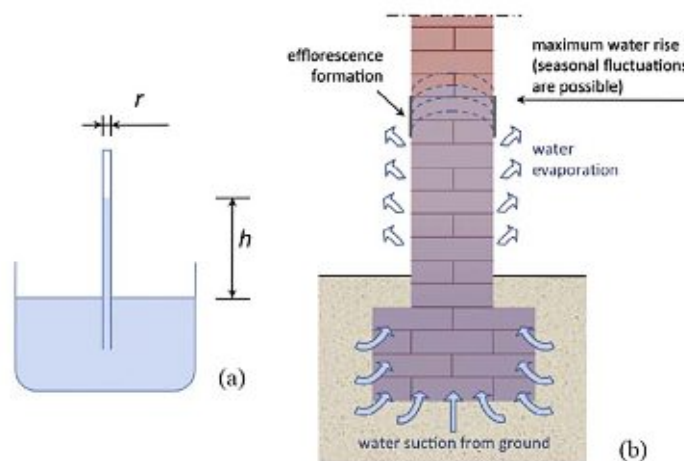


Figure 4.2 (a) water height rise in an ideal capillary tube of radius  $r$  and (b) schematic representation of water capillary rise in masonry wall (source: Franzoni 2014)

Evaporation is a substantial factor affecting rising damp. Moisture risen from the ground that affects the wall surface may be partially subject to evaporation, which is in turn influenced by the following four variables: temperature, humidity, air movement and wall surface condition (e.g., painted or unpainted wall) (Rirsch and Zhang 2010).

Mason (1974) developed a model for rising damp where capillary rise and evaporation coexisted in balance, creating evaporation equilibrium as an n-shape profile of water distribution. With evaporation introduced into the equation, the height of rise is also affected by factors relating to capillary pores, wall thickness and evaporation rate. Figure 4.3 schematically illustrates the equilibrium between capillarity and surface evaporation. An increase in the evaporation rate, as may happen due to higher surface temperatures during the summer, will also reduce the height of rise. Similarly, as the level of groundwater decreases, the height of rise also becomes lower. (Rirsch and Zhang 2010). According to Rirsch and Zhang (2010), “In a thin wall there is proportionally more evaporation than capillary rise which means that the height of rising damp front is reduced” (p.1816). This argument is echoed by Guimaraes et al. (2012b): “Another important conclusion is the effect of wall thickness in the rising damp front, the height of rise increase[s] with the wall thickness” (p. 53). Based on these considerations, it can be concluded that wall thickness has a significant influence on the height of rise.

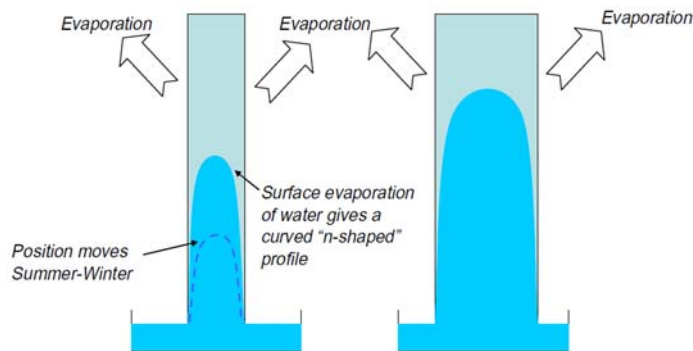


Figure 4.3 Schematic diagram of a brick wall presenting the equilibrium between capillary rise and surface evaporation (source: Rirsch and Zhang 2010)

Considering the boundary between wet and dry parts of the wall as discrete or sharp, Hall and Hoff (2007) have developed the “Sharp Front method” for rising damp with regard to capillarity and water evaporation. The situation is considered when rising damp has stabilized. Disregarding gravitational forces (see Figure 4.4), the following equation describing the height of rise in the wall is obtained (Hall and Hoff 2007, Rirsch and Zhang 2010, Guimaraes et al. 2012a).

$$H = S \left[ \frac{b}{2 e \alpha} \right]^{1/2} \quad (\text{Eq. 4.2})$$

Where,  $H$  is height of the rising damp front,  $S$  is sorptivity of the wall material,  $b$  is wall thickness,  $e$  is rate of evaporation per unit area of the wetted surface (the potential evaporation rate in the local microenvironment),  $\alpha$  is moisture content of the wetted region (as the water bulk volume).

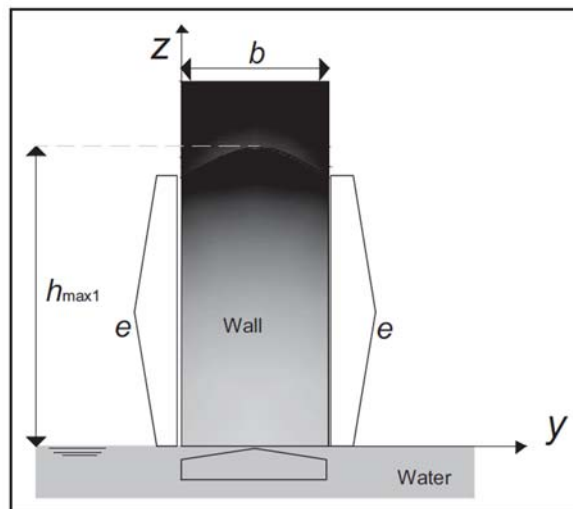


Figure 4.4 Sketch of sharp front model  
(source: Guimaraes et al. 2012a)

Since height of rise varies in direct proportion to the sorptivity of the wall material as described in Equation 3, it can be demonstrated that the sorptivity of water into the material has a strong impact on the height of rising damp front (Hall and Hoff 2007, Rirsch and Zhang 2010). Due to the direct proportion between the sorptivity  $S$  and water absorption coefficient of material  $A$  (Guimaraes et al. 2012a), water capillary height rise increases in materials with higher values of water absorption coefficient (Guimaraes et al. 2012b). Having conducted a numerical study of rising damp phenomenon, Guimaraes et al. (2012b) further substantiates that “regarding the influence of the materials’ properties, the most important parameter is the absorption coefficient of water, which was expected, since it is the parameter that best characterizes the movement of water in liquid phrase, within construction materials” (p. 328). This sentiment is also supported by Torres and Freitas (2010) and Prajapati (2018).

In this context, rising dampness in buildings can be regarded as a challenging issue as different contributing factors involved are unique to each different building and its surrounding conditions.

#### 4.1.4 Thai historical wall and foundation construction

Constructed with traditional techniques in the 19<sup>th</sup> century, a Thai church serves as the selected historical building in this chapter. Typical of Thai traditional wall structures built in the 19<sup>th</sup> century (Watsantachad 2006, Bunjerdskul 2014, Issarathumnoon 2018), both the interior and exterior walls of this church consist of three main layers, namely wall color, lime plaster, and solid clay brick. These layers together constitute the main construction of the walls. Considering that the three main layers of the wall construction are classified as porous materials with permeability (Watsantachad 2006), the passage of water through the structure is inevitable, resulting in accumulation of water in the materials (Franzoni 2014). Moreover, this passageway transports water-soluble salt and mineral substrate contained in those materials into the material's pores which can cause material degradation.

The traditional plaster and wall color, as part of the finishing layers, used in construction during this period is made of the commonly known quicklime, also known as burnt lime (Watsantachad 2006). As the limestone burns, calcium oxide (CaO) is created as a byproduct. This quicklime is later soaked in water until it turns into calcium hydroxide (Ca(OH)<sub>2</sub>), commonly known as hydrated lime, caustic lime, or builders' lime, which is then mixed with other aggregates (such as sand) to produce the lime plaster. Wall components that contain this lime material naturally contain Calcium carbonate (CaCO<sub>3</sub>), a type of water-soluble salt substrate (Watsantachad 2006). Soluble salts and minerals substrate can lead to the occurrence of efflorescence (Wilson 1984, Beall 1999).

The main layer of the wall construction from this time period is the solid brick (see Figure 4.5). Typically made from clay, mud and other mixtures from husk, sawdust and sand, the solid brick naturally contains a variety of mineral compounds such as kaolinite, mica, chlorites and quartz, to name a few (Holdridge 1963, Watsantachad 2006). As these mixtures are chemically separated, compounds such as silicon dioxide, aluminium dioxide, iron dioxide and calcium carbonate can be commonly found (Watsantachad 2006). Abundant in these water-soluble mineral compounds, efflorescence and its impact on the structure can progressively worsen without intervention.

As Wilson (1984) suggests, even where water-soluble salts exist, without water in the construction, efflorescence will not occur. However, due to the fact that such historical buildings were built deep into the ground, such porous materials used in the wall construction as well as the foundation eventually formed a water passageway conducive to rising damp problems.



(a) top view showing the width of the brick (approximately 22 cm)



(b) top view showing the length of the brick (approximately 46 cm)



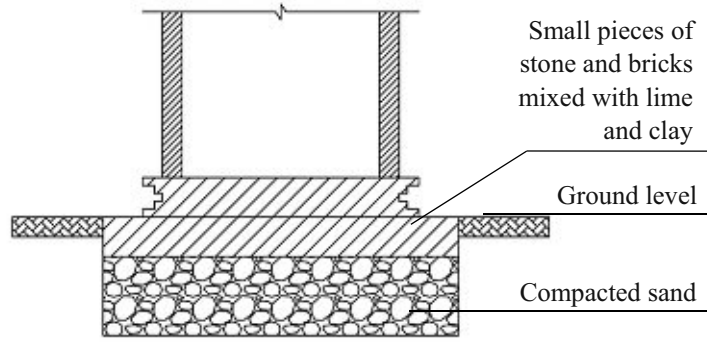
(c) side view showing the height of the brick (approximately 13 cm)

Figure 4.5 A solid brick sample made of clay with its displayed dimensions taken from Holy Rosary Church

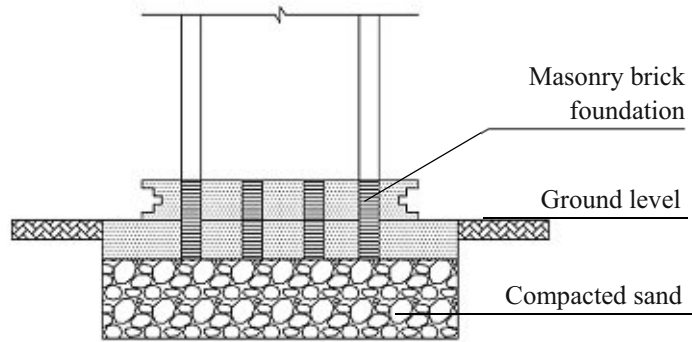
In the case of masonry brick wall, joints (so-called mortar), located vertically or horizontally, and lime plaster (i.e., interior and exterior) are possibly five or ten times more permeable than the brick itself (Wilson 1984). Additionally, in Thailand historical building structures were constructed with the traditional load-bearing wall technique (Jungsiriarrak 1997, Issarathumnoon 2018). As a structural building component, the bearing wall actively carries the weight of the above elements by conducting the whole weight (i.e., its weight and the weight of above elements) to a foundation structure (Jungsiriarrak 1997). The foundation is constructed with the same materials as the wall that spans from the ground to the top of the wall.

Foundations found in Thai historical structures can be classified as: (1) raft foundation; (2) strip foundation; which is the most common; (3) log or jar foundation; (4) buoyancy or tanked or cellular foundation; and lastly (5) pad foundation (Jungsiriarrak 1997) (see Figure 4.6). For the scope of this case study, the strip foundation was selected to represent the typical foundation from the respective era (Sacho 2008). This type of foundation relies on placing a number of masonry bricks to form strips underground as the base of the whole building with a distance of approximately 3-4 meters between each other (see Figure 4.6b). The gaps between the strips are then filled up with compacted sand. The outer foundation line serves as the base of the exterior wall of the building (Jungsiriarrak 1997). As the depth of the foundation has not been specified, an assumption has been made based on the foundation construction of another historical building within the complex of a Thai temple used previously as the case study building in Chapter 3. As Figure 4.7 illustrates, excavating the foundation confirms the construction to be masonry in nature as observed by Sacho (2008). Considering the fact that the same architect designed these buildings, it can be inferred that strip foundations from this time period could be as deep as 2.10 meters below the ground.

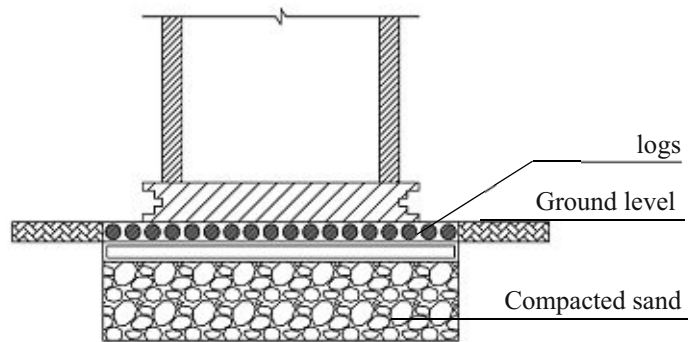
Therefore, it can be concluded that this load-bearing wall construction technique along with this particular type of foundation further aggravate the rising damp problem in allowing moisture from the ground and other water-soluble compounds to be directly absorbed into and throughout the porous masonry wall construction via capillary action.



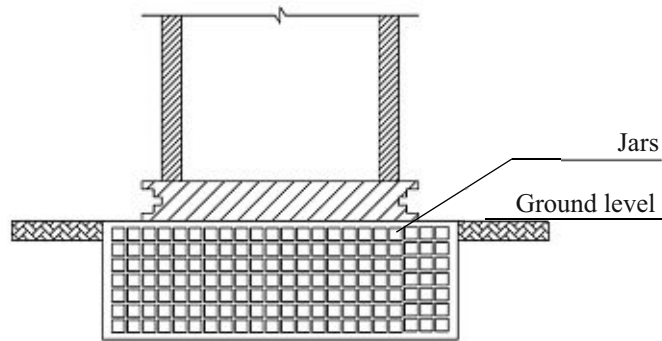
(a) raft foundation



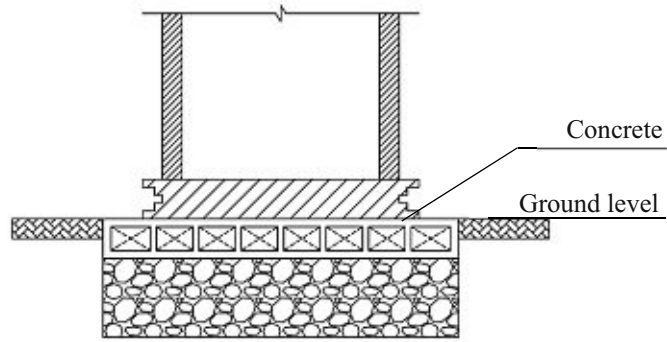
(b) strip foundation



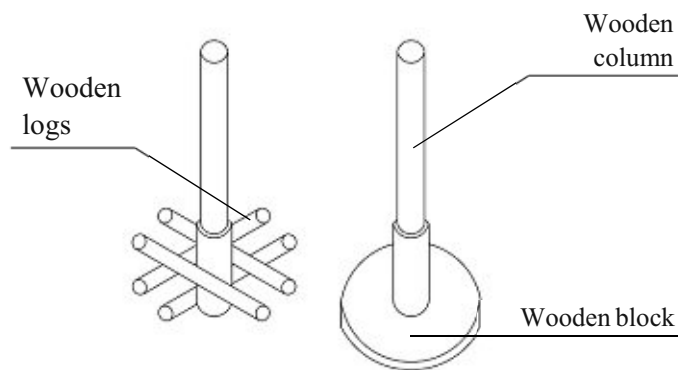
(c) log foundation



(d) jar foundation



(e) buoyancy or tanked or cellular foundation



(f) pad foundation

Figure 4.6 Simplified sketch sections of Thai traditional foundations (source: Jungsiriarrak 1997)



Figure 4.7 Foundation construction of one of the historical building (sermons hall) in Wat-Niwet-Thammaprawat temple, Ayutthaya, Thailand (source: Sacho 2008)

## 4.2 Method

### 4.2.1 Overview

The presence of water in historical brick walls is one of the most prominent problems adversely affecting architectural heritage, causing various considerable building surface and structural damages which in turn could lead to indoor air quality problems (Oxley 2003). A number of related studies have been conducted in different locations, but less attention has been paid to this problem in hot-humid climates, despite the fact that a large number of moisture-related problems exist in historical buildings in these areas. Furthermore, due to lack of diagnosis and investigation, finding causes of building material deteriorations, or so-called building defects, commonly found in historical buildings has been neglect (Halim et a. 2012).

Constructed with traditional techniques in the 19<sup>th</sup> century in Bangkok, Thailand, a hot-humid climate, a historical church affected by moisture-related deteriorations (see Figure 4.9, Figure 4.10 and Figure 4.11) serves as the case study in this chapter. In order to examine the causes of deteriorations and propose effective retrofit solutions for the affected historical facades, integrating visual inspection and a hygro-thermal performance simulation software can provide more detailed results.

Hence, the first procedure of this chapter is to perform dampness assessment using visual inspection. Any physical defects (e.g., blister, decay, stain, rotten timber, and cracks, etc.) found have been recorded in writing. Measurements and photographs have also been taken. Due to the limitations of the first procedure in terms of finding appropriate retrofit options, a numeric hygro-thermal performance simulation was considered as a supportive tool. WUFI, an advanced hygro-thermal simulation software, was used to calculate the transient heat and moisture transport in two dimensions in order to analyze cases of rising damp from groundwater (see, for example, Guimarães et al. 2012b, Torres and Freitas 2007 Holm and Künzle 2003). The simulation was conducted using actual dimensions of the case study building components, particularly, the interior and exterior walls facing four different cardinal directions (e.g., east, west, north and south). The results of the hygro-thermal analysis of historical masonry walls are presented. Retrofit options for these historical walls will be considered and examined in detail in Chapter 5.

#### 4.2.2 Building case study

The case study presented in this chapter is a Roman Catholic church named Holy Rosary Church, known to the locals as Wat-Kalawar in Thai. It is located in Samphanthawong District, on the eastern bank of the Chao Phraya River in Bangkok, Thailand (Figure 4.8). Designed by Architect Joachim Grassi, who also designed the case study building in Chapter 3, the church was constructed in 1891–97 in the style of a Gothic Revival church (Figure 4.9 – Figure 4.12), among the dwellings of Portuguese Catholics who resettled in the area after the fall of Ayutthaya, a former capital city of Thailand (Issarathumnoon 2018). The church was last refurbished in 1989 (Issarathumnoon 2018).

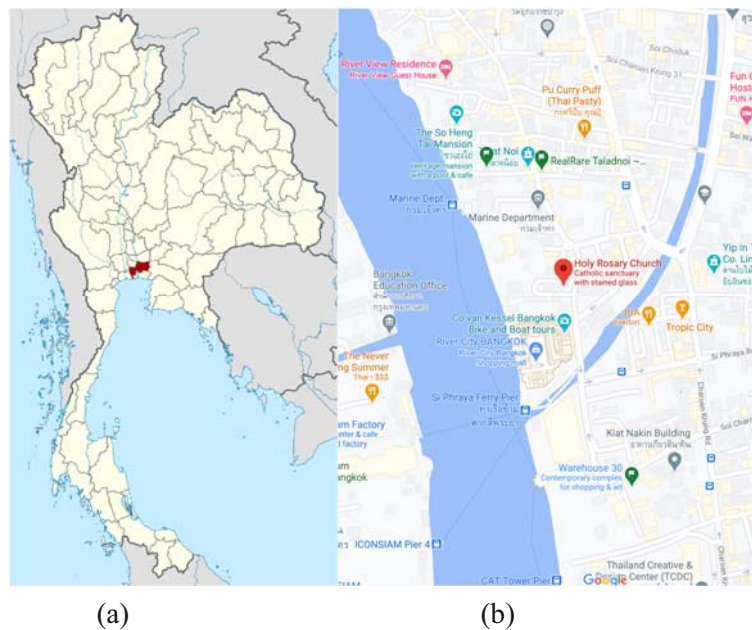


Figure 4.8 The location of (b) Holy Rosary Church (source: Googlemap 2020b), (a) Bangkok, Thailand (source: Wikimedia 2020a)



Figure 4.9 Holy Rosary Church, Bangkok, Thailand  
(source: Wikipedia 2020b)



Figure 4.10 The interior perspective of Holy Rosary Church  
(source: Wikipedia 2020b)

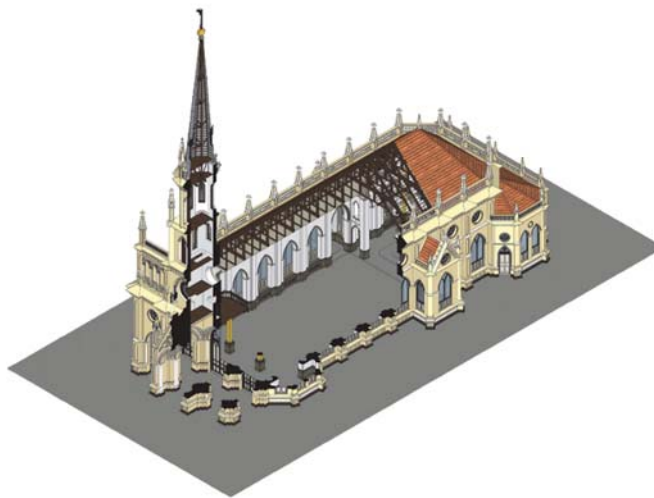
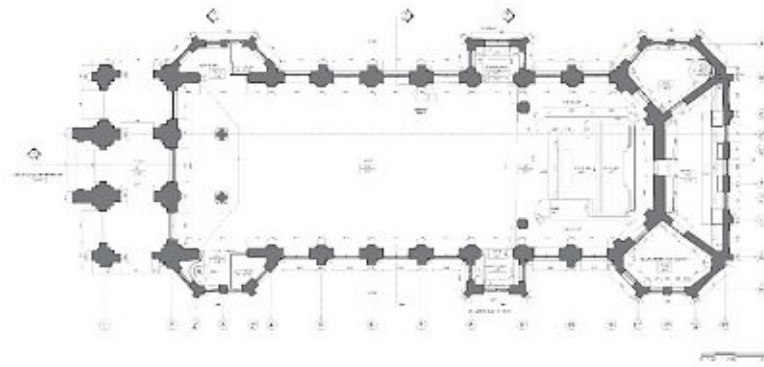
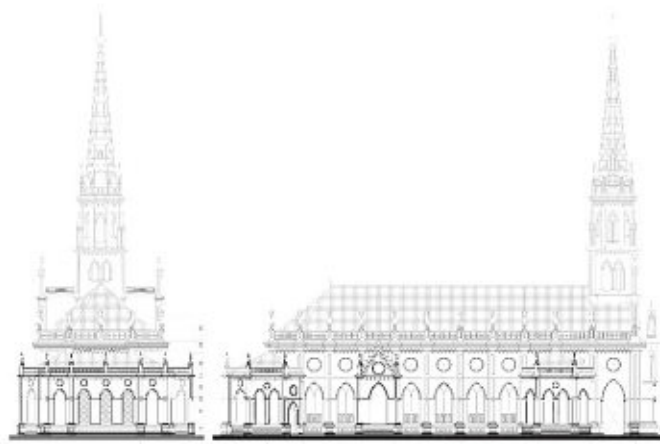


Figure 4.11 The section of isometric model of Holy Rosary Church  
(source: Arch CU 2017)



(a) plan



(b) East elevation

(c) North elevation



(d) West elevation

(e) South elevation

Figure 4.12 Architectural drawings of Holy Rosary Church  
 (i.e., (a) plan and (b) East, (c) North, (d) West, (e) South elevations)  
 (source: Arch CU 2017)

The walls of this church (i.e., interior and exterior walls), typical for Thai traditional temples from the 19<sup>th</sup> century (Watsantachad 2006, Bunjerdskul 2014, Issarathumnoon 2018), were selected for this study. From the outermost to innermost layers, the three main layers of the wall construction are respectively: (i) wall color (0.005 m); (ii) lime plaster (0.045 m); and (iii) solid clay brick (0.45 m for the interior wall and 0.60 m for the exterior walls). The foundation was constructed load bearing brick masonry (Jungsiriarrak 1997, Issarathumnoon, 2018), which is assumed to be approximately 2 m below the ground (Sacho 2008) and 0.45 m in width for supporting the interior wall and 0.60 m in width for supporting the exterior walls. The floor tiles, both interior and exterior, were made of terracotta. The interior wall and the foundation construction are presented in Figure 4.13 and 4.14. The material properties are presented in the following section.

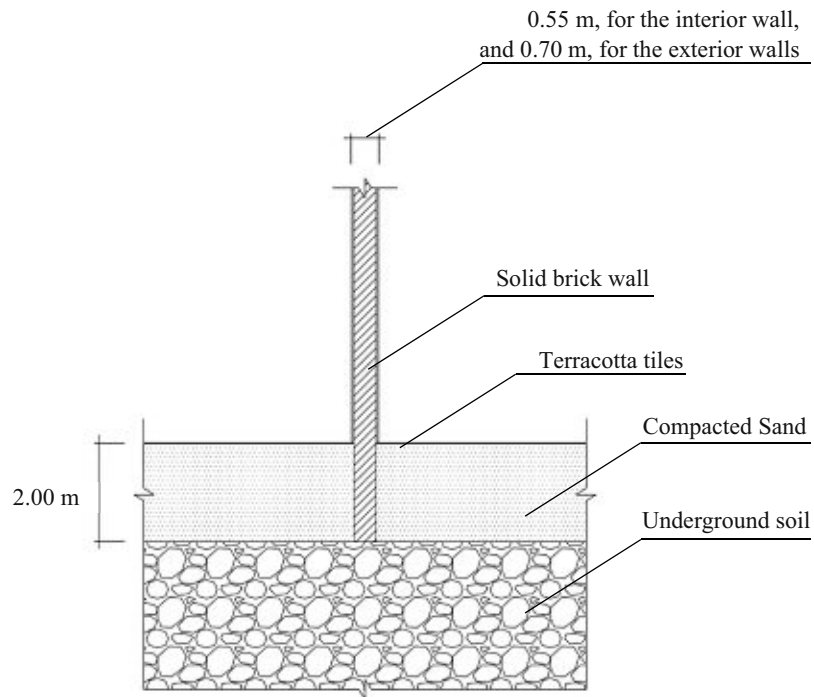


Figure 4.13 The case-study wall and the foundation construction

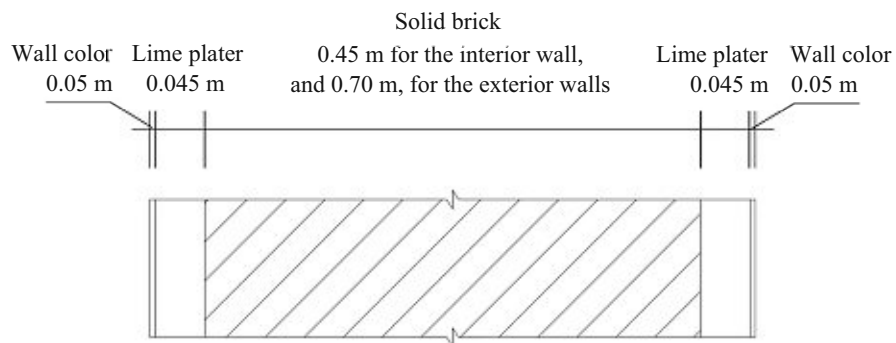


Figure 4.14 The case-study wall construction in enlarged cross-section detail.

### 4.2.3 Hygro-thermal simulation (2D)

The case study wall constructions were simulated in WUFI 2D version 3.3 (WUFI 2020c, Künzel 1998). WUFI works based on the discretization of the Künzel model by means of an implicit finite volume scheme. WUFI 2D expands the scope of WUFI Pro from one-dimensional to two-dimensional analysis, which can be applied to cases involving rising damp.

#### 4.2.3.1 Geometry modelling

There are three layers inside the building wall construction as shown in figure 4.14 consisting of wall color (0.005 m), lime plaster (0.045 m), and solid clay brick (0.45 m for the interior wall and 0.60 m for the exterior walls). The wall color layer was applied with the same material properties as lime plaster since it had lime plaster as a main admixture (Bunjerdskul 2014). The model for the foundation is designed based on an assumption of data provided from literature review (see Section 4.1.3). Figure 4.15 presents the simulation model of the building as a typical historical Thai wall construction from the 19<sup>th</sup> century.

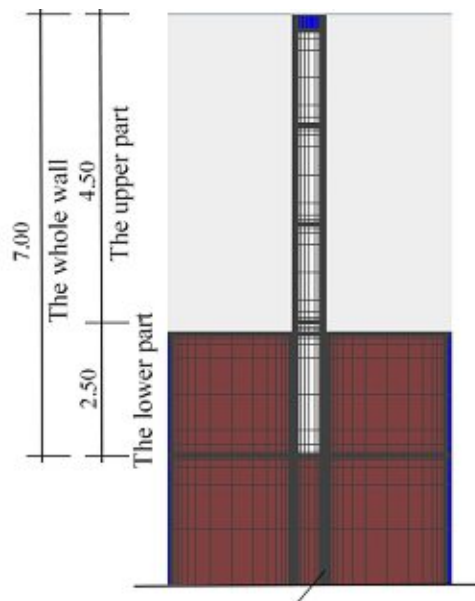


Figure 4.15 The wall and foundation construction's simplified representation in the simulation model

Material properties were assigned based on the material databases of WUFI using the sources of Fraunhofer (IBP) (Germany), North America Database (Germany), Standard DIN EN 12524 (Soil - Sand and Gravel) (Germany) and TU Wien (Austria) (WUFI 2020b). Details regarding the used materials are presented in Table 4.1.

Table 4.1 Information regarding the used materials in the model.

	<b>Layers of wall component</b>	<b>WUFI database sources</b>	<b>Thickness (m)</b>
<b>1</b>	Wall color (Lime Plaster (Stucco, A-value:3.0 kg/m <sup>2</sup> h0.5))	Fraunhofer-IBP – Holzkirchen, Germany	0.005
<b>2</b>	Lime Plaster (Stucco, A-value:3.0 kg/m <sup>2</sup> h0.5)	Fraunhofer-IBP – Holzkirchen, Germany	0.045
<b>3</b>	Solid Brick, historical	TU Wien, Austria	0.450 (for the interior wall) and 0.60 (for the exterior wall)
<b>4</b>	Terracotta tiles	North America Database	0.02
<b>5</b>	Underground soil (Generic Material)	Standard DIN EN 12524: Soil - Sand and Gravel	-

#### 4.2.3.2 Simulation inputs and settings

The design of the generated building model requires several input data and program settings. The outdoor heat transfer coefficient can be calculated by WUFI as a function of wind speed. For the indoor heat transfer coefficient, a default value of 8 W.m<sup>-2</sup>.K<sup>-1</sup> was used (Guimaraes et al. 2012b). The value of short-wave radiation absorptivity was set to 0.4 corresponding to a typical stuccos surface. Long-wave radiation emissivity was assumed to be 0.9. The adhering fraction of rain of the exterior wall surface was set to 0.7, while the exterior floor surface was set to 0 (function of the wall inclination). The input information and settings, including the rain coefficient and surface transfer properties are shown in Table 4.2.

Material properties which were assigned based on WUFI material databases are presented in Table 4.1. The physical and hydro-thermal characteristics of the materials required for the simulations in WUFI are presented in Table 4.3 and Table 4.4.

Table 4.2 Inputs and settings of WUFI

<b>Settings and inputs</b>		<b>Value</b>
Orientation/ Height/ Inclination	Orientation of external surface  Inclination [°]	South, West, East, North  90
Building height-driven rain coefficient	Rain load =Rain*(R1+R2*Wind velocity)	R1[-] = 0 R2[s/m] = 0.07

Surface transfer coefficient	Thermal resistance of exterior surface [m <sup>2</sup> .k.W <sup>-1</sup> ]	Function of wind speed
	Sd-Value of exterior surface [m]	0 (No coating)
	Short wave radiation absorptivity	0.4
		0.9
	Ground short wave reflectivity	0.7
	Adhering fraction of rain (wall)	0
	Adhering fraction of rain (floor)	8
	Thermal resistance of interior surface [m <sup>2</sup> .k.W <sup>-1</sup> ]	
	Sd-Value of interior surface [m]	0 (No coating)

Table 4.3 Material basic properties input data

Basic properties	Lime plaster	Solid brick	Terracotta tiles	Underground soil
Layer thickness [m]	0.05	0.45	0.02	-
Bulk density [kg.m <sup>-3</sup> ]	1600	1560	1670	1500
Porosity [m <sup>3</sup> .m <sup>-3</sup> ]	0.3	0.38	0.196	0.5
Specific heat capacity [J.kg <sup>-1</sup> .K <sup>-1</sup> ]	850	850	840	1000
Thermal conductivity (dry material at 10°C) [W.m <sup>-1</sup> .K <sup>-1</sup> ]	0.7	0.6	0.4	2.0
Water vapor diffusion resistance factor [-]	7	14.93	16	50

Table 4.4 Material hygro-thermal properties input data

Hygro-thermal properties	Lime plaster	Solid brick	Terracotta tiles	Underground soil
Reference water content (RH 80%) [kg.m <sup>-3</sup> ]	Hygrothermal function	4.5	Hygrothermal function	9.2
Free water saturation (RH 100%) [kg.m <sup>-3</sup> ]	Hygrothermal function	230	Hygrothermal function	370
Water absorption coefficient (A-value) [kg.m <sup>-2</sup> .s <sup>-0.5</sup> ]	Hygrothermal function	0.36	Hygrothermal function	Hygrothermal function

Moisture- dependent thermal conductivity supplement [%·M <sup>-1</sup> ·% <sup>-1</sup> ]	8.0	15.0	8.0	Hygrothermal function
Temperature- dependent thermal conductivity [W·m <sup>-1</sup> ·K <sup>-2</sup> ]	0.0002	0.0002	0.0002	Hygrothermal function

The indoor climate condition was created using a utility program in excel format provided by WUFI, called “CreateClimateFile.xls” (WUFI 2020b, Siassi 2013). The program contains input values such as temperature, relative humidity, global horizontal radiation, diffuse radiation, wind direction, wind speed and rain as its input; however, only temperature, relative humidity were applied to create the indoor climate file. The temperature and humidity values required for the calculations were defined based on the actual in-situ measurements from 2016. The output file format is “.wac” which is readable with WUFI. Figure 4.16 presents the utility program.

The climatological parameters are listed in each column header. Weather data values, such as temperature, relative humidity and global horizontal radiation, are written in these columns. The weather data file is generated and placed in the same folder where the excel utility program is located. The generated file can be used in WUFI software for simulation purposes.

Air Temperature [°C]	Air Humidity	Radiation [W/m²]	Rain [L/m²/h]	Wind Direction [°]	Wind Speed [m/s]
Rel. Humidity [%]	Solar Global Horiz.	Solar Diffuse Horiz.	Normal Rain	North = 0, clockwise	Skalar Average
-8.2	0.76751807	0	0	0	0
-7.5	0.88178756	0	0	0	0
-7.6	0.88701941	0	0	0	0
-7.8	0.909882715	0	0	0	1.1
-7.1	0.917901285	0	0	330	1.7
-7.4	0.895929276	0	0	0	0
-7.6	0.895929276	0	0	0	1.3
-9	0.834765217	2.5	2.5	0	1.1
-6	0.809793678	13.61111111	13.61111111	0	2.5
-5.9	0.809651695	22.5	22.5	0	4.2
-5.4	0.876980557	62.5	62.5	0	2.5
-9	0.884214482	139.4844444	137.2222222	0	9.6

Figure 4.16 Utility program provided by WUFI, for creating customized weather file (source: Siassi 2013)

The outdoor climate file generation was based on the measured data from the Thai Meteorological Department, using Meteororm software version 7.1.5 (Meteororm 2020). The data set is from the year 2016 from the weather station in Bangkok, named Don Muang District (TMD 2020), which is used in Chapter 3. The generated weather file contains climatological hourly data.

It is sufficient to repeat the same year (WUFI 2020b) reaching the end of the simulation period. The entire simulation period covers 9 years from 2016 to 2024 (78,849 hours).

Initial conditions in this model included a temperature of 25°C for the whole construction, except for underground soil, which was set as 20°C (Uchida 2011), and a relative humidity of 80% for the pre-retrofit models for the whole construction, except for underground soil, which was set as a relative humidity of 96% which is equal to water content of 50% (see Table 4.5). The initial relative humidity of underground soil was set with a higher value in order to reduce the simulation running time to reach the convergence.

Table 4.5 Initial conditions in this model

Material layers	Initial conditions in component		
	T (°C)	φ (%)	Water content (%)
Wall color	25	80	30
Plaster	25	80	30
Solid brick	25	80	11.8
Terracotta tiles	25	80	3.3
Underground soil (foundation level)	25	96	50
Underground soil (below foundation)	20	96	50

#### 4.2.3.3 Hygro-thermal simulation outcomes

The outcomes of hygro-thermal simulation presented in this chapter is water content ( $\text{kg}\cdot\text{m}^{-3}$ ). The detailed definition of the outcome is listed in Chapter 2, section 2.2.3.3.

#### 4.2.4 Evaluation criteria

In order to understand the occurrence of rising damp and moisture-related problem of the case-study historical masonry wall, two goals were formulated.

The first goal is, by means of on-site survey, to identify the moisture-related deteriorations, or defects, and preliminarily diagnose the dampness problems on the building surfaces via visual inspection. The criteria for selecting the damaged areas are based on the severity of the problem, area accessibility, and representativeness of the selected building components (namely, the interior wall surface, exterior wall outer surface, exterior wall inner surface, and column surface). As a

result, five damaged building surface areas were selected: (1) the surface of the interior wall of the sacristy room, (2) the inner surface of the exterior wall of the northern hall connecting to the sacristy room, (3) the outer surface of the exterior wall (specifically, on the over-hanged component surface), (4) the outer surface of the exterior wall, and (5) the surface of the entrance column (see Figure 4.17). Regarding the description of the damaged surface areas, defects caused by dampness can be identified with specific defect characteristics such as cracks, stains (e.g., black gray or green water-soluble mineral stain), or crystal deposits (i.e., water-soluble salts), and biological plants (e.g., fungi, mosses, creeping plants). Moisture-related defects effecting the wall paint are commonly seen as paint flaking, paint peeling, and blistering of paint (Halim et al. 2012).

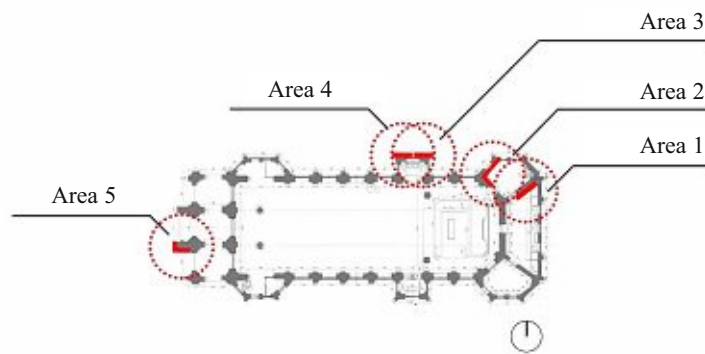


Figure 4.17 Building plan with investigation areas

The second goal of this study is to explore the hygro-thermal performance of the wall construction in terms of water content (%). The initial and final moisture content for the entire brick wall of the base cases were evaluated in both wall conditions (interior and exterior) over a 6-year period (from 2019 to 2024). The entire simulation period covers 9 years (from 2016 to 2024). The last 6-year period was taken given the stability of the respective results.

After performing the simulations, the total water content ( $\text{kg}\cdot\text{m}^{-3}$ ) values of the three parts of the wall, namely the whole, the upper part, and the lower part (including the foundation) of the solid brick wall construction (see Figure 4.15) were obtained. The total water content ( $\text{kg}\cdot\text{m}^{-3}$ ) of the whole wall indicates the ability of wall assembly to dry out over time (Ibrahim et al. 2014, Arena and Mantha 2013). If the final value at the end of the simulation period is less than the initial value (at the beginning of the simulation), it can be concluded that the wall has the potential to dry out.

## 4.3 Results and discussion

### 4.3.1 Results

#### 4.3.1.1 The visual inspection of moisture problems

The visual inspection is performed according to the symptoms of defects influenced by the presence of moisture on the case-study building surfaces. The moisture problems can still be seen on the walls today (see Figure 4.18 - Figure 4.22). Overall, the surface damages, the so-called defects, are more severe on the interior wall surfaces than the exterior ones.

Starting with Area 1, the interior wall in the sacristy room was inspected (see Figure 4.18). Due to the severity, it was chosen to represent the interior wall damages in the case study. Moreover, this particular wall was selected for the simulation model. As shown in the photograph (Figure 4.18), there are black and grey stains, with paint peeling off the wall surface from around 0.20 m above the interior floor level up to 1.50 m on the left side of the wall and 2.00 m near the corner. Below the aforementioned area, there are also visible water stains, especially in the corner area. Due to the severity of the damage growing progressively from the lower part to the higher part of the wall, it can be indicated that the problems are caused by capillary rise or rising damp (Bakri and Mydin 2014).

The occurrence of black and grey stains can be identified as efflorescence since there are many sources of water-soluble salts and minerals in solid bricks, lime plaster, and mortar used in Thai historical constructions (Watsantachad 2006). In addition, the bearing wall foundation acts as an ideal underground water passage, supplying soluble salts readily available in the groundwater up and into the walls. The surface hairline cracks are also visible on the wall surface. On account of very thin crack lines, approximately 1-2 mm wide, appearing on the wall plaster layer, it can be assumed that the cracks were caused by the constant expansion and contraction of the substrate due to moisture locked inside the wall during its wet-dry cycle. This type of cracks falls in the category of slight harmful damage since the width of the cracks is not larger than 5 mm (Bakri and Mydin 2014).

As far as Area 2 (i.e., the inner surface of the exterior wall of the northern hall connecting to the sacristy room) is concerned, the damages are less severe compared to those of the wall in the sacristy room (see Figure 4.19). The defects are quite similar to the ones in the sacristy room. There are black and gray stains with paint peeling off. However, the heights of the damaged areas are around 0.80 - 1.00 m from the room floor. It can be inferred that the height of water rise is not greater than around 1.00 m.

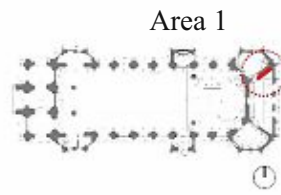


Figure 4.18 The defects on the interior wall of sacristy room

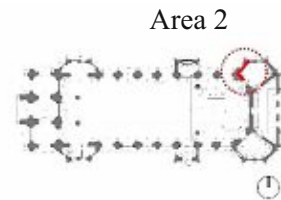


Figure 4.19 The defects on the inner surface of exterior wall of the northern hall connecting to sacristy room

In cases of the exterior wall on the external surfaces, Area 3 (see Figure 4.20) and Area 4 (see Figure 4.21) are faced with similar conditions influenced by outdoor climate. Directly impacted by rainfall, the black stains that appear mainly on the building elements projecting from the main building parameter are clearly visible (see Figure 4.20). Upon inspection of the vertical wall surface (see Figure 4.21), the decorative paint films can be seen blistering and peeling off (see Figure 4.21b), resulting in localized loss of adhesion between the paint layer and the underlying surface. These problems particularly occur on the surfaces exposed to the rain, sunlight, and the fluctuation of the temperature (Bakri and Mydin 2014). In fact, accumulated moisture in wall materials caused by rising damp can lead to

blistering and peeling paint (Halim et a. 2012, Bakri and Mydin 2014).

Lastly, Area 5 (see Figure 4.22) shows the surface damages on the exterior column surfaces, specifically those of the column at the main entrance of the building. The defects can be seen as black stains similar to the ones on the exterior building component shown in Figure 4.20. Nevertheless, there are also some cracks visible on the surface with the blistering and peeling of paint films. The exterior cracks can lead to severe moisture problems on the wall since rainwater can penetrate through the cracks and accumulate in the layer under the wall plaster (Bakri and Mydin 2014).

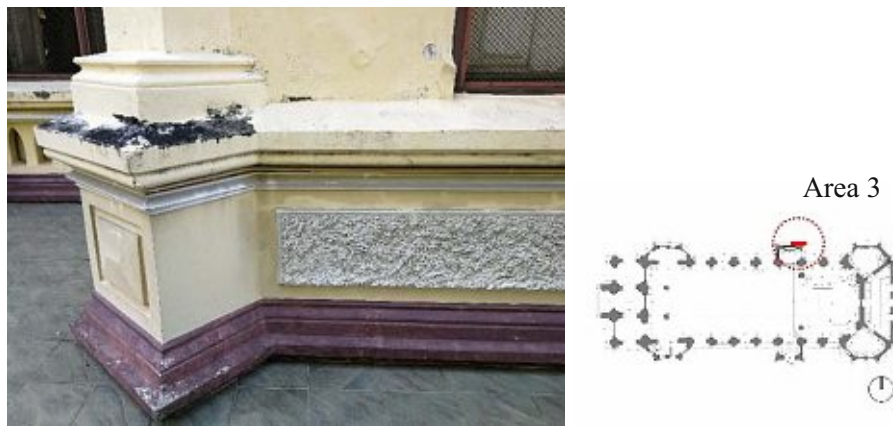


Figure 4.20 The defects on the outer surface of exterior wall



(a)



(b)

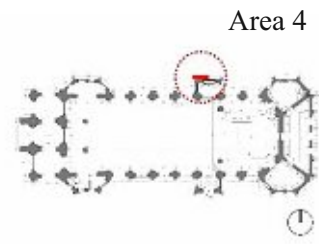


Figure 4.21 The defects on the outer surface of exterior wall



(a)



(b)

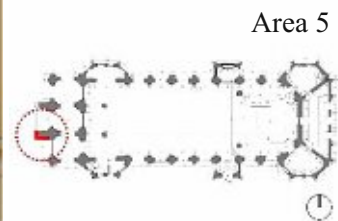


Figure 4.22 The defects on the surface of the entrance column

### 4.3.1.1 Simulation outputs

The potential to dry out is one of the indicators of hygrothermal performance (Ibrahim et al. 2014). Simulation results show a steady accumulation of the whole wall water content from 2019 to 2023 converging onto a stable level in 2024.

Table 4.6 presents the average water content ( $\text{kg.m}^{-3}$ ) of the three parts of the walls (interior and exterior walls), comprising of the entire wall, the upper part, and the lower part of solid brick wall (see Figure 4.15). These were calculated from the converged results in 2024. The calculated data provide the initial values for post-retrofit cases simulation, which will be presented in Chapter 5. Regarding the results shown in Table 4.6, it can be seen that water content in the whole interior wall is around 40% more than that in the exterior wall. However, if we only focus on the upper part of the wall, ignoring the moisture in the foundation part, water content on the interior wall is approximately 70% greater than the exterior ones.

The results found in this case study support the observations that the exterior walls, accumulate less moisture than the interior walls: The exterior walls are exposed to outdoor climatic conditions with a higher rate of ventilation, solar radiation, and lower relative humidity in the air. These are likely to increase the evaporation rate (Rirsch and Zhang 2010, Hall and Hoff 2007).

Table 4.6 The computed average water content given for the entire wall, the upper part, and the lower part of solid brick wall

		<b>The average water content (<math>\text{kg.m}^{-3}</math>) in 2024</b>		
		<b>The whole wall</b>	<b>The upper-part wall</b>	<b>The lower-part wall</b>
Interior		162.2	88.1	324.0
Exterior	South	98.02	27.62	251.95
	West	96.90	26.02	251.91
	East	95.43	23.91	251.83
	North	94.88	23.08	251.88

In order to examine the influence of rising damp on the upper part of the wall, the upper-part wall was divided into 3 parts, namely the top of the upper-part wall, the middle of the upper-part wall, and the bottom of the upper-part wall (see Figure 4.23).

The average water content ( $\text{kg.m}^{-3}$ ) of the three parts of the upper-part walls (interior and exterior walls) are presented in Table 4.7. It can be seen that the exterior walls, facing four orientations, are influenced by underground water only until the bottom part of the wall, which is not higher than 1.80 m above the

ground level, since water content remains constant in the middle and the top parts (see Figure 4.25). However, the interior wall is impacted by capillary rise from the bottom to the middle part of the wall (see Figure 4.24). The top part of the interior wall is as an area found to be in balance with the environmental humidity. These findings point to consistency of simulation results and observed surface damages from the investigation for the surfaces of both the interior and exterior walls (see Figure 4.18, Figure 4.19, and Figure 4.20).

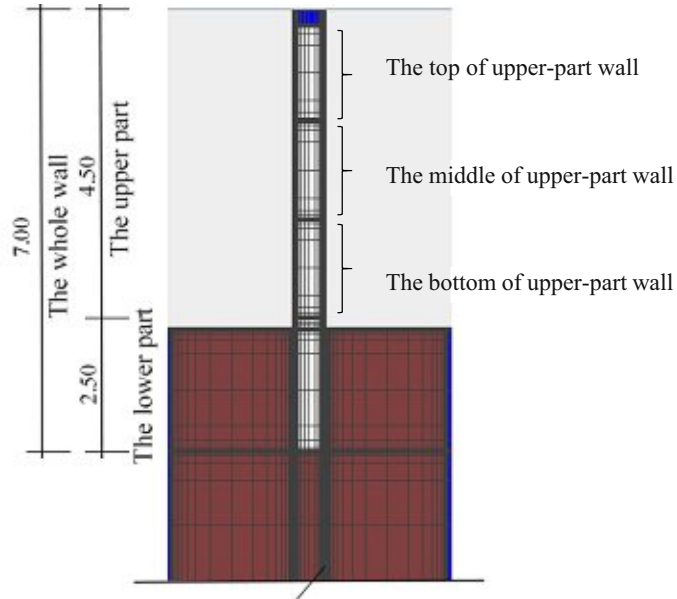


Figure 4.23 Simplified construction representation in the simulation model with the specification of the defined upper-part wall segments

Table 4.7 The average water content given for the top of upper-part wall, the middle of upper-part wall, and The bottom of upper-part wall.

Cases	The average water content (kg.m <sup>-3</sup> ) in 2024		
	The top of upper-part wall	The middle of upper-part wall	The bottom of upper-part wall
Interior	8.65	24.7	231.03
Exterior	South	14.67	14.72
	West	13.19	13.23
	East	11.24	11.27
	North	10.43	10.46

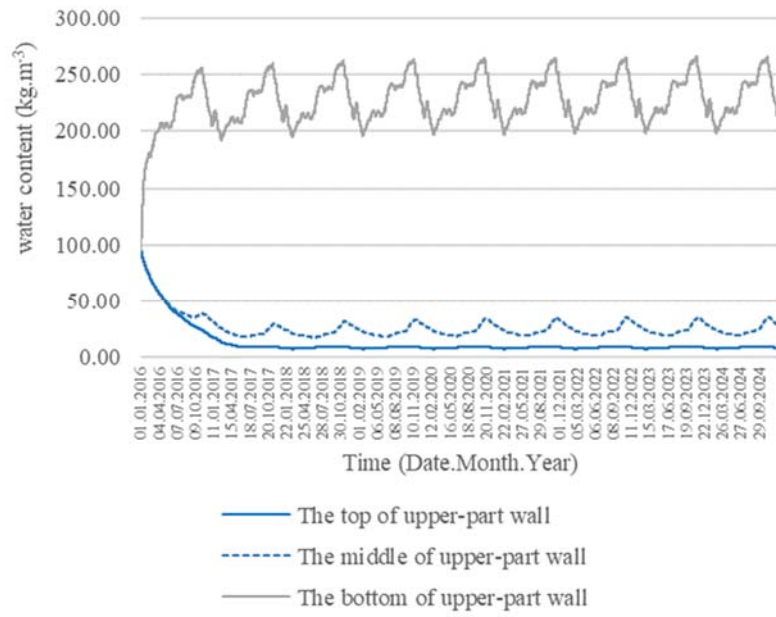


Figure 4.24 Time evolution of the water content ( $\text{kg.m}^{-3}$ ) given for three segments of the upper part of interior wall

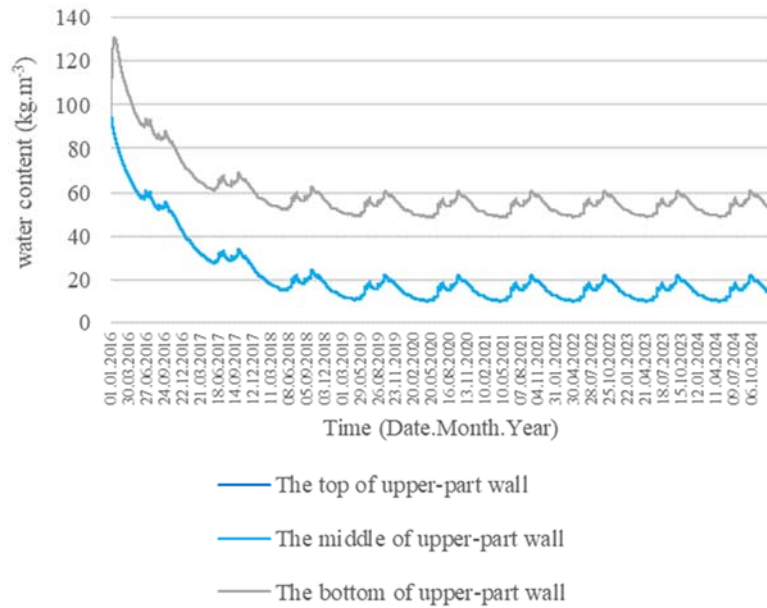


Figure 4.25 Time evolution of the water content ( $\text{kg.m}^{-3}$ ) given for three segments of the upper part of exterior wall facing south

### 4.3.2 Conclusion

In this chapter, the existing moisture-related problems in the selected case study building surfaces are diagnosed via on-site visual inspection as the first step of the overall investigation. Moreover, the results of a simulation-based analysis of the hygro-thermal performance of historical brick wall in tropical climate is presented.

Regarding the damages' characteristics, growing progressively from the lower part to the higher part of the wall, it can be concluded that the problems are caused mainly by capillary rise. This behavior is mostly and clearly found on the surfaces of the interior walls. Further findings from the on-site visual inspection indicate that there are more severe problems on the interior wall surfaces compared to the exterior wall surfaces, which correlates with the simulation results. In congruence with the simulation results, the findings show that there is more water content in the interior wall than in the exterior walls.

For future studies related to the diagnosis of moisture-related problems, it is important to investigate and evaluate all the damages and failure in every part of the building in order to address the primary causes of the damages. Performing the diagnosis with supportive devices, such as moisture measurement equipment, additional confidence in the diagnosis can be gained. Furthermore, an understanding of results, from both numeric simulation and on-site investigation, is a significant part of the building damage diagnosis since accuracy of diagnosis of the dampness problems in historical buildings can be substantially improved.

## Chapter 5

# Evaluation of historical building retrofit options

## 5.1 Background

### 5.1.1 Intervention Methods against rising damp: Wall cutting or insertion of impermeable layer method

For decades, finding good refurbishment options for the affected historical building façade has been a challenge. In order to gain a better understanding and find suitable solutions, current methods used in rising damp reduction in masonry constructions are reviewed in this chapter.

There are a wide variety of intervention methods used in targeting rising damp problems in masonry constructions over the last century. Franzoni (2018) conducted a comprehensive study looking at studies concerning the intervention methods against rising damp in masonry construction and found a total of 65 papers. The literature in this field is concentrated mostly after 2005. With increased interest, as many as six studies were published in 2017 (see Figure 5.1).

Among the three evaluation methods of investigation (i.e., laboratory setting, in situ observation, and computational modelling) reviewed, about 50% were conducted in laboratory settings (e.g., using real-scale masonry model) (see Figure 5.2). While 35% of the results were based on in situ observation, only 13% were based on computational modelling, which is suggested by the growing interest in the number of papers published between 2010 and 2017 (Franzoni 2018). As such, advanced hygro-thermal simulation (see, for example, Holm and Künzle 2003) is rarely applied as a methodology in studies related to rising damp.

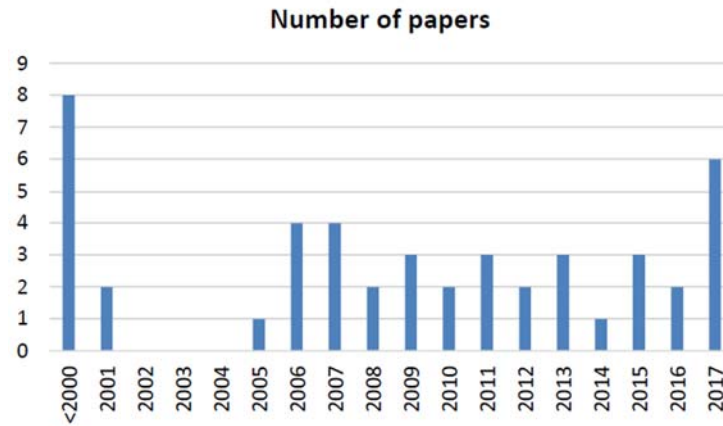


Figure 5.1 International papers per year (source: Franzoni 2018)

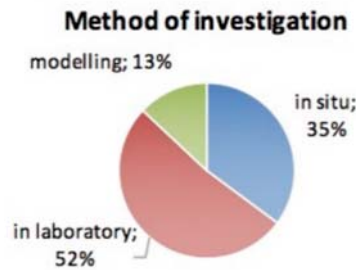


Figure 5.2 Research approach in the international papers examined (source: Franzoni 2018)

In an attempt to categorize intervention methods currently used in rising damp reduction in masonry constructions, two recent studies were reviewed. According to EMERISDA (2014), “existing methods include mechanical interruption, chemical interruption i.e. injection (with pressure) and impregnation (without pressure or with hydrostatic pressure only), methods based on evaporation increase and several electrokinetic methods (as electro-osmosis)” (p.3). These methods were categorized into two main groups by EMERISDA (2014): (1) methods which stop or limit rising damp (i.e., damp-proof course including mechanical interruption and chemical interruption, evaporation increase and electrokinetic); and (2) methods which tackles symptoms (i.e., additional measures including special plaster, veneer walls, and drainage).

Franzoni (2018) later categorized intervention methods against rising damp into four main groups known as “repair systems” according to the three factors involved in determining the rising damp height, which are water supply, evaporation, and materials and wall structure (see Figure 5.3), and lastly systems based on electro-osmosis. The four repair systems are aimed at: (1) reducing water supply from the ground; (2) boosting water evaporation; (3) modifying the materials in the wall; and (4) using electro-osmosis to redirect unwanted moisture in the

materials elsewhere. Since these categories are similar to and consistent with the ones defined by EMERISDA (2014). However, as they appear to be more clearly defined, they were chosen as a guideline for explaining the intervention methods described in this chapter.

Repair systems considered in the 46 scientific papers examined by Franzoni (2018) are presented in Figure 5.4 (Note: papers investigating more than one system were counted more than once). Overall, chemical damp-proofing, one of the systems aimed at modifying the materials in the wall, receives the most attention from researchers at 30.9% of the number of related scientific papers, followed by wall base ventilation method (evaporation increase system), and repaired plaster at 21.8% and 18.2%, respectively (Figure 5.4).

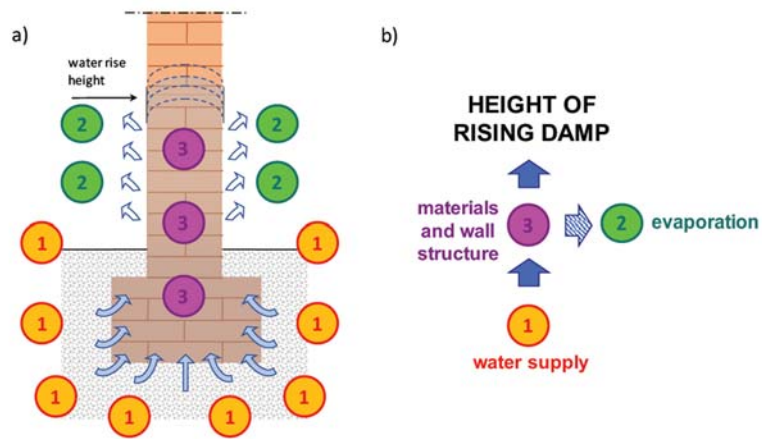


Figure 5.3 (a) Dynamics of capillary water rise in masonry, and (b) schematic representation of the three factors involved, which determine the resulting height of rising damp (source: Franzoni 2018)

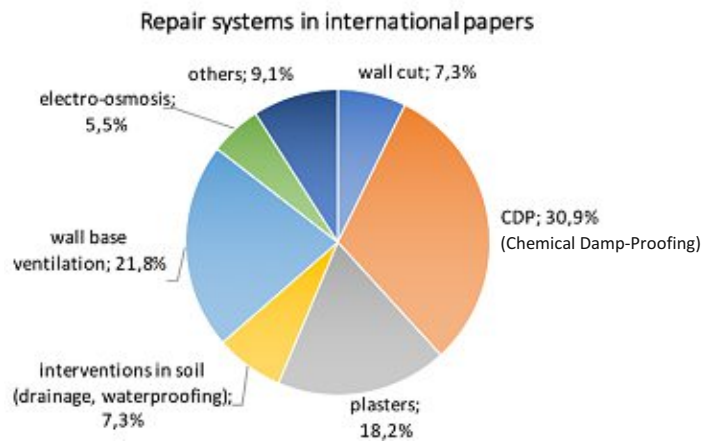


Figure 5.4 Repair systems in 46 international papers examined by Franzoni (2018)

The repairs systems found in the literature are described below, in accordance with the categories proposed by Franzoni (2018) (see Figure 5.5). The concept of each repair system is described in terms of its construction process as an intervention method aimed at rising damp mitigation. Examples of post-retrofit buildings using each different repair system and the advantages and disadvantages thereof are also given.

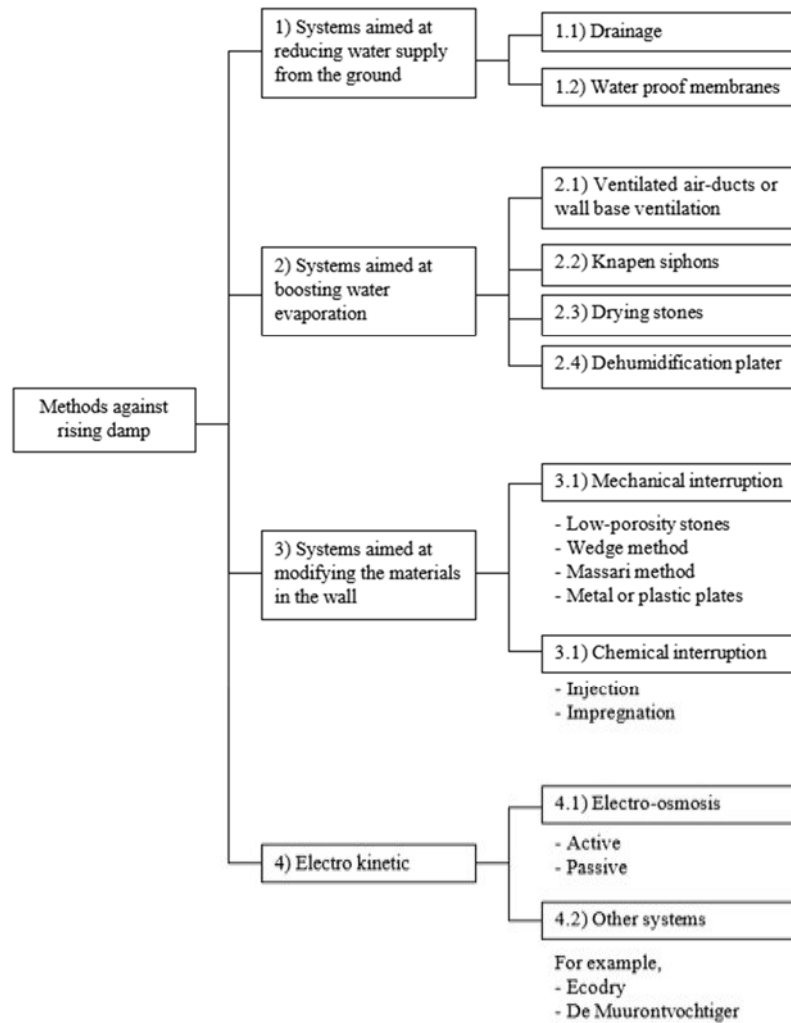


Figure 5.5 Overview of current repair methods, according to the groups categorized by Franzoni (2018)

First, systems aimed at reducing water supply from the ground have been proposed and studied in order to cope with rising damp. In order to do so, drain or water proof membranes (i.e., polymer-based sheet) are constructed along the perimeter of the building under the ground. This method not only reduces water supply from the ground but also increases the evaporation rate of ground moisture (Franzoni 2018). Trotman (2007) suggests that this type of systems is widely recommended as a means for rising damp mitigation; however, Franzoni

(2018) points to the lack in literature related to conducting a systematic investigation of its drying effectiveness. This is in fact confirmed by the small number of related papers (see Figure 5.4).

Second, systems aimed at increasing water evaporation, specifically ventilated air-ducted, or wall-based ventilation, have been recently proposed to reduce the level of height rise achieved by rising damp front (for example, Torres and Freitas 2007, Torres and Freitas 2010, Guimaraes et al. 2012a, and Pazderka et al. 2017) (see Figure 5.6). This method has been investigated in several papers as shown in Figure 5.5.

Numeric simulation was found to be an effective tool for evaluating the performance of retrofit option design in order to select the duct size and adjust air ventilation speed (Torres 2013, Tazky and Sedlakova 2015, and Pazderka et al. 2017). Experimental results show that significant moisture decrease has been reported in low thickness walls, which can be as much as 40% (Pazderka et al. 2017) or more (Torres 2013). Certain levels of drying were found also on-site observation studies (Freitas et al. 2015). However, there is only a limited amount of experiment data since the comprehensive testing of this system is yet to be completed (Franzoni 2018).

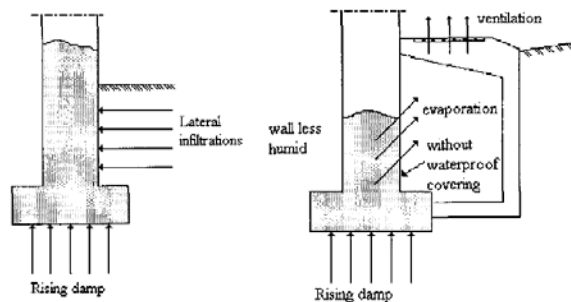


Figure 5.6 Functioning principle of ventilated peripheral channels (wall base ventilation system) (source: Freitas and Torres 2003)

Another approach proposed based on evaporation increase, established since the early 20<sup>th</sup> century, is the so-called “Knapen siphons” or “Knapen tubes” or “Atmospheric siphons,” which are tubes made of porous materials (e.g., fired-clay, or perforated plastic or metal) (EMERISDA 2014). These tubes are inserted into the wall and inclined towards the external wall surface in order to release the damp air within the wall materials (see Figure 5.7). However, the results found in the previous studies are proven to be hardly successful, where the bare hole is found to be more effective (Heiman et al. 1973).



Figure 5.7 Different types of Knapen siphons in wall  
(source: EMERISDA 2014)

By the same principle, the “drying stones” were invented to enhance evaporation of masonry wall by placing the stone containing aerodynamically shaped holes (see Figure 5.8) at the base of the wet wall with a distance of about 30 cm. Scientific literature is not positive about this system (EMERISDA 2014). The further approach is based on the application of repair plasters, that are dry-ready-to-use mortars, known as dehumidification plaster, which are expected to promote evaporation with respect to traditional ones. However, these plasters are produced mainly for the purpose of reducing the damage related to salt crystallization (Lubelli and van Hees 2006, EMERISDA 2014, Franzoni 2018).



Figure 5.8 (a) A stone containing aerodynamic shape holes, and (b)  
After retrofit with drying stone application  
(source: EMERISDA 2014)

Third, regarding the aim at modifying the materials and structure of the wall to reduce height of rise, two main systems have been proposed: (1) mechanical interruption, and (2) chemical interruption. Mechanical interruption, also known as wall cutting, consists of inserting an impermeable layer or a layer with a low water absorption in the wall. The cut is executed by means of different technologies, for example, hammering sheets or slabs into the mortar joints or soft brick (EMERISDA 2014). A wide range of materials, such as steel or lead plates, bitumen-based membranes, polyethylene or polyester-based or PVC membranes, can be used to make the sheets (Freitas and Torres 2003, EMERISDA 2014).

In the past it was possible to use low absorption materials such as natural low-porosity stones to create a barrier in the wall in order to prevent rising damp. In a given geographical area affected by rising damp, for example, brick masonry walls in Venice were commonly built with layers of low-porosity stones as a curb or base for the walls (EMERISDA 2014). In 1827, in the wall construction, the insertion of lead slabs or stones, impregnated with a glue composed of boiled linseed oil and litharge, was suggested as a method to reduce the rising damp level (EMERISDA 2014).



Figure 5.9 Horizontal courses of low-porosity stones brick were used at the base of the walls in order to limit the water capillary rise in two affected buildings in Venice; (a) Alberaria Tower, and (b) Salt Emporium (source: EMERISDA 2014)

To perform a mechanical interruption, there are other techniques apart from the sheet or thin layer insertion. One of the techniques is the so-called “wedge method.” This method requires removing a brick or stone course, and replacing it with concrete wedges. The joints are later filled up with a mortar containing resin (EMERISDA 2014). Another technique with the same concept is known as the “Massari method” (Massari and Massari 1985). Developed in Italy by Massari, this mechanical interruption method requires drilling two overlapping series of holes into the wall. Before drilling the second series, however, the first series of holes is filled up with synthetic, water repellent mortar (EMERISDA 2014).

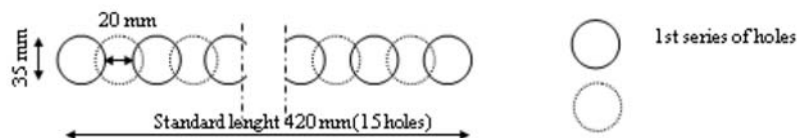


Figure 5.10 Massari method: two series of overlapping holes are cored and filled with water repellent mortar (source: EMERISDA 2014)

Since this system has been known and practiced for centuries, the insertion of a water impermeable layer, or the so-called wall cutting, is considered to be amongst one of the most effective interventions to stop the migration of capillary water from the ground. If carried out properly, from the construction point of view, the moisture transport above the insertion plane of an impermeable material layer is completely stopped (Alfano et al. 2005, Franzoni 2018). Meticulous attention to details in construction is required for this intervention to succeed, especially during the overlapping of the sheets and the filling of repairs mortar into the cut. Despite the high probability of success, there are some significant limitations to these interventions.

One of the major limitations of mechanical wall cutting is the potential structural instability and increased seismic vulnerability as cracks can occur in the wall and pose a structural risk (EMERISDA 2014, Franzoni 2018). Another limitation is the possibility of forming a pathway for water from the masonry below the cut, which is close to saturation, to the area above the cut, when lime plaster is applied as the finishing layer. In terms of maintaining aesthetics and the original facade of the historical buildings, mechanical interruption may cause the building to lose its authenticity. Without applying the wall finishing layer, the mechanical interruption, for example, thin metal plate insertion, can leave an unpleasant visible layer on the masonry wall (EMERISDA 2014) (see Figure 5.11b).



Figure 5.11 (a) Mechanical interruption Italy (Universita Ca'Foscari Venezia), and (b) Mechanical Interruption in Belgium (BBRI) (source: EMERISDA 2014)

Another type of mechanical intervention is known as chemical interruption or chemical damp-proofing (CDP). Franzoni (2018) describes CDP as a process in which a moisture barrier layer is formed by injecting a hydrophobic or pore-blocking chemical substance into cross-sectional holes drilled into the wall as close to the ground as possible. Chemical injections have been largely investigated in the scientific literature (Franzoni 2014), however, there is no standard procedure for testing its effectiveness in laboratory setting and the guidelines for CDP vary from country to country (Franzoni 2018). Since the chemical spreading ability is the main factor responsible for creating

the continuous barrier between the holes, it must be ensured that the chemical barrier covers the entire width and length of the affected wall. Regarding the various unknown parameters possibly involved in the drying of the masonry resulting from chemical damp-proof barrier and due to lack of conclusive study results (Franzoni 2018), chemical interruption is still a considerable challenge.



Figure 5.12 (a) Wall treatment using pressure (injection), and (b) wall treatment using only hydrostatic (Impregnation)  
(source: EMERISDA 2014)

Finally, intervention systems based on electrokinetic phenomena, known as electro-osmosis, both passive and active, have been investigated. There are very few scientific studies that address the effects of electro-osmosis on masonry walls, especially the in-situ observation (Franzoni 2018) (see Figure 5.4). According to Franzoni (2018), “the active electro-osmosis is expected to cause the migration of water in the pores from the electrodes applied in the moist wall (anode) to the electrodes applied in the soil (cathode), through the application of an external dc electric field” (p.11). Figure 5.13 illustrates a schematic of an electro osmosis set up applied on a masonry wall. This method was found efficient in a Russian building, upon application of a very high voltage (up to 200 V), however, it was not in use because of the danger of high voltages in presence of people (Ivliev 2007). The literature on the effectiveness of this method is controversial and causing some experts to remain skeptical (EMERISDA 2014).

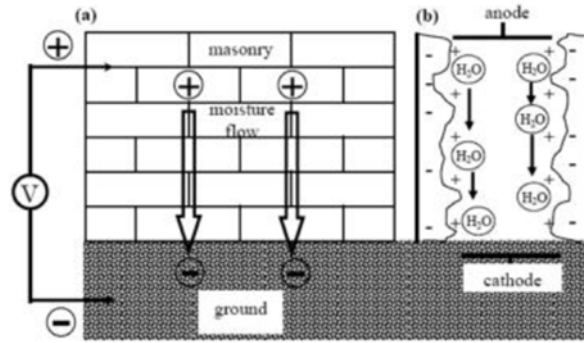


Figure 5.13 Schematic of an electro osmosis set up used on a masonry wall (source: EMERISDA 2014)

Although these systems have theoretically clear operating principles and have been already applied for decades in masonry buildings, the reviewed scientific literature indicates that the effectiveness of the aforementioned intervention methods against rising damp still require further investigations and full elucidation (Franzoni 2018). Moreover, regarding the complexity of historical masonry buildings (e.g., unknown material properties), the assessment of the effectiveness of the repair systems is still a great challenge, either in terms of laboratory testing, in-situ survey or simulation software modelling, which requires more detailed and systematic investigation.

In this study, the wall cutting method is found to be a promising retrofit method for historical masonry buildings located in hot humid climate affected by rising damp problems, given the positive results from the related literature and the fact that this method has been practiced for centuries. Regarding the high cost of using this method and the lengthy amount of time required to fully observe the dampness occurrence and its impact, however, an alternative tool, such as numeric simulation softwares, is deemed more supportive and useful, specifically in retrofit decision making for historical buildings (see, for example, Holm and Künzel 2003, Torres and Freitas 2007, and Guimarães et al. 2012). Hence, in this study, wall mechanical intervention also known as wall cutting will be selected as the retrofit method for the case-study building. Its performance will be evaluated by using A hygro-thermal simulation software (WUFI 2020a).

## 5.2 Method

### 5.2.1 Overview

Rising damp is one of the most relevant problems affecting historic masonry buildings leading to severe consequences both in terms of building material and structure deteriorations and poor indoor air quality. Due to the complexity and the number of unknown factors involved in rising damp in historical buildings, finding good solutions for rising

damp mitigation has been a challenge. Over the last few centuries, many repair systems have been studied and proposed for coping with rising damp, for example, mechanical interruption, chemical interruption and electro-osmosis (Franzoni 2018). Mechanical intervention method, consisting of the insertion of a water impermeable layer or wall cutting, is considered to be amongst one of the most effective measures to stop the migration of capillary water from the ground (EMERISDA 2014).

To support the retrofit decision making procedure, numeric hygro-thermal simulation application is considered to be more cost-effective since the cost of realizing the proposed options is significantly high (EMERISDA 2014). Furthermore, since observing the rising damp phenomenon can span the course of several years to more than a decade, tedious longitudinal studies, either real-size-modelling or in situ observation studies, may not be practical or timely. Hence, in this study, an advanced hygro-thermal simulation software named WUFI was used to calculate the transient heat and moisture transport in two dimensions in order to analyze cases of rising damp (see, for example, Guimarães et al. 2012b, Holm and Künzel 2003), and to evaluate the effectiveness of the building retrofit options with the purpose of finding suitable solutions for rising damp problems in historical buildings (see, for example, Torres and Freitas 2007, 2010).

The case study building discussed previously in Chapter 4 addressed hot-humid climate and the dampness occurrence. The same historical church constructed with traditional load-bearing wall technique in the 19th century also serves as the case study in this chapter (see Section 4.2.2 for background details). After performing a series of hygro-thermal analyses of the case study building components, specifically the interior and exterior walls facing four different cardinal directions in the previous chapter, retrofit options for these particular instances will be considered and examined in this chapter.

### 5.2.2 Retrofit options for the case-study building

The mechanical wall cutting or the insertion of impermeable material method was selected and evaluated as a retrofit option for the historical church. Bitumen was used as the cutting layer material. The cutting plate is located 0.20 m above the floor level (see Figure 5.14). The cut goes through the entire wall construction layers including wall color (0.005 m), lime plaster (0.045 m), and solid clay brick (0.45 m) (see Figure 5.15). The material properties of bitumen layers are presented in the following section.

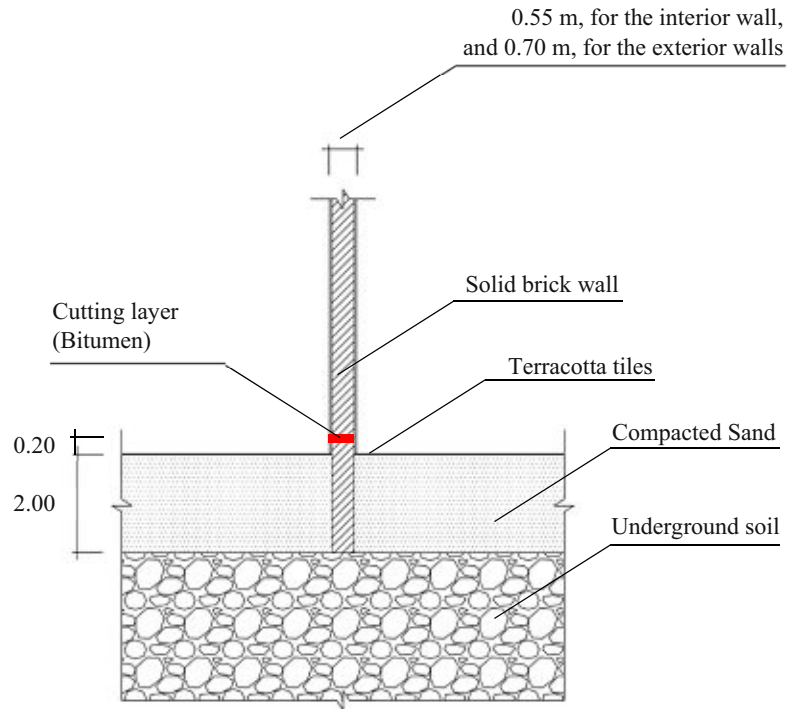


Figure 5.14 The wall cutting location on the building construction

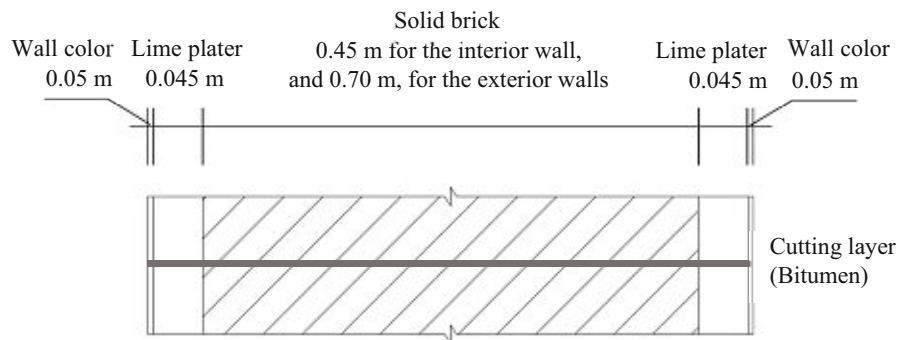


Figure 5.15 The case-study wall construction in enlarged cross-section detail.

### 5.2.3 Hygro-thermal simulation (2D)

The case study wall constructions were simulated in WUFI 2D version 3.3 (WUFI 2020e, Künzle 1998).

#### 5.2.3.1 Geometry modelling

The simulation model in this chapter is based on the model in Chapter 4 with the same construction and materials (see Section 4.2.3.1). Figure 5.16 presents the simulation model of a typical

historical Thai wall construction in the 19<sup>th</sup> century with the retrofitted method, namely wall cutting, using a bitumen layer. Bitumen properties were assigned based on the material databases of WUFI (WUFI 2020c) (see Table 5.1).

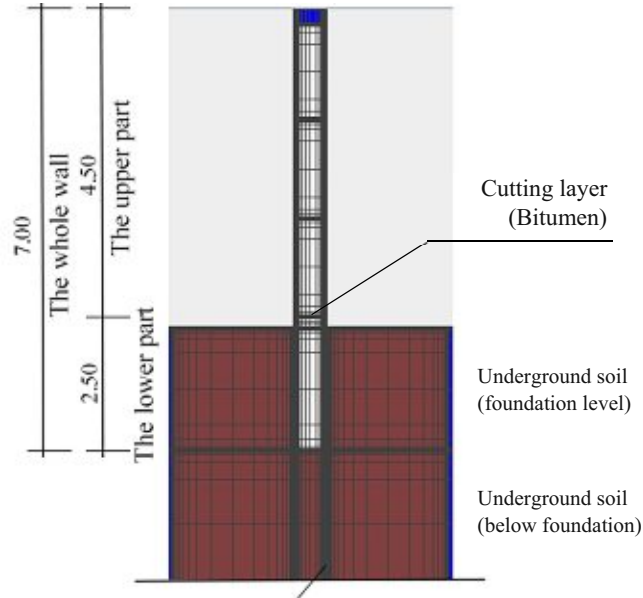


Figure 5.16 The location of the cutting plate, as an element of retrofitted method, on the wall construction, simplified as a representation in the simulation model

Table 5.1 Information regarding the used materials in the model.

Layers of wall component	WUFI database sources	Thickness (m)
Bitumen layer (Roof Membrane V13 (bitumen felt))	Generic Material	0.005

### 5.2.3.2 Simulation inputs and settings

The design of the generated building model requires several input data and program settings. The model inputs and settings in this chapter are the same as the input data and settings in Chapter 4 (see the details of model inputs and settings in Chapter 4, section 4.2.3.2). The material's basic and hygro-thermal properties input data of bitumen layer model are presented in Table 5.2 and 5.3. The initial value for the post-retrofit simulation cases are assigned in terms of the converged results of the pre-retrofit cases in 2014 (see Table 5.4).

Table 5.2 Basic properties input data of bitumen layer model

Basic properties	Bitumen layer
Layer thickness [m]	0.05
Bulk density [ $\text{kg.m}^{-3}$ ]	2400
Porosity [ $\text{m}^3.\text{m}^{-3}$ ]	0.001
Specific heat capacity [ $\text{J.kg}^{-1}.\text{K}^{-1}$ ]	1000
Thermal conductivity (dry material at $10^\circ\text{C}$ ) [ $\text{W.m}^{-1}.\text{K}^{-1}$ ]	0.5
Water vapor diffusion resistance factor [-]	100000

Table 5.3 Hygro-thermal properties input data of bitumen layer model

Hygro-thermal properties	Bitumen layer
Reference water content (RH 80%) [ $\text{kg.m}^{-3}$ ]	Hygrothermal function
Free water saturation (RH 100%) [ $\text{kg.m}^{-3}$ ]	Hygrothermal function
Water absorption coefficient (A-value) [ $\text{kg.m}^{-2}.\text{s}^{-0.5}$ ]	Hygrothermal function
Moisture-dependent thermal conductivity supplement [ $\%.\text{M}^{-1}\%^{-1}$ ]	Hygrothermal function
Temperature-dependent thermal conductivity [ $\text{W.m}^{-1}\text{K}^{-2}$ ]	0.0002

Table 5.4 Initial conditions in this model provided as per converged results of the pre-retrofitted cases in 2014

Material layers	Initial conditions in component	
	T ( $^\circ\text{C}$ )	Water content (%)
Wall color	25	186.8
Plaster	25	186.8
Solid brick (upper-part wall)	25	95.3
Solid brick (upper-part wall, except foundation)	25	305.9
Solid brick (foundation)	25	325.8
Terracotta tiles	25	193.9
Underground soil (foundation level)	25	360.4
Underground soil (below foundation)	20	368.1

### 5.2.3.3 Hygro-thermal simulation outcomes

The outcome of hygro-thermal simulation presented in this chapter is water content ( $\text{kg.m}^{-3}$ ). The detailed definition of the outcome is listed in Chapter 2, section 2.2.3.3.

### 5.2.4 Evaluation criteria

The aim of this chapter is to explore the hygro-thermal performance of the retrofit wall construction, using wall cutting method, in terms of water content (%). The initial and final moisture content for the entire brick wall of the retrofit cases were evaluated for both wall conditions (interior and exterior) over a 6-year period (from 2019 to 2024). The entire simulation period covers 9 years (from 2016 to 2024). The last 6-year period data set was taken given the stability of the respective results. Obtained values included the total water content ( $\text{kg.m}^{-3}$ ) of the three parts of the wall, namely the whole, the upper part, and the lower part (foundation included) of the retrofitted solid brick wall construction (see Figure 5.16). However, the upper-part wall is focused more in this chapter since it is the main area influenced by the retrofit.

In order to evaluate the retrofitted options, total water content ( $\text{kg.m}^{-3}$ ) (Ibrahim et al. 2014, Arena and Mantha 2013), water content reduction (%) due to the retrofit (Torres and Freitas 2010), and drying out time (year) were estimated. The total water content ( $\text{kg.m}^{-3}$ ) of the whole post-retrofit wall indicates the ability of the wall assembly to dry out over time. The potential for the wall to dry out can be inferred when the final value at the end of the simulation period is less than the initial value (at the beginning of the simulation). The relative water content reduction (%) after the retrofit is the difference between the initial water content and the final water content at the end of the simulation period in relation to the initial water content (see Eq. 5.1). The drying out time (in years) is estimated from the line graph presenting the time evolution of the water content ( $\text{kg.m}^{-3}$ ) given for the upper-part wall.

$$\text{The water content reduction (\%)} = \frac{W_{ini} - W_{final}}{W_{ini}} (100) \quad (\text{Eq. 5.1})$$

where  $W_{ini}$  is the initial water content and  $W_{final}$  is the final water content at the end of the simulation period

## 5.3 Results and discussion

### 5.3.1 Results

Simulation results show a steady accumulation of the whole wall water content from 2019 to 2023 converging onto a stable level in 2024. The average water content ( $\text{kg}\cdot\text{m}^{-3}$ ) of the three parts of the walls (interior and exterior walls), comprising the entire wall, the upper part, and the lower part of solid brick wall (see Figure 5.16) is presented. Nevertheless, more attention has been given to the upper-part wall since this is the main area influenced by the retrofit.

The results, given for the entire wall, the upper part, and the lower part of solid brick wall, of the post-retrofit cases for both interior and exterior wall constructions are shown in Table 5.5. Considering the wall part influenced by the intervention, the mean water content of the upper part of the solid brick wall (the part above the cutting plane) in 2024 is significantly less than the initial (stable pre-retrofit) value as shown in Table 5.6 and Figure 5.17. The water content reduction potential (%) as affected by the wall cutting method is shown in Table 5.6.

Focusing on the results of the upper-part walls, it becomes clear that in all conditions of the walls the insertion of permeable materials leads to a significant water content reduction. The water content reduction potential in the interior walls reaches 90% as compared to the pre-retrofit state, while the water content reduction potential in the exterior walls is around 45 to 55 %. The average water content of the upper part of the solid brick interior wall significantly decrease from  $88.1 \text{ kg}\cdot\text{m}^{-3}$  to  $8.7 \text{ kg}\cdot\text{m}^{-3}$ . As Figure 5.17 suggests, the major process of drying out occurs in the first two years after the intervention for the interior wall, while it takes around three years for the exterior wall.

The steady accumulation period of the upper part of the solid brick wall of the post-retrofit cases over the last six years (2016-2019) is presented in Figure 5.18. Regarding the line graphs shown in Figure 5.18, it can be inferred that during the steady accumulation period water content in the interior wall has a low fluctuation, whereas the higher fluctuation of water content is found in the exterior walls, specifically the ones facing south and west. The water content of exterior wall facing south and west are higher due to the influence of the southwest monsoon during the rainy season which generally cover from the middle of May to October (TMD 2020).

Table 5.5 The average water content given for the entire wall, the upper part, and the lower part of solid brick wall, of the post-retrofit cases

Cases	The average water content (kg.m <sup>-3</sup> ) in 2024		
	The whole wall	The upper-part wall	The lower-part wall
Interior	120.0	8.7	363.5
Exterior	South	89.4	15.3
	West	88.3	13.7
	East	88.2	11.3
	North	87.6	10.5

Table 5.6 The average water content of the upper part of solid brick wall of post-retrofit cases comparing with pre-retrofit cases

Cases	The average water content (kg.m <sup>-3</sup> ) of the upper part of solid brick wall in 2024		Water content reduction (%) by the retrofit
	Pre-retrofit cases	Post-retrofit cases	
Interior	88.1	8.7	90.1
Exterior	South	27.6	15.3
	West	26.0	13.7
	East	23.9	11.3
	North	23.1	10.5

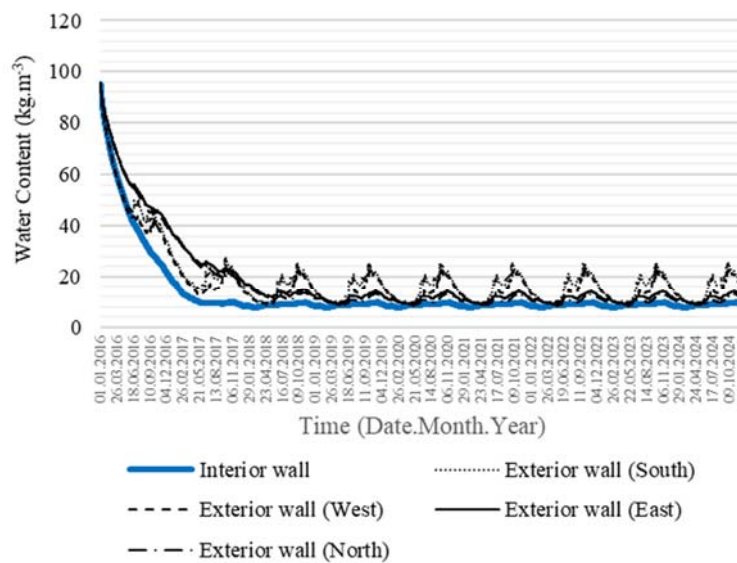


Figure 5.17 Simulated water content of the upper part of solid brick wall of the post-retrofit cases over a period of 9 years (2016 to 2024)

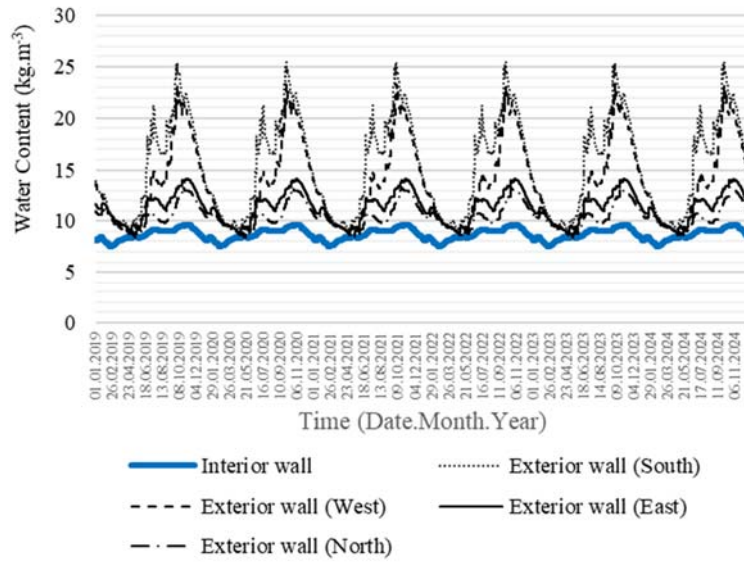


Figure 5.18 Simulated water content of the upper part of solid brick wall of the post-retrofit cases over a steady accumulation period of 6 years (2016 to 2024)

Considering water content in the lower wall parts (both the post-retrofit interior and exterior ones), moisture accumulations become higher compared to moisture accumulations pre-retrofit especially in the exterior wall facing east and the exterior wall facing north (see Table 5.7). However, moisture accumulation remains constant (very minimal increase by only 0.2%) in the exterior walls facing south and west. As a limitation, the results are in fact indicative of the fact that the post-retrofit masonry below the cut will be close to saturation (EMERISDA 2014, Franzoni 2018).

Table 5.7 The average water content of the lower part of solid brick wall of post-retrofit cases comparing with pre-retrofit cases

Cases	The average water content (kg.m <sup>-3</sup> ) of the lower part of solid brick wall in 2024		Water content reduction (%) by the retrofit	
	Pre-retrofit cases	Post-retrofit cases		
Interior	324.0	363.5	-12.2	
Exterior	South	251.95	251.4	0.2
	West	251.91	251.4	0.2
	East	251.83	256.2	-1.7
	North	251.88	256.3	-1.8

Since wall thickness is one of the factors affecting the water height of rise (Mason 1974, Rirsch and Zhang 2010, Guimaraes et al. 2012b), the exterior walls were simulated also with the thickness of 0.55 m, which is similar to the interior wall thickness, in order to evaluate the performance of the wall cutting method on thinner exterior walls. Regarding the cases of the exterior wall with thickness of 0.55 m, the results show that the percentages of water reduction (%) after implementing the wall cutting method in all cases are less than the cases with the thickness of 0.70 m around 14-15% (see Table 5.8). Moreover, the interior wall was also simulated with the thickness of 0.70 m in order to examine the influence of wall thickness on the wall under the indoor condition. However, the results of the interior wall cases show that there is virtually no difference (1%) between the cases with the 0.55 m and 0.7 m wall (see Table 5.8). It can be summarized that the performance of wall cutting method is higher when the wall thickness is greater in cases of exterior wall.

Table 5.8 The average water content (in 2024) of the upper part of solid brick wall of post-retrofit cases comparing with pre-retrofit cases in the interior wall and exterior walls with the thickness of 0.55 m and 0.70 m

			The average water content (kg.m <sup>-3</sup> ) of the upper part of solid brick wall in 2024		Water content reduction (%)
			Pre-retrofit cases	Post-retrofit cases	
<b>Wall cases (0.55 m thickness)</b>	Interior		88.1	8.7	90.1
	Exterior	South	22.1	15.3	30.8
		West	20.5	13.7	33.2
		East	18.2	11.5	36.8
		North	17.4	10.6	39.1
<b>Wall cases (0.70 m thickness)</b>	Interior		96.2	8.7	91.0
	Exterior	South	27.6	15.3	44.6
		West	26.0	13.7	47.3
		East	23.9	11.3	52.7
		North	23.1	10.5	54.5

### 5.3.2 Conclusion

Since the results of a simulation-based analysis of the hygro-thermal performance of historical brick wall in tropical climate were previously discussed in Chapter 4, the effects of a moisture mitigation measure (insertion of impermeable layers) concerning both internal and external walls were investigated in this chapter.

The main findings of the study may be summarized as follows:

- In historical buildings, the wall cutting methods appear to be an effective measure against rising damp. If carried out properly from the construction point of view, the moisture transport above the insertion plane of an impermeable material layer can be successfully interrupted. This however does not rule out the possible impact from humidity due to indoor climate and outdoor weather conditions.
- The wall cutting method was found to be more efficient for interior walls, with 90% of water content reduction, compared to the exterior cases with 45% to 55%. During the steady accumulation period water content in the interior wall is fluctuating more compare to the exterior walls. In the interior case, the walls, after implementing the impermeable material insertion, displayed a notable drying out phase in the first two years after the retrofit. All cases of the exterior wall took around three years to dry out. The simulation results also suggest that the masonry below the cut would be close to saturation after the intervention. Moreover, it can be concluded that the performance of wall cutting method may be higher when and only if the exterior walls are thicker.
- As an intervention, the wall cutting method is not without limitations. The structure may become unstable or more vulnerable to seismic events as a result of improper execution. Moreover, the saturation near the masonry below the cut cannot be avoided. These problems and the lack of simulation validation studies based on in-situ data imply the need for further investigations.

## Chapter 6

# Conclusion

### 6.1 Contributions

This dissertation presents the results of the hygro-thermal analysis, using two-dimensional numerical simulation, of historical building walls in a hot-humid climate in order to investigate the rising damp mechanism in the historical building construction. Specifically, the focus has been placed on historical buildings and the relevant building components commonly found in 19th-century Thailand, a Southeast Asian nation located just 15° 00' N above the equator, where less attention is given by the field despite the wide range of rising damp problems and lack of effective retrofit solutions. Constructed with traditional techniques from the respective era in Bangkok, Thailand, a historical church affected by various moisture-related deteriorations serves as the primary case study of this dissertation.

In order to examine and identify the possible causes of the deteriorations and prescribe effective retrofit solutions for the affected historical facades, on-site visual inspection and a hygro-thermal performance simulation software were strategically integrated. WUFI, an advanced hygro-thermal simulation software, was used to calculate the transient heat and moisture transport in two dimensions in order to analyze cases of rising damp from groundwater. The simulation was conducted using actual dimensions of the case study building components, particularly, the interior and exterior walls facing four different cardinal directions (i.e., eastward, westward, northward and southward). Regarding the characteristics of the deteriorations growing progressively from the lower part to the higher part of the wall, it can be concluded that the problems are caused mainly by capillary moisture rise. This behavior is mostly and clearly found on the surfaces of the interior walls. Further findings from visual inspection indicate that there are more severe problems on the interior wall surfaces compared to the exterior wall surfaces, which is consistent with the simulation results. In congruence with the simulation results, the findings show that there is more water content exists in the interior wall than in the exterior walls.

Given the results of the hygro-thermal performance of the concerned historical facades concerning both the internal and external walls, the effectiveness of a mechanical intervention method as a rising damp mitigation measure in masonry constructions was chosen for effectiveness evaluation in

order to identify appropriate retrofit solutions. In particular, wall cutting has been used for centuries and considered to be amongst one of the most effective measures to stop the migration of capillary water from the ground as a water impermeable layer is inserted into the walls. The aforementioned simulation software (WUFI) was thus deployed for modelling the case study building components (i.e., the interior and exterior walls) with the selected retrofit method (wall cutting) in order to analyze and evaluate the performance of the intervention. The results of the hygro-thermal analysis of the historical masonry walls with the retrofit are then presented. The main findings of the study can be summarized that in historical buildings, the wall cutting method appears to be an effective rising damp mitigation measure. If carried out properly from the construction point of view, the moisture transport above the insertion plane of an impermeable material layer can be blocked successfully. Nevertheless, there still exists potential impact from humidity due to indoor climate and outdoor weather conditions. Moreover, the cutting wall method was found to be more effective for retrofitting the interior wall (90% of water content reduction) compared to the exterior cases (45% to 55% water content reduction). In fact, in contrast with the interior wall's water content during the 2019 to 2023 period (which involved a gradual water accumulation), the water content of the exterior cases tended to fluctuate more. With regard to the interior wall, a notable drying out phase appeared in the first two years after the retrofit whereas all cases of the exterior walls took around three years to dry out. The simulation results also suggest that the masonry below the cut is close to saturation even after the intervention. Moreover, the simulation results also point to the positive impact of wall thickness for the exterior walls on the performance of wall cutting.

Since this dissertation relies mainly on simulation results, it benefited from the results of a simulation calibration effort at TU Wien, Austria. The simulation results for a retrofitted wall at TU Campus, including relative humidity and temperature, were compared with data measured at the positions within the different layers of the existing wall construction in order to evaluate the reliability of the employed simulation tool. Whereas this calibration effort was not conducted for a case study building in Thailand, it still provided some relevant and valuable information concerning the predictive performance of the deployed simulation model, as a number of input settings were analyzed and chosen based on their influence on the simulation results. In order to achieve better agreement between measured and calculated data, some simulation settings and inputs (i.e. initial condition, indoor and outdoor climate, and some material properties) were adjusted. The results of the comparisons between calculated and measured values were analyzed. The results show a noticeable improvement of the predictive potency of the simulation model when input variables were adjusted based on measurements. A key implication of this study is that it is of great importance to apply a local indoor and outdoor climate. Additionally, accurate initial conditions (i.e., starting values of layer temperatures and humidities) can contribute to more reliable simulation results.

Moreover, since the reliable knowledge of material-specific parameters is essential to generating dependable simulation models, this dissertation also investigated the degree of sensitivity of hygro-thermal analysis to the choice of model input data (material properties). A hygro-thermal performance model

of a wall construction was generated and subjected to a sensitivity analysis to identify a subset of the input variables concerning material properties, with significant influence on the simulation outcomes, comprising of material water content, temperature and the relative humidity of the air pores in the material. The calculations were performed under the condition of hot-humid climate for a Thai historical wall (Thai temple wall) in the central region, constructed in 19th-century. The results illustrated that the most influential parameters are the water vapor diffusion resistance factor ( $\mu$ ), the water absorption coefficient ( $A$ ), and the thermal conductivity ( $\lambda$ ), based on the mean relative deviations. While considering the coefficient of variation (CV of deviations), the most influential parameter was shown to be porosity.

## 6.2 Future research

The outcomes of this research highlight a number of issues that can be addressed further in future studies:

- Regarding the predictive performance of hygro-thermal simulations of an existing wall, the number of adjusted input variables were limited with only four modification scenarios in this study. More modification scenarios of model inputs such as adjusting material surface properties (e.g., sd-value, heat transfer coefficient, and adhering fraction of rain), would be beneficial to improve the predictive potency of the simulation model.
- In performing a sensitivity analysis in order to determine the most appropriate choice of model input data for hygro-thermal simulation, six material-related input parameters were examined. More effort is required to evaluate the sensitivity of the hygro-thermal performance indicators to other material properties, such as water absorption isotherm. Due to the fact that the same model used in different climate conditions could result in a different sensitivity classification, the simulation models simulating under other climate conditions are suggested to perform a sensitivity analysis. In addition, the results obtained are relative to 0.8 m thick solid wall (i.e., clay brick, lime plaster and lime stucco). Therefore, for future research, other construction types and configurations should be studied.
- For future studies related to the diagnosis of moisture-related problems, it is important to investigate and evaluate all the damages and failure in every part of the building in order to address the primary causes of the damages. Performing the diagnosis with supportive devices (e.g., moisture measurement equipment), additional confidence in the diagnosis can be gained. Additionally, an understanding of results, from both numerical simulation and on-site investigation, is a substantial part of the building damage diagnosis since accuracy of diagnosis of the dampness problems in historical buildings can be significantly improved. In terms of enhancing the hygro-thermal simulation accuracy, the simulation model calibration using in situ monitoring data is highly recommended.

- Limitations imposed by wall cutting as a retrofit method should be addressed in future studies. For example, improper execution may cause more damage to the construction, resulting in cracks or increased seismic vulnerability. Moreover, the saturation near the masonry below the cut may have negative implications. In-situ empirical validation of the simulation models also needs to be addressed in future studies.

## References

- Aien, S., Taheri, M., Pinich, S., Schuss, M., and Mahdavi, A. (2017), 'Predictive performance of hygro-thermal simulation models: A case study,' Proceedings of the 12th International EnviBUILD Conference (7th & 8th September 2017): 7.
- Alev, Ü., Uus, A., Teder, M., Miljan, M-J., and Kalamees, T. (2014), 'Air leakage and hygrothermal performance of an internally insulated log house,' NSB 2014 10th Nordic Symposium on Building Physics, 15-19 June 2014, Lund, Sweden. pp. 55-62. URL:<https://wufi.de/en/wp-content/uploads/sites/11/2014/12/Alev-Uus-et-al-2014-Air-leakage-and-hygrothermal-performance.pdf>
- Alfano, G., Chiancarella, C., Cirillo, E., Fato, I., and Martellotta, F. (2005), 'Long-term performance of chemical damp-proof courses: twelve years of laboratory testing,' Build Env. 2005; 41, pp. 1060-9.
- Aranyanak, C. (1984), 'Effects of soluble salts in the deterioration of monuments,' Academic conference Kasetsart University 22<sup>nd</sup> Environment Program, 30 January - 2 February 1984, Bangkok, Part 24, 18 pages.
- Arch CU (2017), 'Initial and Planning Stages in Preservation Process, Contributions to Recommendation for Appropriate Conservation Treatments: A Case of Conservation of the Our Lady of the Rosary Church Project,' Department of Architecture, Chulalongkorn university, Bangkok, Thailand.
- Arena, L. and Mantha, P. (2013), 'Moisture Research - Optimizing Wall Assemblies,' U. S. Department of Energy.
- ASHRAE (2006), 'Proposed New Standard 160, Design Criteria for Moisture Control in Buildings,' American Society of Heating, Refrigerating, and Air-Conditioning Engineers, Atlanta, GA.
- Bakri, N.N.O. and Mydin, M.A.O. (2014), 'General building defects: causes, symptoms and remedial work,' European Journal of Technology and design, Vol. (3), No.1.
- Beall, C. (1999), 'Thermal and moisture protection manual for architects, engineers, and contractors,' McGraw-Hill company, Inc., USA, pp. 1-19.
- Biology dictionary (2020). 'biology online.'  
URL:<https://www.biologyonline.com/dictionary/hydrophobic>

- Browne, D. (2012), 'The SPAB Hygrothermal Modelling: Interim Report,' The SPAB research report 3, October 2012, Society for the Protection Ancient Buildings, UK, 98 pages.
- BSI (2007), 'BS EN 15026: 2007 – Hygrothermal performance of building components and building elements – Assessment of moisture transfer by numerical simulation,' British Standards Institution, London, UK.
- Bunjerdskul, K. (2014), 'Changes of slaked lime formula in traditional Thai architectural conservation,' Master thesis dissertation, Chulalongkorn University, Thailand.
- Campian, C. and Pop, M. (2016), 'Methods for elimination of dampness in Building walls,' IOP Conf. Series: Materials Science and Engineering, Vol. 133; 012049, International Conference on Innovative Research - ICIR Euroinvent 2016, 19–20 May 2016, Iasi, Romania.
- Claridge, D. E. (2011), 'Building simulation for practical operational optimization,' Build. Perform. Simul. Des. Oper., p. 365.
- Climatemps (2020), 'Bangkok Climate & Temperature.'  
URL: <http://www.bangkok.climatemps.com/>
- DIN 4108-3 (2001), 'DIN 4108-3:2001-07; Thermal protection and energy economy in buildings - Part 3: Protection against moisture subject to climate conditions; Requirements and directions for design and construction,' Beuth Verlag GmbH, Berlin, Germany.
- DIN 52617 (1987), 'Bestimmung des Wasseraufnahmekoeffizienten von Baustoffen (Determination of the water uptake coefficient of building materials),' Beuth Verlag GmbH, Berlin, Germany.
- DIN 52620 (1991), 'Bestimmung des Bezugsfeuchtegehalts von Baustoffen (Determination of the reference moisture content of building materials),' Beuth Verlag GmbH, Berlin, Germany.
- Dullien, F.A. and Batra, V.K. (1970), 'Determination of the structure of porous media,' Ing Eng Chem 1970; 62 (10): 25-53.
- EMERISDA (2014), 'Existing methods against rising damp,' Summary report, D2.1 Final version 31-07-2014, TU Delft, Netherlands.
- Falchi, L., Slamzi, D., Balliana, E., Drussi, G., and Zendri E. (2018), 'Rising damp in historical Building: A Venetian perspective,' Building and Environment 131, pp. 117-127.
- Fiacco, A.V. (1983), 'Introduction to Sensitivity and Stability Analysis in Nonlinear Programming,' Academic Press, New York.
- Fixit group (2017), 'Restoration and remediation products.' URL: <http://www.fixit.ch/Home/Produkte/Restaurierungs-und-Sanierungsprodukte/>
- Franzoni, E. (2014), 'Rising damp removal from historical masonries: A still open challenge,' Construction and Building Materials 54, pp. 123-136.

- Franzoni, E. (2018), 'State-of-the-art on methods for reducing rising damp in masonry,' *Journal of Cultural Heritage* 31, Supplement, p. S3-S9, URL: <https://doi.org/10.1016/j.culher.2018.04.001>
- Fraunhofer IBP (2007), 'WUFI Presses Benchmark Test of EN 15026,' Fraunhofer Institute for Building Physics, Holzkirchen, Germany. URL: [https://wufi.de/en/wp-content/uploads/sites/11/2015/04/WUFI-Pro-Benchmarktest-EN15026\\_en.pdf](https://wufi.de/en/wp-content/uploads/sites/11/2015/04/WUFI-Pro-Benchmarktest-EN15026_en.pdf)
- Freitas, V.P. and Torres, M.I.M. (2003), 'The influence of the boundary conditions in rising damp in historical constructions,' *WITT Transaction on the Built Environment*, ISSN: 1743-3509, Vol. 66. 12 pages.
- Freitas, V.P., Guimarães, A.S., and Delgado, J.M.P.Q. (2015), 'Wall-Base Ventilation System to Control Rising Damp: A Case Study of Vilar de Frades Historical Church in Portugal,' *International Journal of Architectural Heritage*, 9(7), pp. 859-865.
- Geving, S. and Holme J. (2010), 'The drying potential and risk for mold growth in compact wood frame roofs with built-in-moisture,' *Journal of Building Physics* 33(3): 249–69.
- Geving, S., Kvalvik, M., and Martinsen, E. (2011), 'Rehabilitation of basement walls with moisture problems by the use of vapour open exterior thermal insulation,' *Proceedings of the 9th Nordic Symposium on Building Physics—NSB 2011, Tampere, Finland*, 1: 323–30.
- Googlemap (2020a), 'Location of Wat Niwet Thammaprawat, Ayutthaya.' URL: <https://www.google.com/maps/place/Wat+Niwet+Thammaprawat+Ratchaworawihan/@14.2314861,100.5739654,17z/data=!3m1!4b1!4m5!3m4!1s0x30e2784153bf4345:0xe1ef0ffc1bd09288!8m2!3d14.2314809!4d100.5761541>
- Googlemap (2020b), 'Location of Holy Rosary Church, Bangkok.' URL: <https://www.google.com/maps/place/Holy+Rosary+Church/@13.7313057,100.5114269,17z/data=!3m1!4b1!4m5!3m4!1s0x30e298d9390005f5:0xbc6756f8caa4fdcd!8m2!3d13.7313005!4d100.5136156>
- Guimaraes, A.S., Delgado, J.M.P.Q., and Freitas, V.P. (2012a), 'Rising damp in walls: Evaluation of the level achieved by the damp front,' *Journal of Building Physics* 37(1), pp. 6-27.
- Guimaraes, A.S., Delgado, J.M.P.Q., and Freitas, V.P. (2012b), 'Numerical Simulation of Rising Damp Phenomenon,' *Defect and Diffusion Forum*, ISSN: 1662-9507, Vols. 326-328, pp. 48-53.
- Hagentoft, C.-E. (2001), 'Introduction to Building Physics,' *Studentlitteratur AB*, 444 Pages.
- Hägerstedt S.O. and Arfvidsson, J. (2010), 'Comparison of field measurements and calculations of relative humidity and temperature in wood framed walls,' In O. Zmeskal (Ed.), *Conference proceedings – Thermophysics 2010*, Faculty of Chemistry, Brno University of Technology, Czech Republic, pp. 93-101.

- Hägerstedt, S.O. and Harderup L.-E. (2011a), 'Comparison of measured and calculated temperature and relative humidity with varied and constant air flow in the facade air gap,' Proceedings of the 9th Nordic Symposium on Building Physics – NSB 2011, Tampere, Finland, 1:147–54.
- Hägerstedt, S.O. and Harderup L.-E. (2011b), 'Control of moisture safety design by comparison between calculations and measurements in passive house walls made of wood,' Proceedings of the 12th International Conference on Durability of Building Materials and Components – XII DBMC, Porto, Portugal, 1: 25–32.
- Halim, A.A., Harun, S.N., and Hamid, Y. (2012), 'Diagnosis of dampness in conservation of historic building,' Journal design + built, Vol. 5.
- Hall, C. and Hoff, W.D. (2007), 'Rising damp: capillary rise dynamics in walls,' Proceedings of the Royal Society A. 2007, Vol. 463, pp. 1871-1884.
- Heiman, J., Waters, E., and McTaggart, R. (1973), 'The treatment of rising damp,' Archit Sci Rev, 16(4), pp. 170-7.
- Hens, H. (1996), 'Modelling Heat Air and Moisture Transfer in Insulated Envelope Parts,' Final Report IEA-Annex 24, KU, Leuven,
- Holdridge, D.A. (1963), 'The composition of some British clays used in the fine ceramic industries,' in the international clay conference, Vol. 1, New York: Macmillan, pp. 351-364.
- Holm, A. and Künzel, H.M. (2003), 'Two-dimensional transient heat and moisture simulations of rising damp with WUFI 2d,' Fraunhofer Institute for Building Physics, Holzkirchen, Germany, 7 pages. URL: <https://wufi.de/literatur/>
- Iaqsolutions (2020), 'IAQS – Indoor air quality Solutions.' URL: <https://iaqsolutions.com.au/what-is-efflorescence/>
- Ibrahim, M., Wurtz, E., Biwole, P. H., Achard, P., and Sallee, H. (2014), 'Hygrothermal performance of exterior walls covered with aerogel-based insulating rendering,' Energy Build., Vol. 84, pp. 241–251.
- ISO (2001), 'EN 13788 – Hygrothermal performance of building components and building elements - Internal surface temperature to avoid critical surface humidity and interstitial condensation - Calculation methods,' International Organization for Standardization.
- Issarathumnoon, W. (2018), 'Initial and Planning Stages in Preservation Process, Contributions to Recommendation for Appropriate Conservation Treatments: A Case of Conservation of the Our Lady of the Rosary Church Project,' NAJUA: Architecture, Design and Built Environment, Vol. 33, (Jun. 2018), B3-B21.
- Ivliev E.A. (2007), 'Electroosmotic drying of building walls and basements,' Surf. Eng. Appl. Electrochem 43(4), pp. 291–296.
- Jungsiriarrak, S. (1997), 'Conservation of structure and material of Thai historical building,' Handout of the course no. 262-407 Preservation of

historical buildings and ancient sites, Faculty of Architecture, Silpakorn University (Thailand), pp. 8-11.

Krus, M. (1996), 'Moisture Transport and Storage Coefficients of Porous Mineral Building Materials. Theoretical Principles and New Test Methods, Fraunhofer IRB Verlag.

Künzel, H.M. (1995), 'Simultaneous Heat and Moisture Transport in Building Components. – One- and two-dimensional calculation using simple parameters,' Fraunhofer IRB Verlag Stuttgart 1995 (ISBN 3-8167-4130-7), 65 pages.

Künzel, H.M. (1998), 'Effect of interior and exterior insulation on the hygrothermal behavior of exposed walls,' Materials and structures 31, H. 206, pp. 99-103.

Lubelli, B., van Hees, R.P.J., and Groot C.W.P. (2006), 'Sodium chloride crystallization in a "salt transporting" restoration plaster,' Cement Concrete Res 36, 1467-1474.

Lyu, C., Nastase, G., Ukpai, G., Serban, A., and Rubinsky, B. (2017), 'A comparison of freezing-damage during isochoric and isobaric freezing of the potato,' PeerJ 5: E3322, DOI: 10.7717/peerj.3322.

Mapsofworld (2020), 'Thailand Location Map.' URL: <https://www.mapsofworld.com/thailand/thailand-location-map.html>

Mason, G. (1974), 'Rising damp,' Build Sci. 1974; 9, pp. 227-31.

Massari, G. and Massari, I. (1985), 'Damp buildings old and new,' Bulletin of the Association for Preservation Technology, Vol. 17, No. 1, pp. 2-30. [translation of Risanamento igienico dei locali umidi. Milano: Hoepli, 1985]

Mendes, N., Philippi, P.C., Lamberts, R. (2002), 'A new mathematical method to solve highly coupled equations of heat and mass transfer in porous media,' International Journal of Heat and Mass Transfer, Vol. 45, Issue 3, January 2002, pp. 509-518.

Meteonorm (2020), 'Meteonorm Software,' Meteotest AG, Swiss Federal Office of Energy, Bern, Switzerland.  
URL:<https://meteonorm.meteotest.ch/en/>

Monetti, V., Davin, E., Fabrizio, E., Andre, P., and Filippi, M. (2015), 'Calibration of building energy simulation models based on optimization: A case study,' in Energy Procedia, Vol. 78, pp. 2971–2976.

Morgan, R.F. (2011), 'A New Journal for the Torrid Zone,' Journal of Tropical Psychology, Vol. 1, p. 1.

Mundt-Petersen, S.O. (2012), 'Literature study/State-of-the-art—Mould and moisture safety in constructions,' Report TVBH-3053, Lund University, Sweden.

- Mundt-Petersen, S.O. (2013a), 'Comparison of hygrothermal measurements and calculations in a single-family wooden house on the west coast of Sweden,' Report TVBH-3054, Lund University. In press.
- Mundt-Petersen, S.O. (2013b), 'Comparison of hygrothermal measurements and calculations in a single-family wooden house in the Swedish municipality of Upplands-Bro,' Report TVBH-3058, Lund University. In press.
- Mundt-Petersen, S.O. (2015), 'Moisture Safety in Wood Frame Buildings - Blind evaluation of the hygrothermal calculation tool WUFI using field measurements and determination of factors affecting the moisture safety,' Byggnadsfysik LTH, Lunds Tekniska Högskola.
- Mundt-Petersen, S.O. and Harderup L. (2013), 'Validation of a one-dimensional transient heat and moisture calculation tool under real conditions,' Thermal Performance of the Exterior Envelopes of Whole Buildings XII International Conference.
- Nicastro, D.H., ed. (1997), 'Failure Mechanism in Building construction,' ASCE Press, New York.
- Othmen, I., Poullain, Ph., Caucheteux, A., and Leklou, N. (2014), 'Sensitivity analysis of the Künzel model: application to the study of the hygrothermal transfer in a tuffeau wall,' Advanced Computational Methods and Experiments in Heat Transfer XIII 417.
- Oxley, R. (2003), 'Survey and Repair of Traditional Buildings, A Sustainable Approach,' Great Britain: Bath Press.
- Pannell, D.J. (1997), 'Sensitivity analysis of normative economic models: Theoretical framework and practical strategies,' Agricultural Economics 16: 139-152. URL: <https://dpannell.science.uwa.edu.au/dpap971f.htm>
- Pazderka, J., Hájková, E., and Jiránek, M. (2017), 'Underground air duct to control rising moisture in historic buildings: improved design and its drying efficiency,' Acta Polytechnica 57(5), pp. 331-339.
- Phumkokrux, N. (2020), 'A Study of Köppen-Geiger Climate Classification Change in Thailand from 1987–2017,' In: Monprapussorn S., Lin Z., Sitthi A., Wetchayont P. (eds), Geoinformatics for Sustainable Development in Asian Cities, ICGGS 2018, Springer Geography. Springer, Cham., pp. 109-117. URL: [https://doi.org/10.1007/978-3-030-33900-5\\_11](https://doi.org/10.1007/978-3-030-33900-5_11)
- Pinich, S., Taheri, M., and Mahdavi, A. (2018), 'Sensitivity Analysis of the hygro-thermal simulation model of a historical building façade in hot-humid climate,' Poster: BauSIM2018 - 7. Deutsch - Österreichische IBPSA - Konferenz Tagungsband, Karlsruhe, Germany; 26.09.2018 - 28.09.2018; in: Proceedings of BauSim2018, Paper-Nr. 1157, 6 pages.
- Prajapati, S. (2018), 'Effect of aging on water absorption coefficient of commercial grade stucco,' Master Thesis, Master of Engineering, Department of Mechanical Engineering at University of Victoria, Victoria, British Columbia, Canada.

- PVsyst (2020), 'PVsyst – Meteonorm data and program'  
 URL: [https://www.pvsyst.com/help/meteo\\_source\\_meteonorm.htm](https://www.pvsyst.com/help/meteo_source_meteonorm.htm)
- Qinru, L., Rao, J., and Fazio, P. (2009), 'Development of HAM tool for building envelope analysis, Building and Environment,' Vol. 44, Issue 5, May 2009, pp. 1065–1073.
- Ramsom, W.H. (1981), 'Building Failure; Diagnosis and avoidance,' E & F.N Spon, New York.
- Reimondo, M., Dondi, M., Gardini, D., Guarini, G., and Mazzanti, F. (2009), 'Predicting the initial rate of water absorption in clay brick,' Construct Build Mater 2009; 23: pp. 2623-30.
- Rirsch, E. and Zhang, Z. (2010), 'Rising damp in masonry walls and the importance of mortar properties,' Construction and Building Materials 24, pp. 1815-1820.
- Sacho, T. (2008), 'Wat Niwet Thammaprawat Worawihan,' Fine Arts Department. Lannkam, Bangkok, Thailand.
- Sandrolini, F. and Franzoni, E. (2007). 'Repair systems for the restoration of ancient buildings – Dampness rise problem,' Restoration of Buildings and Monuments, Vol. 13, No. 3, pp. 161-172.
- Santamouris, M. and Dascalaki, E. (2002), 'Passive retrofitting of office buildings to improve their energy performance and indoor environment: The OFFICE project,' Build. Environ., Vol. 37, no. 6, pp. 575–578.
- Sassi, S. (2013), 'Validation of wind-driven rain module for HAM-tools,' A thesis presented to Ryerson University, Master of Applied Science, Building science, Toronto, Ontario, Canada.
- Schuss, M., Mahdavi, A., Pont, U., Sustr, C., Aien, S., Ghazi Wakili, K. and Stahl, T. (2017), 'Strukturierte Aerogelputze'; in: 'Bauphysik-Kalender 2017,' 1, Ernst & Sohn. Architektur und technische Wissenschaften Berlin, Berlin, ISBN: 9783433031698, 153 - 175.
- Stephan, E., Caucheteux, A., Cantin, R., Tasca-Guernouti, S., and Michel, P. (2013), 'Sensitivity analysis of an energyplus simulation model of the ambient humidity in an old building,' Proceedings of the 13<sup>th</sup> Conference of International Building Performance Simulation Association, Chambéry, France.
- Stevenandrewmartin (2020), 'Steven A. Martin. – Political Geography of Thailand-Six Regions w/77 Provinces.'  
 URL:<https://www.stevenandrewmartin.com/thai-geography/>
- Tahmasebi, F. and Mahdavi, A. (2012), 'Optimization-based simulation model calibration using sensitivity analysis,' IBPSA-CZ. Conference Brno, 8. a 9. 11.
- Tahmasebi, F. and Mahdavi, A. (2013), 'A two-staged simulation model calibration approach to virtual sensors for building performance data,' Proc. 13th Int. Conf. Int. Build. Perform. Simul. Assoc., pp. 608–613.

- Tazky, L. and Sedlakova, A. (2015), 'Design of the ventilated air channel to resolve moisture problems in the historical church,' *Energy Procedia* 78, pp. 1323 – 1328.
- TMD (2020), 'Climate in Thailand,' Thai Meteorological Department, Bangkok, Thailand. URL: [https://www.tmd.go.th/info/knowledge\\_weather01\\_n.html](https://www.tmd.go.th/info/knowledge_weather01_n.html)
- Torres, M.I.M. and Freitas, V.P. (2007), 'Treatment of rising damp in historical buildings: wall base ventilation,' *Building and Environment* 42, pp. 424-435.
- Torres, M.I.M. and Freitas, V.P. (2010), 'The influence of the thickness of the walls and their properties on the treatment of rising damp in historic buildings,' *Construction and Building Materials* 24, pp. 1331-1339.
- Torres, M.I.M., (2013), 'Wall base ventilation system to treat rising damp: the influence of the size of the channels,' *J. Cult. Herit.* 2013, doi: 10.1016/j.culher.2013.03.005.
- Trotman, P. (2007), 'Rising damp in walls: diagnosis and treatment,' BRE Digest 245 (Building Research Establishment). Watford: HIS BRE Press.
- Uchida, Y., Yasukawa, K., Tenma, N., Taguchi, Y., Ishii, T., Suwanlert, J., and Lorphensri, O. (2011), 'Subsurface Temperature Survey in Thailand for Geotherma Application,' *J. Geotherm Res. Soc. Japan*, Vol. 33, No.2, pp. 93-98.
- Wasantachad, N. (2006), 'Salts in brick wall,' *NAJUA: Architecture, Design and Built Environment*, v. 22, pp. 237-254.
- Wikimedia (2020a), 'File: Thailand Bangkok locator map. svg.' URL: [https://commons.wikimedia.org/wiki/File:Thailand\\_Bangkok\\_locator\\_map.svg](https://commons.wikimedia.org/wiki/File:Thailand_Bangkok_locator_map.svg)
- Wikipedia (2020a), 'Datei: Thailand Ayutthaya locator map.svg.' URL: [https://de.wikipedia.org/wiki/Datei:Thailand\\_Ayutthaya\\_locator\\_map.svg](https://de.wikipedia.org/wiki/Datei:Thailand_Ayutthaya_locator_map.svg)
- Wikipedia (2020b), 'Holy Rosary Church, Bangkok.' URL: [https://en.wikipedia.org/wiki/Holy\\_Rosary\\_Church,\\_Bangkok](https://en.wikipedia.org/wiki/Holy_Rosary_Church,_Bangkok)
- Wilson, F. (1984), 'Building materials evaluation handbook,' Van Nostrand Reinhold Company Inc., New York, USA, pp. 101-111.
- Woloszyn, M. and Rode, C. (2008), 'Tools for performance simulation of heat, air and moisture conditions of whole building,' *Building simulation*. 1: 5–24.
- Wongchaturaphat, W. (2011), 'Lai-sen Bohransthan, Wat Niwet Thammapravat Ratchaworawihan,' Fine Arts Department, Bangkok, Thailand, ISBN 9789744174796, 200 pages.
- WTA (2004), 'WTA-Guideline 6-2-01/E – Simulation of Heat and Moisture Transfer,' WTA-International, Munich, Germany.

WUFI (2020a), 'WUFI – the transient coupled heat and moisture transport simulation,' Fraunhofer Institute for Building Physics (IBP), Holzkirchen, Germany. URL: <https://wufi.de/en/>

WUFI (2020b), 'WUFI – WUFI® Pro 5 software on-line help,' Fraunhofer Institute for Building Physics (IBP), Holzkirchen, Germany.

WUFI (2020c), 'WUFI – WUFI® 2D software on-line help,' Fraunhofer Institute for Building Physics (IBP), Holzkirchen, Germany.

WUFI (2020d), 'WUFI – WUFI® Pro 5 manual,' Fraunhofer Institute for Building Physics (IBP), Holzkirchen, Germany. URL: [https://wufi.de/en/wp-content/uploads/sites/9/2014/09/WUFI-Pro-5\\_Manual.pdf](https://wufi.de/en/wp-content/uploads/sites/9/2014/09/WUFI-Pro-5_Manual.pdf)

WUFI (2020e), 'WUFI – WUFI® 2D Installation & Introduction,' Fraunhofer Institute for Building Physics (IBP), Holzkirchen, Germany. URL: [https://wufi.de/en/wp-content/uploads/sites/9/2014/09/WUFI2D-3\\_Manual.pdf](https://wufi.de/en/wp-content/uploads/sites/9/2014/09/WUFI2D-3_Manual.pdf)

WUFI-Wiki (2020a), 'WUFI-Wiki – WUFI Manuals and Tutorials,' Fraunhofer Institute for Building Physics (IBP), Holzkirchen, Germany. URL: <https://www.wufi-wiki.com/mediawiki/index.php/Hauptseite>

WUFI-Wiki (2020b), 'WUFI-Wiki – WUFI Manuals and Tutorials: WUFI 2D Details: Physics,' Fraunhofer Institute for Building Physics (IBP), Holzkirchen, Germany. URL: [https://www.wufi-wiki.com/mediawiki/index.php/Details:Physics#The\\_Calculation\\_Model](https://www.wufi-wiki.com/mediawiki/index.php/Details:Physics#The_Calculation_Model)

## List of Figures

Figure 1.1	Schematic diagrams showing the effect and distribution of moisture inside and outside wall (source: Künzle 1995).....	10
Figure 2.1	(a) A material surrounded by humid air with a part of the pore structure absorbing moisture (source: Hagentoft 2001), and (b) a scanning electron micrograph of cellular concrete with 22x magnification, showing its pore structure (source: Künzle 1995) .....	14
Figure 2.2	Sorption isotherm (source: Hagentoft 2001) .....	15
Figure 2.3	Schematic diagram of the moisture storage function of a hygroscopic capillary-active building material (source: Künzle 1995).....	16
Figure 2.4	Diffusion of water vapor through a porous material layer (source: Hagentoft 2001) .....	18
Figure 2.5	Chain of pores inside the material (source: Hagentoft 2001) ...	19
Figure 2.6	Transport of water in a partially filled pore system (source: Hagentoft 2001) .....	20
Figure 2.7	The flow chart for the WUFI model (source: WUFI-Wiki 2020a) .....	25
Figure 2.8	Temperatures of the exterior air compared with temperatures of the ground at a depth of 1 m (source: WUFI-Wiki 2020a).....	33
Figure 2.9	Moisture storage function, and (b) the moisture storage function of solid brick masonry provided in WUFI database (source: WUFI 2020b).....	38
Figure 2.10	Liquid transportation function provided in the software (source: WUFI 2020b).....	39
Figure 2.11	Section of the layers of the tested façade (source: Schuss et al. 2017).....	42
Figure 2.12	Position of the Sensors in a façade (source: Schuss et al. 2017) .....	42
Figure 2.13	View of installed sensors on the existing wall; temperature and humidity sensors as well as the heat flow plates of the test areas on the south façade (source: Schuss et al. 2017) .....	43
Figure 2.14	External surface after retrofit (source: Schuss et al. 2017).....	43
Figure 2.15	Position of sensors in different layers of construction (01, 02, 04, and 05) .....	44
Figure 2.16	An example of Box plot with whiskers. (source: Othmen et al. 2014).....	49

Figure 2.17	Distribution of relative humidity (Left) and temperature (Right) of measured values, initial model values and values from all scenarios in each node (source: Aien et al. 2017).....	50
Figure 2.18	R <sup>2</sup> of relative humidity (Left) and temperature (Right) of measured values, initial model values and values from all scenarios in each node (source: Aien et al. 2017).....	51
Figure 2.19	(CV)RMSD of relative humidity (Left) and temperature (Right) of measured values, initial model values and values from all scenarios in each node (source: Aien et al. 2017).....	51
Figure 2.20	Absolute error of relative humidity (Left) and temperature (Right) of measured values, initial model values and values from all scenarios in each node (source: Aien et al. 2017).....	52
Figure 2.21	Relative error of relative humidity of measured values, initial model values and values from all scenarios in node 01 (Left) and node 02 (Right). (source: Aien et al. 2017).....	52
Figure 2.22	Relative error of relative humidity of measured values, initial model values and values from all scenarios in node 04 (Left) and node 05 (Right). (source: Aien et al. 2017).....	53
Figure 2.23	Trend of relative humidity in middle of the wall (node 04) comparing between the measured data, the calculated data in scenario 3 and scenario 4 (source: Aien et al. 2017) .....	53
Figure 3.1	Thailand location map (source: Mapsofworld 2020).....	55
Figure 3.2	Regions of Thailand and surrounding countries (source: Stevenandrewmartin 2020).....	55
Figure 3.3	Average monthly temperature in each region in Thailand during 1981-2010 (30 years) (source: TMD 2020).....	57
Figure 3.4	The location of (a) Wat-Niwet-Thammaprawat temple (source: Googlemap 2020a), (b) Ayutthaya, Thailand (source: Wikipedia 2020a) .....	61
Figure 3.5	Wat-Niwet-Thammaprawat temple, Ayutthaya, Thailand (source: Pinich 2018).....	61
Figure 3.6	Interior perspective of Wat-Niwet-Thammaprawat temple, Ayutthaya, Thailand .....	61
Figure 3.7	Last refurbishment of the temple's exterior wall in 2015 (source: Pinich 2018).....	62
Figure 3.8	Signs of post-retrofit moisture problems on the middle and lower parts of the walls (photo taken in 2017) (source: Pinich 2018).....	62
Figure 3.9	Architectural drawings of the building (i.e., (a) plan and (b) section) (source: Wongchaturaphat 2011) .....	63
Figure 3.10	Photographs (a) and (b) from the renovation in 2015 with the Massari method (EMERISDA 2014).....	64
Figure 3.11	The wall construction in cross-section details. ....	64
Figure 3.12	The simulation model of the case-study building (typical historical Thai wall construction) (source: Pinich 2018).....	65
Figure 3.13	Mean relative deviations (from the initial model) of calculated hourly water content values in the three layers as a result of varying (a) A, (b) n, (c) $\rho$ , (d) $\lambda$ , (e) $C_p$ , (f) $\mu$ .....	72
Figure 3.14	Mean relative deviations (from the initial model) of calculated hourly relative humidity values in the three layers as a result of varying (a) A, (b) n, (c) $\rho$ , (d) $\lambda$ , (e) $C_p$ , (f) $\mu$ .....	73

Figure 3.15	Mean relative deviations (from the initial model) of calculated hourly temperature values in the three layers as a result of varying (a) $A$ , (b) $n$ , (c) $\rho$ , (d) $\lambda$ , (e) $C_p$ , (f) $\mu$ .....	74
Figure 3.16	Box plots of relative deviations (from the initial model) of calculated hourly water content values in the brick layer as a result of varying $A$ (Upper chart) and $\mu$ (Lower chart) (source: Pinich 2018).....	77
Figure 3.17	Box plot of relative deviations (from the initial model) of calculated hourly relative humidity in the brick layer as a result of varying $\mu$ (source: Pinich 2018) .....	77
Figure 3.18	Time evolution of the water content for water vapor diffusion resistance ( $\mu$ ).....	78
Figure 4.1	Efflorescence on the wall surface (source: Iaqsolutions 2020)	80
Figure 4.2	(a) water height rise in an ideal capillary tube of radius $r$ and (b) schematic representation of water capillary rise in masonry wall (source: Franzoni 2014).....	83
Figure 4.3	Schematic diagram of a brick wall presenting the equilibrium between capillary rise and surface evaporation (source: Rirsch and Zhang 2010).....	84
Figure 4.4	Sketch of sharp front model.....	85
Figure 4.5	A solid brick sample made of clay with its displayed dimensions taken from Holy Rosary Church.....	87
Figure 4.6	Simplified sketch sections of Thai traditional foundations (source: Jungsiriarrak 1997) .....	90
Figure 4.7	Foundation construction of one of the historical building (sermons hall) in Wat-Niwet-Thammaprawat temple, Ayutthaya, Thailand (source: Sacho 2008).....	90
Figure 4.8	The location of (b) Holy Rosary Church (source: Googlemap 2020b), (a) Bangkok, Thailand (source: Wikimedia 2020a) ....	92
Figure 4.9	Holy Rosary Church, Bangkok, Thailand (source: Wikipedia 2020b).....	93
Figure 4.10	The interior perspective of Holy Rosary Church (source: Wikipedia 2020b) .....	93
Figure 4.11	The section of isometric model of Holy Rosary Church (source: Arch CU 2017) .....	93
Figure 4.12	Architectural drawings of Holy Rosary Church (i.e., (a) plan and (b) East, (c) North, (d) West, (e) South elevations) (source: Arch CU 2017) .....	94
Figure 4.13	The case-study wall and the foundation construction.....	95
Figure 4.14	The case-study wall construction in enlarged cross-section detail. ....	95
Figure 4.15	The wall and foundation construction's simplified representation in the simulation model .....	96
Figure 4.16	Utility program provided by WUFI, for creating customized weather file (source: Siassi 2013).....	99
Figure 4.17	Building plan with investigation areas .....	101
Figure 4.18	The defects on the interior wall of sacristy room .....	103
Figure 4.19	The defects on the inner surface of exterior wall of the northern hall connecting to sacristy room .....	103
Figure 4.20	The defects on the outer surface of exterior wall.....	104
Figure 4.21	The defects on the outer surface of exterior wall.....	105

Figure 4.22	The defects on the surface of the entrance column.....	105
Figure 4.23	Simplified construction representation in the simulation model with the specification of the defined upper-part wall segments .....	107
Figure 4.24	Time evolution of the water content ( $\text{kg}\cdot\text{m}^{-3}$ ) given for three segments of the upper part of interior wall .....	108
Figure 4.25	Time evolution of the water content ( $\text{kg}\cdot\text{m}^{-3}$ ) given for three segments of the upper part of exterior wall facing south.....	108
Figure 5.1	International papers per year (source: Franzoni 2018).....	111
Figure 5.2	Research approach in the international papers examined (source: Franzoni 2018).....	111
Figure 5.3	(a) Dynamics of capillary water rise in masonry, and (b) schematic representation of the three factors involved, which determine the resulting height of rising damp (source: Franzoni 2018).....	112
Figure 5.4	Repair systems in 46 international papers examined by Franzoni (2018).....	112
Figure 5.5	Overview of current repair methods, according to the groups categorized by Franzoni (2018).....	113
Figure 5.6	Functioning principle of ventilated peripheral channels (wall base ventilation system) (source: Freitas and Torres 2003)....	114
Figure 5.7	Different types of Knapen siphons in wall .....	115
Figure 5.8	(a) A stone containing aerodynamic shape holes, and (b) After retrofit with drying stone application .....	115
Figure 5.9	Horizontal courses of low-porosity stones brick were used at the base of the walls in order to limit the water capillary rise in two affected buildings in Venice; (a) Alberaria Tower, and (b) Salt Emporium (source: EMERISDA 2014).....	116
Figure 5.10	Massari method: two series of overlapping holes are cored and filled with water repellent mortar (source: EMERISDA 2014) .....	116
Figure 5.11	(a) Mechanical interruption Italy (Universita Ca'Foscari Venezia), and (b) Mechanical Interruption in Belgium (BBRI) (source: EMERISDA 2014).....	117
Figure 5.12	(a) Wall treatment using pressure (injection), and (b) wall treatment using only hydrostatic (Impregnation).....	118
Figure 5.13	Schematic of an electro osmosis set up used on a masonry wall (source: EMERISDA 2014).....	119
Figure 5.14	The wall cutting location on the building construction .....	121
Figure 5.15	The case-study wall construction in enlarged cross-section detail. ....	121
Figure 5.16	The location of the cutting plate, as an element of retrofitted method, on the wall construction, simplified as a representation in the simulation model .....	122
Figure 5.17	Simulated water content of the upper part of solid brick wall of the post-retrofit cases over a period of 9 years (2016 to 2024) .....	126
Figure 5.18	Simulated water content of the upper part of solid brick wall of the post-retrofit cases over a steady accumulation period of 6 years (2016 to 2024).....	127

# List of Tables

Table 2.1	Thermal conductivity supplement (b) of building materials (Künzel 1995) .....	21
Table 2.2	Average surface transfer coefficients for calculating the heat and moisture exchange between exterior or interior component surfaces and the environment (WUFI-Wiki 2020a).....	29
Table 2.3	Short-wave absorptivity and brightness reference value of various building material surfaces (source: Künzel 1995) .....	29
Table 2.4	Lists of the material basic properties .....	35
Table 2.5	Lists of the hygro-thermal functions of material regarding WUFI software simulation.....	37
Table 2.6	Inputs and settings of WUFI (source: Aien et al. 2017) .....	45
Table 2.7	Material basic properties input data .....	45
Table 2.8	Material hygro-thermal properties input data .....	46
Table 2.9	Initial conditions assumptions in the initial simulation model (source: Aien et al. 2017).....	46
Table 2.10	Simulation scenarios (source: Aien et al. 2017) .....	47
Table 3.1	Thermal conditions in each region in Thailand during 1981-2010 (30 years) (source: TMD 2020) .....	56
Table 3.2	Information regarding the used materials in the model. ....	65
Table 3.3	Inputs and settings of WUFI.....	66
Table 3.4	Material basic properties input data .....	67
Table 3.5	Material hygro-thermal properties input data .....	67
Table 3.6	The temperature and humidity values required for the indoor climate condition calculations.....	68
Table 3.7	Initial conditions in this model as well as calculation period .....	68
Table 3.8	The properties of lime stucco, lime plaster and solid clay brick serving as the model input parameters (the model initial values) (source: Pinich 2018).....	69
Table 3.9	The properties of solid clay brick with 6-step varied values .....	69
Table 3.10	Threshold of the sensitivity classification based on mean relative deviation and coefficient of variation (CV) values (source: Pinich 2018).....	70
Table 3.11	Calculated mean relative deviation and coefficient of variation (CV) values over the 6 steps of respective input variable alteration averaged over the three positions (source: Pinich 2018) .....	75
Table 3.12	Classification of six input parameters with respect to the mean relative deviation (source: Pinich 2018) .....	76
Table 3.13	Classification of six input parameters with respect to the coefficient of variation, CV (source: Pinich 2018) .....	76

Table 4.1	Information regarding the used materials in the model. ....	97
Table 4.2	Inputs and settings of WUFI .....	97
Table 4.3	Material basic properties input data .....	98
Table 4.4	Material hygro-thermal properties input data .....	98
Table 4.5	Initial conditions in this model .....	100
Table 4.6	The computed average water content given for the entire wall, the upper part, and the lower part of solid brick wall .....	106
Table 4.7	The average water content given for the top of upper-part wall, the middle of upper-part wall, and The bottom of upper-part wall..	107
Table 5.1	Information regarding the used materials in the model. ....	122
Table 5.2	Basic properties input data of bitumen layer model .....	123
Table 5.3	Hygro-thermal properties input data of bitumen layer model....	123
Table 5.4	Initial conditions in this model provided as per converged results of the pre-retrofitted cases in 2014 .....	123
Table 5.5	The average water content given for the entire wall, the upper part, and the lower part of solid brick wall, of the post-retrofit cases .....	126
Table 5.6	The average water content of the upper part of solid brick wall of post-retrofit cases comparing with pre-retrofit cases .....	126
Table 5.7	The average water content of the lower part of solid brick wall of post-retrofit cases comparing with pre-retrofit cases .....	127
Table 5.8	The average water content (in 2024) of the upper part of solid brick wall of post-retrofit cases comparing with pre-retrofit cases in the interior wall and exterior walls with the thickness of 0.55 m and 0.70 m.....	128

# Curriculum vitae

## Sarin Pinich

- 2020 – present Instructor at Faculty of Architecture Chulalongkorn University, Bangkok, Thailand.
- 2015 – 2020 PhD student/ candidate, Department of Building Physics and Building Ecology, TU Wien, Vienna, Austria
- 2011 – 2015 Instructor at Faculty of Architecture Chulalongkorn University, Bangkok, Thailand.

## Educational background

- 2009 M. Arch., Architecture (Environment and Technology in Architecture), Chulalongkorn University, Bangkok, Thailand
- 2005 B. Arch., Architecture, Chulalongkorn University, Bangkok, Thailand

## Publications

### PhD Project related publications

- Aien, S., Taheri, M., Pinich, S., Schuss, M., and Mahdavi, A. (2017), 'Predictive performance of hygro-thermal simulation models: A case study,' Proceedings of the 12th International EnviBUILD Conference (7th & 8th September 2017): 7.
- Pinich, S., Taheri, M., and Mahdavi, A. (2018), 'Sensitivity Analysis of the hygro-thermal simulation model of a historical building façade in hot-humid climate,' Poster: BauSIM2018 - 7. Deutsch - Österreichische IBPSA - Konferenz Tagungsband, Karlsruhe, Germany; 26.09.2018 - 28.09.2018; in: Proceedings of BauSim2018, Paper-Nr. 1157, 6 pages.
- Pinich, S. and Mahdavi, A. (2020), 'Rising damp in historical buildings in tropical climate: A case study of hygro-thermal analysis,' Oral Presentation (Online): Indoor Air 2020 conference, Seoul, Korea, 1<sup>st</sup> – 4<sup>th</sup> November, 2020, in: Proceedings of Indoor Air 2020 conference.

## Other publications

- Pinich, S. and Sreshthaputra, A. (2015), 'Relationship between Moisture Content and Decay of Walls in Ancient Building: A Case of Wat Nivet Dhammaprawat, Ayudhya,' AJA, Department of Architecture, Chulalongkorn University, Bangkok, Thailand.
- Sreshthaputra, A., and Pinich, S. (2012), 'Status of Green Design, Construction, and Operation of Thai Government Buildings,' KKU Conference 2012, Khon Kaen University, Bangkok, Thailand.
- Sreshthaputra, A., Vongveeranonchai, N., Pinich, S. (2012), 'An Approach to Solving of Humidity Problem in the Reclining Buddha Statue of Wat Statue, Ayutthaya,' KKU Conference 2012, Khon Kaen University, Bangkok, Thailand.
- Pinich, S. (2010), 'Stack Ventilation Design Guidelines for Residential Building: Case Study Eur Ar Thorn Housing Project,' CU: ADS, 2011. Department of Architecture, Chulalongkorn University, Bangkok, Thailand.
- Pinich, S. (2009), Natural Ventilation: Planning Design Guidelines for Residential Building: Case Study Eur Ar Thorn Housing Project,' Master Thesis, Department of Architecture, Chulalongkorn University, Bangkok, Thailand.